ADAR1 mutation causes ZBP1-dependent immunopathology

Nicholas Wesley Hubbard

A dissertation

submitted in partial fulfillment of the

requirements for the degree of

Doctor of Philosophy

University of Washington

2022

Reading Committee:

Andrew Oberst, Chair

Jakob von Moltke

Ram Savan

Program Authorized to Offer Degree:

Department of Immunology

University of Washington

Abstract

ADAR1 mutation causes ZBP1-dependent immunopathology

Nicholas Wesley Hubbard

Chair of the Supervisory Committee:

Andrew Oberst

Department of Immunology

In this dissertation, we describe a novel role for the antiviral protein ZBP1 in mediating the pathology associated with the type-I interferonopathy associated with deficiency in the protein ADAR1. Through these studies, we gain novel insight both into the mechanisms controlling ZBP1 activation, as well as a better understanding of the downstream physiologic outcomes of ZBP1 activation.

Summary: The RNA editing enzyme ADAR1 is essential for suppression of innate immune activation and pathology caused by aberrant recognition of self-RNA, a role it carries out by disrupting the duplex structure of endogenous double-stranded RNA species. A point mutation in the Z-nucleic-acid binding domain (ZBD) of ADAR1 is associated with severe autoinflammatory disease. ZBP1 is the only other ZBD-containing mammalian protein and its activation can trigger both cell death and transcriptional responses via the kinases RIPK1 and RIPK3, and the protease

caspase-8. Here, we show that the pathology caused by ADAR1 ZBD mutation is driven by activation of ZBP1. We found that ablation of ZBP1 fully rescued the overt pathology caused by ADAR1 mutation, without fully reversing the underlying inflammatory program caused by this mutation. While loss of RIPK3 partially phenocopied the protective effects of ZBP1 ablation, combined deletion of caspase-8 and RIPK3, or of caspase-8 and MLKL, unexpectedly exacerbated the pathogenic effects of ADAR1 mutation. These findings indicate that ADAR1 is a negative regulator of sterile ZBP1 activation, and that ZBP1-dependent signaling underlies the autoinflammatory pathology caused by mutation of ADAR1.

TABLE OF CONTENTS

LIST OF FIGURES

Chapter 1:

Chapter 2:

Supplemental Figures:

Chapter 3:

ACKNOWLEDGEMENTS

I thank my advisor, Andrew, for his patience and advice over the last 6 years. I've enjoyed our many conversations about interesting data, future experiments, and wild scientific speculation. I appreciate him frequently coming to me with an interesting possible future idea or experiment he thought I might find interesting, though, "…I should under no circumstances do…" but I also thank him for putting his foot down and making me to do the not-so-fun but important experiments to finish this project, publish, and finish this PhD. I didn't always appreciate it immediately, but in retrospect I gratefully acknowledge the importance of these nudges, especially knowing that we would both prefer to continue talking/thinking about/doing the fun experiments rather than grind through the necessary but boring ones. Andrew has been a spectacular example of scientific focus and clarity – I'm continually impressed with his ability to write and think in a way that both captures the complexity, challenges, and impact of the science we are doing, while somehow avoiding becoming mired in the unnecessary complexity that I so often find myself becoming distracted with. I hope that I have learned from his excellent example.

To the members of my thesis committee, thank you for your time, support, and valuable feedback. I have looked forward to our meetings and your criticism has always been helpful and fair. I'm grateful to be part of a community with such excellent scientists who are still willing to take the time out of their busy schedules to support and mentor others working to develop their own scientific careers.

I also want to thank the past and present Oberst lab members. Between a global pandemic and everyday scientific challenges, the last few years have not been a particularly fun time to do science. Thank you for being patient with me, even when I have been quiet, grumpy, and

generally not a joy to be around. The last few months interviewing for postdoc positions and preparing to graduate, have reminded me of the shared excitement and collegiality of academic science that keeps me here – academia may not always reflect the easiest work-life balance or financial security, but somehow, it's worth it when you're surrounded by people who continually help make this work interesting, unexpected, and weird. Thank you for making this fun.

DEDICATION

I dedicate this work to my grandparents, Barbara and Dick Hubbard. Because of their hard work and commitment to their family, my opportunities in life have been essentially limitless. I haven't always made the most responsible or forward-thinking choices, particularly in terms of my academic pursuits, but their hard work has privileged me with the luxury to stumble and make many, MANY mistakes along the way to graduate school and this work. I am very aware that not everybody has been as lucky as me, and so I hope that I can somehow contribute to future generations having the same opportunity you worked so hard to give me.

Chapter 1

Introduction

1.1 Introduction

Programmed cell death represents an extremely effective mechanism to combat infection, yet must be tightly controlled in order to avoid excessive host immunopathology. Necroptosis is an inflammatory cell death program mediated by Receptor Interacting Protein Kinase 1 (RIPK1) and 3 (RIPK3), which likely evolved as an antiviral mechanism allowing deletion of infected cells[1–6].

In contrast to passive cell death processes such as necrosis, programmed cell death is a rapid event orchestrated by a series of defined molecular mechanisms, typically occurring within minutes to several hours[7,8]. For example, the commonly known cell death mechanism, apoptosis, is canonically orchestrated by the activation of several cysteine proteases, known as caspases. The molecular mechanisms by which programmed cell death is executed also has important consequences on the outcomes of that cell death. Again, taking apoptosis as an example, apoptotic caspase activation results in a cell shrinking and 'blebbing' into membrane bound apoptotic bodies, which are subsequently phagocytosed before they can spill their contents into the extracellular space. This is in contrast with the lytic forms of programmed cell death, pyroptosis and necroptosis (the subject of this dissertation). In these forms of cell death, the plasma membrane is disrupted by a molecular pore formed by (respectively) gasdermins or MLKL (Mixed Lineage Kinase domain Like pseudokinase)[9–11]. In addition to the release of cellular contents, both pyroptosis and necroptosis also orchestrate distinct inflammatory events: respectively, maturation and release of IL-1β or activation of the NFκB transcriptional pathway.[12–16]

Necroptosis was originally described in association with the Tumor Necrosis Factor (TNF) signaling pathway – this first description of necroptosis occurred in L929 cells stimulated with TNF in the presence of caspase inhibition; upon stimulation rapid necrosis was observed[17]. Subsequent studies revealed that this result was due to the activity of the Receptor-Interacting-Protein-Kinases (RIPK) molecules RIPK1 and RIPK3[18–22]. Briefly, upon TNF signaling, RIPK1 recruits RIPK3 into large oligomeric structures via their shared RHIM (RIP Homotypic Interaction Motif) domain; this RIPK1/RIPK3 complex is termed the 'necrosome'. Following this oligomerization event, RIPK1 phosphorylates RIPK3, which in turn phosphorylates MLKL, resulting in its oligomerization into large

molecular pores which then translocate to the plasma membrane, resulting in membrane permeabilization and lytic cell death[23].

Although TNF activation of the necroptotic signaling pathway is not the focus of this dissertation, the mechanisms of crosstalk between RIPK1 dependent transcription, necroptosis and apoptosis were largely defined in this context and will become relevant in later chapters, so a summary is warranted here. Upon TNF signaling (Fas-L and TRAIL signal in a largely identical fashion), RIPK1 and FADD (Fas associated protein with death domain) are recruited to the TNF-receptor via their Death Domains (DD) through the adapter protein TRADD (TNF Receptor Associated Death Domain); this complex is termed 'complex-I'[24–27]. Complex-I is responsible for TNF dependent transcription and is mediated by kinase independent functions of RIPK1; RIPK1 is poly-ubiquitinated by a family of ubiquitin ligases known as the IAPs (inhibitor of apoptosis), and this ubiquitination facilitates the recruitment and activation of the IKK/NFκB signaling cascade **(Fig. 1)**. A more detailed description of this mechanism is beyond the scope of this discussion, but generally, the stability of complex-I is largely determined by the state of RIPK1 polyubiquitination; if ubiquitination is maintained, NFκB activation drives additional pro-survival factor transcription (including IAP family proteins), while if RIPK1 is deubiquitinated (this will rapidly occur unless actively counteracted), the cell will activate a programmed cell death pathway[28].

Complex-I formation may immediately begin transition into complex-IIa following the recruitment of procaspase-8 via FADD's CARD (Caspase activation and recruitment domain). Importantly, Casp8 may either form homodimers, or heterodimers, with the protein cellular FLICE (FADD-like IL-1β-converting enzyme)-inhibitory protein (cFLIP)[12,19,29,30]. Casp8/cFLIP heterodimers possess the proteolytic capacity to cleave components of the necrosome but are not competent for triggering the apoptotic signaling cascade (in contrast to Casp8 homodimers, which will be discussed shortly)[31]. **(Fig. 1)** Notably, cFLIP is strongly induced downstream of NFκB transcription (complex-I) and is therefore an important pro-survival component of TNF signaling. Casp8 (and cFLIP) plays an enigmatic role where it may, 1) inhibit RIPK1 through proteolytic cleavage of necrosome components[32],

or 2) trigger apoptotic cell death[29]. To briefly introduce the Casp8 apoptotic signaling cascade (also known as 'extrinsic' apoptosis), upon homodimerization, procaspase-8 undergoes proteolytic maturation into the mature Casp8 homodimer. Active Casp8 may then cleave the Bcl-2 family protein Bid into its truncated version, tBid[33], resulting in the activation the mitochondrial proteins Bax and Bak, which subsequently forms pores in the mitochondrial outer membrane. Mitochondrial Outer Membrane Permeabilization (MOMP) results in the release of cytochrome-C[34], which triggers the oligomerization of APAF1 (Apoptosis peptidase activating factor 1) and Caspase-9 (Casp9)[35]; in a similar fashion to Casp8, Casp9 oligomerization results in its dimerization and activation. Finally, in its active form, Casp9 cleaves and activates the 'executioner caspases, Caspase-3 and Caspase-7, whose direct activity results in the cellular dismantling associated with apoptosis (DNA laddering, cell shrinkage, membrane blebbing, etc)[7,36,37].

Finally, in the case where complex-IIa is not resolved through either apoptosis or Casp8/cFLIP activity (proteolytic dismantling of the necrosome), it may transition into complex-IIb, where RIPK3 and MLKL may be recruited, triggering necroptotic cell death as described earlier[19,21,22,27,38]. **(Fig. 1)** The dynamic relationship between complex-IIa and complex-IIb is underscored by the observation that loss of Casp8 results in embryonic lethality due to unrestrained necroptosis, but that this lethality is fully rescued by combinatorial deletion of either RIPK3 or MLKL (mice with a single deletion of either appear normal)[19,29,39]; this rescue suggests that the necroptotic signaling pathway is continually poised for activation and a key component for its activation is modulation of Casp8. Furthermore, RIPK1 deletion is also embryonically lethal, but can be rescued by simultaneous deletion of RIPK3 and Casp8 ($RIPK1^{-/-}$ ::$Casp8^{-/-}$::$RIPK3^{-/-}$)[40], suggesting a requirement for regulation of TNF signaling during embryonic development. Although few physiologic mechanisms for Casp8 regulation have been defined, these observations are consistent with the original report describing necroptosis upon TNF signal in combination with caspase-inhibition, and further suggests that translational control (cFLIP) and Casp8 modulation are central requirements for the activation of necroptosis.

The signaling described above, although complicated, is a vastly simplified version of the necroptotic signaling pathway; despite an enormous body of work characterizing this pathway, the decision to engage transcriptional, apoptotic, or necroptotic mechanisms (or a combination) remains poorly understood, but likely depends on cellular lineage and location ques, as well as homeostatic versus inflammatory context. For the purposes of this dissertation though, it is simply worth noting that the signaling processes associated with necroptosis are diverse and dynamic, with multiple signaling outputs possible, the consequences of which we will explore in the next chapter.

1.2 ZBP1 is an activator of necroptosis

Although initially characterized in the context of the TNF signaling pathways, necroptosis likely evolved primary as an antiviral pathway: the action of necroptosis has been implicated in control of a diverse array of viral infections by both DNA and RNA viruses, including herpes simplex virus-1 (HSV-1)[4,18], influenza A virus (IAV)[41,42], *Vaccinia* virus[5,43,44], murine cytomegalovirus (MCMV)[43,45,46], West Nile virus (WNV) and Zika Virus (ZIKV)[47,48]. Across these diverse pathogens, the protein Z-DNA binding protein 1 (ZBP1) has been established as the critical sensor upstream of programmed cell death. Despite extensive characterization of the molecular mechanisms underlying necroptotic signaling, the ligand responsible for activating ZBP1 remains unclear[49], and is complicated by the lack of an obvious common ligand shared by the DNA and RNA viruses capable of triggering necroptosis.

ZBP1, also known as DLM-1 or DAI (DNA Activator of Interferon) is a strongly interferon inducible protein, which contains two N-terminal 'Z-DNA Binding Domains' and three central RHIM domains[50]. **(Fig. 2)** Despite several misleading early reports, later work on ZBP1 demonstrated that in response to a diverse set of viral infections, ZBP1, via its RHIM domains is capable of directly recruiting and activating the necroptosis-inducing kinase RIPK3, leading to activation of mixed lineage kinase-like protein (MLKL) and programmed cell death[6-8, 25, 29]. This contrasts with TNF and TNF-like signaling mechanisms which are primarily mediated through RIPK1, leading to the subsequent recruitment of RIPK3; in fact, ZBP1 signaling has been previously described as entirely dependent on RIPK3, and a

contribution of RIPK1 to ZBP1 dependent necroptosis has not been described in response to viral infection[41,51,52]. It is potentially also worth noting that although ZBP1 contains three putative RHIM domains (denoted RHIM1, RHIM2 and RHIM3), only RHIM1 appears to be critical for interactions with RIPK3. While there are a range of possibilities for what these domains could be doing, it appears likely that there are yet undefined ZBP1 interactions mediated by these additional domains.

Activation of ZBP1 relies on its two N-terminal 'Z-DNA binding domains' (ZBDs), and despite their name, the ligand to which they bind remains unclear[45,53–58]. While the specific ZBD ligand remains unknown, it is clear that the Z-DNA binding domains of ZBP1 are crucial for recognition of viruses, and any deletion or modification of Zα1 in particular abrogates ZBP1 function in response to viral infection.[41,43,50,59,60] Although ZBP1 contains two N-terminal ZBD domains (denoted Zα1 and Zα2), only Zα1 seems to be strictly required for recognition of most viral infections. Importantly, 'Z-DNA Binding Domain' is something of a misnomer: ZBDs are equally capable of binding to Z-DNA, as well as Z-RNA[61–63]. In contrast to the commonly known right handed double helix of B-DNA, Z-form nucleic acid is a left-handed double stranded nucleic acid structure which takes its name from the characteristic zig-zag conformation of the phosphate backbone[64]. This conformation has been proposed to arise in response to torsional strains in regions adjacent to where Z-NA is formed, for example, during protein-nucleic acid binding or DNA replication. While some sequences of nucleic acids have been characterized as more prone to adopting a Z-form conformation, ZBDs have been biochemically characterized to bind Z-form nucleic acids in a sequence independent fashion through recognition of the minor groove-minor groove structure of Z-NA. Interestingly, as Z-form nucleic acid is thermodynamically unstable and transient, there is some evidence that upon binding, ZBD's may stabilize these nucleic acid species[65]. And although a physiologic context for this ZBD/Z-NA interaction has remained undefined, based on the dynamic nature of these structures, it is interesting to consider how nucleic acids themselves may act as a sort of cellular sensor for danger by undergoing conformational changes such as the formation of Z-form nucleic acid structures, either through protein binding or other unknown interactions.

Although ZBP1 activation has primarily been shown in response to viral infection, in several early *in vitro* experiments, we demonstrated that ZBP1 may also be activated in the absence of infection. Using a doxycycline inducible system **(Fig 3A)**, we show that overexpression of ZBP1 alone results in necroptotic cell death **(Fig 3B)**. Moreover, overexpression of ZBP1 with a mutated ZBD failed to trigger any death (data not shown). Finally, by replacing the Z-DNA binding domains with a tandem 'FKBP' domain (termed 2xFV-ZBP1), we can artificially induce the oligomerization of ZBP1 by the addition of a 'B/B' homodimerizer drug, also known as AP-1. Using this system, we show that while overexpression of 2xFV-ZBP1 has no effect, but upon AP-1 addition and oligomerization of ZBP1, rapid necroptotic cell death occurs (**Fig. 3C**). These experiments suggest the potential for a ligand and mechanism for ZBP1 activation in sterile nonviral setting.

Two recent *in vivo* studies have demonstrated instances of ZBP1-dependent pathology occurring under sterile settings, suggesting that this pathway may be activated by endogenous ligands[51,66,67]. Briefly, these studies independently generated mouse models where the RHIM domain of RIPK1 was mutated, thereby removing its ability to interact with either RIPK3 or ZBP1. RIPK1$^{mutRHIM/mutRHIM}$ mice are embryonically lethal but are rescued by further deletion of RIPK3 or MLKL. Surprisingly, these mice were also fully rescued by further deletion of ZBP1. Intriguingly, while RIPK1 has not been shown to be involved in ZBP1 dependent necroptosis in response to viral infection, these sterile models demonstrate a role for RIPK1 in regulating ZBP1 activity. Although not specifically shown in these reports, presumably this control of ZBP1 activation occurs through RIPK1 and homotypic DD recruitment of FADD/Casp8/cFLIP to the necrosome. We note that this hypothesis is potentially in line with our own observations that stimulation of murine LET1 (Lung epithelial type-I) cells with IFN and the caspase inhibitor ZVAD results in ZBP1 dependent cell death **(Fig 4)** Generally, these studies suggest that the ZBP1-RIPK3 signaling axis requires tightly controlled negative regulation mechanisms (reminiscent of those associated with the TNFR pathway), which may be differentially modulated between the contexts of homeostasis versus infection.

1.3 Relationship of ADAR1 and ZBP1

Although the role of ZBD's in biology and ZBP1 function is unclear, a brief survey of ZBD containing proteins leads us to one potentially illuminating observation: only one other mammalian protein contains a ZBD, the protein ADAR1 (adenosine deaminase acting on dsRNA 1), and more specifically the cytoplasmic interferon inducible long 'p150' isoform of ADAR1[31] (**Fig 2**).[53,54,57,68,69]

ADAR1 binds to double stranded RNA (dsRNA) and modifies its structure via deamination[70–74]; in this way, it acts as a negative regulator of the cellular response to dsRNA. More specifically, deamination of dsRNA by ADAR1 blocks its recognition by the dsRNA sensor MDA5[75–80]. Accordingly, loss of ADAR1, or polymorphisms within the ZBD motif of ADAR1, are associated with the auto-inflammatory disease, Aicardi-Goutières Syndrome (AGS)[79,81–84]. Despite no clear physiologic role for ZBD's, this association with ADAR1 activity suggests that they may play a role in the response to dsRNA. We also note that in addition to its two N terminal Z-DNA Binding domains, ADAR1 also contains three central dsRNA binding domains **(Fig 2)**. The combined presence of these two distinct types of nucleic acid binding domain may suggest that ADAR1 is capable of responding to a wider variety of nucleic acid structures, or, that these domains potentially act in concert to increase specificity or affinity (or both) to key regions of dsRNA[85].

Loss of ADAR1 in mice is embryonically lethal, but this lethality is partially rescued by concurrent deletion of the dsRNA sensor, melanoma-associated differentiation protein 5 (MDA5)[70,76,77,80]. MDA5 is a cytosolic protein that recognizes long dsRNA structures[86,87]. In contrast to the closely related RIG-I (Retinoic Acid Inducible Gene I) which recognizes short dsRNA species (thought to be mediated by 5'triphsphate recognition), MDA5 triggers a type-I IFN response to dsRNA regions of 1 kb or longer, with IFN production increasing progressively with longer and longer dsRNA structures[86–89]. This specificity to longer dsRNA structures appears to be mediated by an oligomerization requirement; where monomeric MDA5 only weakly binds to dsRNA, longer stretches of dsRNA allow MDA5 to form a filament along the dsRNA axis, and these protein-protein interactions increase affinity by several orders of magnitude. In fact, mutations in MDA5 which stabilize these protein-protein interactions and allow

recognition of shorter stretches of RNA are also associated with a different genetic version of AGS[86,87,90,91]. The primary source of these long dsRNAs is thought to be from endogenous Alu retroelements; Alu elements are extremely successful mobile genetic elements and represent the most abundant repetitive sequences in the human genome[87,92,93]. Sequence analysis of the ADAR1 'editome' reveals a high number of A to I edits in mRNAs containing hairpin forming Alu elements in their untranslated regions[85,94]. Critically, introduction of A to I edits to dsRNA Alu hairpins by ADAR1 creates mismatches in the double-stranded structure, disrupting the formation of MDA5 filaments along their length, thereby abrogating the production of type-I IFN in response to these abundant endogenous elements[86,87,91].

As mentioned earlier, a full knockout of ADAR1 (or a p150 isoform specific knockout) results in embryonic lethality in mice[76]. Although full loss of ADAR1 is not observed in humans, a variety of mutations have been observed across ADAR1 which are associated with AGS **(Fig 5)**. These mutations are primarily comprised of either early frameshift and nonsense mutations, or missense mutations in the deaminase domain. Interestingly, while these mutations are quite rare and occur only as single heterozygous mutations (they would likely be embryonically lethal if homozygous), they only cause disease when paired on the opposite allele with a proline to an alanine mutation at amino acid position 193 (P193A)[79,95]. This P193A mutation is noteworthy for several reasons: 1) P193A is a highly prevalent mutation in human populations, with approximately 1:360 people of Northern European descent carrying it[78,79,96], 2) proline 193 lies within the first ZBD of ADAR1, specifically in the p150 isoform, and 3) by itself, this mutation causes no obvious signs of disease either in a heterozygous or homozygous form. This ADAR$^{P195A/null}$ disease haploinsufficiency indicates the ZBD of ADAR1 has a critical biologic function, and that there is a gene dose requirement for proper ADAR1 function. To better understand the role of this P195A mutation in ADAR1 function, a mouse model was recently developed by making the homologous ADAR1 mouse mutation at position 195 (P195A)[96]. Like the genetics of human AGS, mice homozygous for P195A showed no signs of inflammation (or any observable difference in transcription);

mice lacking a single allele of ADAR1 were also phenotypically normal; mimicking the human disease genotype, when these two alleles were combined ($ADAR1^{P195A/-}$) mice were born, but were severely runted, and had strongly decreased survival (median survival ~d.21)[96]. In comparison to a full ADAR1 deletion, this phenotype is a far better representation of that observed in human disease and represents a highly attractive model for understanding if a relationship between ZBP1 and ADAR1 may exist. Moreover, as these mice are viable, any differences in phenotype upon ZBP1 modification may be much more readily observable.

It is also worth noting that the disease associated with ADAR1 mutation in humans and in mice is primarily driven by type-I interferon; in particular, the $ADAR^{P195A/-}$ model is fully rescued by MDA5 and IFNAR deletion (compared to the partial rescue of a full knockout)[96]. Given that ZBP1 is a potently interferon inducible gene[49,97], this led us to hypothesize that ZBP1 could represent an important distal mediator of the auto-inflammatory pathology associated with this particular type-I interferonopathy. While it seems less likely that ZBP1 is ubiquitously associated with all forms of type-I interferon mediated pathology, based on the shared Z-DNA binding domains of ADAR1 and ZBP1, we wonder if there is a specific role for ZBP1 in this instance of interferon driven disease. We also note that loss of the RNA sensor, protein kinase RNA-activated (PKR) rescues *in vitro* cell death upon ADAR1 loss and, *in vivo* rescues the $ADAR^{P195A/-}$ phenotype[75,96,98]. However, activation of neither MDA5 nor PKR represents a direct mechanism to explain the cell death and downstream pathology associated with ADAR1 deficiency. We suggest that ZBP1 represents a common dsRNA sensor that initiates necroptosis, and that upon loss of ADAR1 function, ZBP1 activity may be positively coordinated through the action of other dsRNA sensors such as PKR and MDA5. Importantly, while several studies have examined the signaling responsible for cell death upon loss of ADAR1, these studies have relied on commonly-used cultured cell lines which have lost expression of components of the necroptotic machinery[20, 21, 35]. Because most primary cells maintain sensitivity to necroptosis[13,75,99–101], these studies may have inadvertently overlooked the contribution of this pathway on the physiologic response to ADAR1 loss.

1.6 Concluding Remarks

ZBP1 appears to be the critical sensor by which viral infections activate the necroptotic signaling pathway, but the molecular mechanisms governing this process remain unclear. Furthermore, although we have a detailed understanding of the signaling processes associated with RIPK1 and RIPK3, this is largely based on studies involving the TNF signaling pathway; while some of the same rules may apply, ZBP1 recruitment of the necrosome is clearly distinct, both in cellular localization and molecular interactions – for instance, ZBP1 is believed to interact nearly exclusively with RIPK3, and the contribution of RIPK1 to ZBP1 dependent necroptosis is unclear. Therefore, a more detailed understanding of both the upstream signals and downstream outcomes of ZBP1 activation is warranted.

In this dissertation, I will investigate these questions by characterizing *in vivo* ZBP1 dependent effects in this new P195A model of ADAR1 deficiency. Although viral infections appear to be the primary mechanism for activating ZBP1, using this nonviral approach offers several benefits:

1) Unlike previous studies, this model of sterile ZBP1 activation does not otherwise perturb any other components of the necroptotic signaling pathway. For example, although the pathology associated with the RIPK1^{RHIM} model clearly exerts itself in a ZBP1 dependent fashion, by removing the ability of RIPK1 (and thereby Casp8) to associate with the necrosome, we have removed a key regulatory mechanism associated with this pathway, thereby precluding a physiologic understanding of upstream activation mechanisms, as well as any ZBP1/RIPK1 dependent signaling outcomes.

2) Using a sterile model, we can focus on ZBP1, rather than the complicated biology associated with any individual viral infection. As mentioned before, ZBP1 responds to a surprising variety

of viruses, each of which modulates the host interferon response in their own unique fashion; by avoiding these complications, the common features of ZBP1 specific activation and signaling will be more apparent and interpretable.

3) These findings have the potential to implicate ZBP1 in a variety of inflammatory pathologies, both in pathogen and non-pathogen settings. Generally speaking, current therapies targeting inflammatory disease rely on broad spectrum inhibition of the immune response, in many cases leaving the recipient vulnerable to infection[102–105]. Therefore, interferon mediated disease and immune pathology represents a major scientific and clinical challenge: by nature our immune response is comprised of hundreds of distinct effector mechanisms, often acting simultaneously; despite their important roles in anti-pathogen immunity, many of these effector pathways may also drive severe adverse pathology in the host. Therefore, it follows that among this multitude of inflammatory mechanisms, some may disproportionately contribute to immune pathology. If these mechanisms could be identified and the circumstances of their activation understood, they could be specifically targeted to relieve damaging immune pathology, while maintaining the overall anti-pathogen response.

1.7 Figures

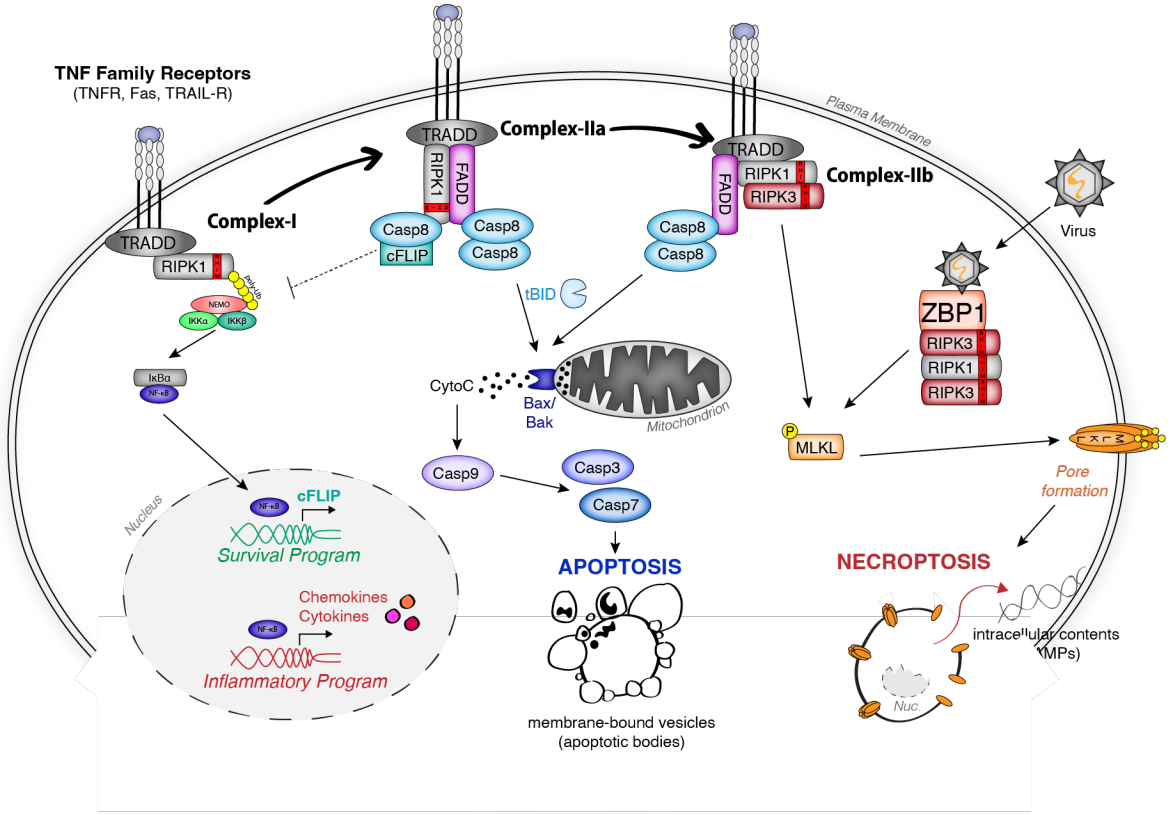

Figure 1. Activation and regulation of the necroptotic signaling pathway. Necroptosis may be triggered by a downstream of a variety of molecules including TNF and ZBP1. Binding of the TNF receptor or TNF-receptor like pathways results in a RIPK1 dependent recruitment of transcriptional, apoptotic and necroptotic signaling components. This pleiotropic signaling mechanism may result in survival, apoptosis or necroptosis, depending on the cellular conditions at the time of signaling. In contrast to TNF activation of the necroptotic pathway, ZBP1 is activated in response to viral infection, and is believed to directly recruit RIPK3 and trigger necroptotic cell death, although RIPK1 may also be recruited to the ZBP1 signaling complex and regulate its activity through the recruitment of FADD/Casp8/cFLIP.

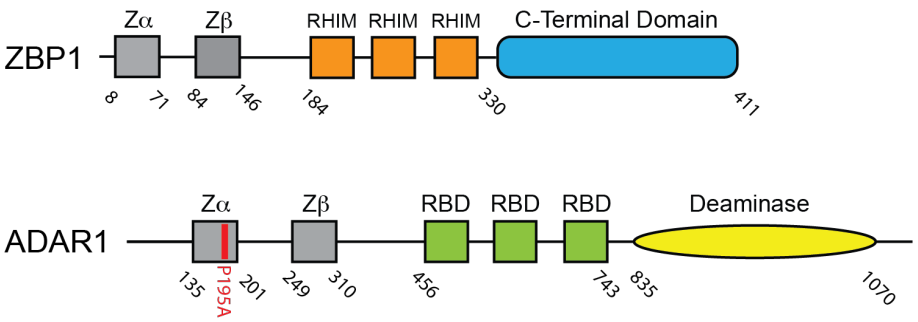

Figure 2. Schematic diagram of ZBP1 and ADAR1 domain structure. ZBP1 contains two tandem N-terminal Z-DNA biding domains, are commonly referred to as Zα and Zβ, or Zα1 and Zα2, respectively. ZBP1 also contains three central RHIM domains and a poorly characterized intrinsically disorganized C-terminal domain. ADAR1 also contains two N-terminal Z-DNA followed by three central RNA Binding Domains and finally a C-terminal deaminase domain.

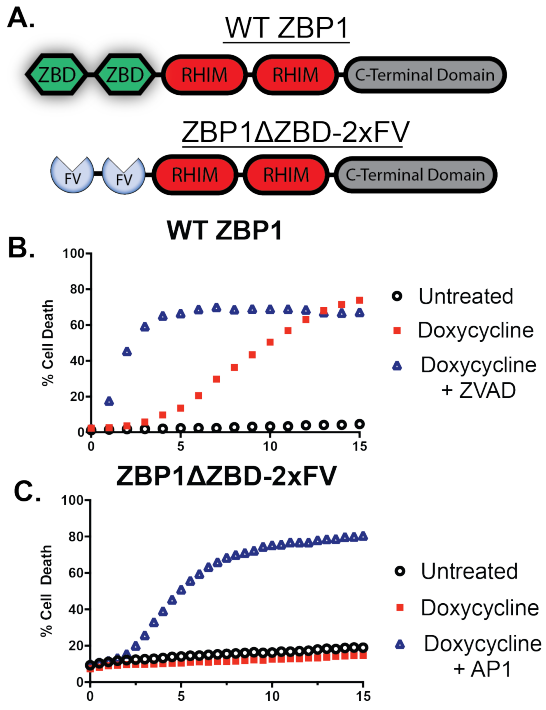

Figure 3. Overexpression or oligomerization of ZBP1 triggers cell death. (A) Full length ZBP1 was cloned into a tetracycline inducible expression system (pSLIK), or, two tandem FKBP domains were fused to an N-terminal truncation of ZBP1 lacking its two Z-DNA Binding Domains. (**B)** Doxycline induced overexpression of ZBP1 results in programmed cell death, which appears to be a combination of apoptosis and necroptosis based on altered death kinetics upon the addition of zVAD. **(C)** Oligomerization of ZBP1 by addition of the drug AP-1 (or B/B) induces rapid ZBP1 dependent cell death in the absence of viral infection.

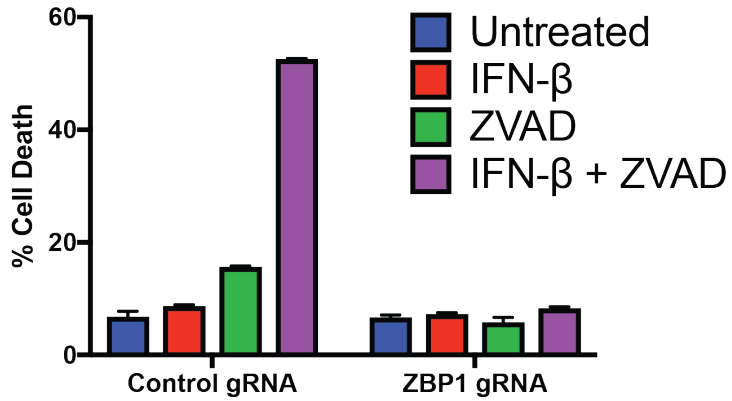

Figure 4. ZBP1 dependent cell death induced by IFN-β treatment and caspase inhibtion. WT (Control gRNA) or ZBP1 knockout (ZBP1 gRNA) LET1 cells were treated with 1000 IU/mL IFN-β overnight (12 hours), at which pint ZVADD was added and cell death was analyzed by IncuCyte analysis. Graph shows cell death 4 hours post ZVAD treatment.

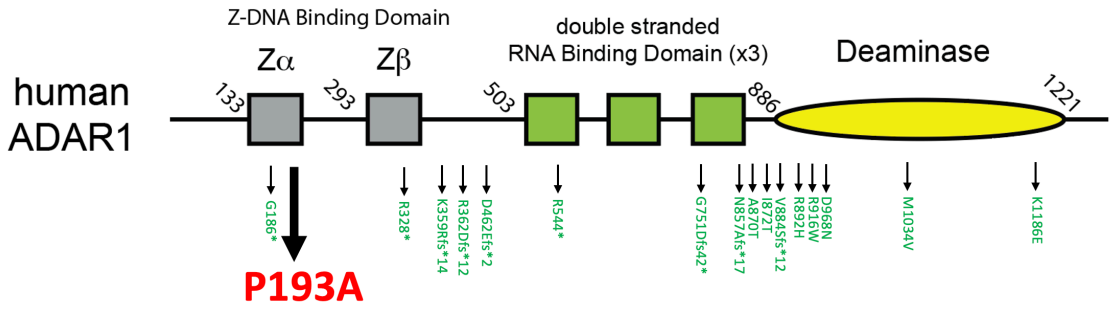

Figure 5. ADAR1 mutations associated with Aicardi-Goutières Syndrome. Mutations listed in green have been reported as heterozygous mutations in *Adar* which are associated with AGS. The P193A mutation listed in red occurs throughout the population (homozygous and heterozygous) at a relatively high rate, while not causing disease. When the P195A is paired with any of the other mutations listed, disease has been reported.

Chapter 2

ZBP1 underlies pathology in a model of ADAR1 mutation

This chapter is adapted from the following publication:

Hubbard, N.W., Ames, J.M., Maurano, M. *et al.* ADAR1 mutation causes ZBP1-dependent immunopathology. *Nature* (2022). https://doi.org/10.1038/s41586-022-04896-7

2.1 Introduction

ADAR1 modifies endogenous RNAs to prevent activation of the innate immune RNA sensors MDA5, OAS/RNAseL, and PKR[75,76]. The interferon-inducible p150 isoform of ADAR1 includes an N-terminal ZBD, and a naturally occurring point mutation in this region causes a proline-to-alanine substitution at position 193 in human ADAR1[79] **(Fig 1A)**. This mutation is present at a remarkably high rate (~1/360 in individuals of northern European descent), and if paired with a loss-of-function mutation on the second allele of ADAR1 causes the severe autoinflammatory disease Aicardi-Goutières Syndrome (AGS)[81]. Recently, a mouse model of this mutation was reported that recapitulates the genetic underpinnings and aspects of the pathology of AGS; mice carrying the P195A mutation (homologous to human P193A) on one or both alleles of ADAR1 are phenotypically normal, but animals with this mutation combined with deletion of the p150 isoform in the second allele of ADAR1 (*Adar*$^{P195A/p150null}$) display liver, kidney, and spleen pathology, are runted, and have a median survival of 25 days[96].

2.2 Results

ZBP1 loss rescues ADAR1 mutation

The *Adar*$^{P195A/p150null}$ model is driven by a point mutation in the ZBD of ADAR1 **(Fig 1A)**. Since ZBP1 contains the only other mammalian ZBD, we wondered whether these two proteins might functionally interact. Consistent with this possibility, we found that ADAR1 co-immunoprecipitated with ZBP1, but that this interaction was abrogated when point mutations were introduced to the ZBD of ZBP1 that prevented RNA binding **(Supplemental Figure 1A,B**). We also observed that the interaction between ZBP1 and ADAR1 was strengthened by UV crosslinking, which covalently links protein to nucleic acid **(Supplemental Figure 1C)**. As these data suggested that ADAR1 and ZBP1 bind a common ligand via their ZBDs, we wondered if the pathology caused by mutation of the ZBD of ADAR1 in the *Adar*$^{P195A/p150null}$ mouse model was driven by aberrant ZBP1 activation**.** To test this idea, we crossed *Adar*$^{P195A/p150null}$ mice to animals lacking ZBP1, using a widely-used ZBP1 knockout mouse strain[106], referred to here as ZBP1-a **(Fig. 1B)**. We observed that *Adar*$^{P195A/p150null}$*:: Zbp1-a*$^{-/-}$ mice were born at expected frequencies and appeared phenotypically normal **(Fig 1C,D, Supplemental Figure 2A,B).** Following birth, *Adar*$^{P195A/p150null}$*:: Zbp1-a*$^{-/-}$ mice gained weight slightly more slowly than *Adar*$^{P195A/WT}$ littermates **(Fig 1E,F)**, but otherwise displayed normal phenotype, fertility, and survival. The kidney and liver pathology previously reported in *Adar*$^{P195A/p150null}$ animals[96] was also largely normalized by ablation of *Zbp1-a* **(Supplemental Figure 2C)**.

As we were generating these data, it was reported that the *Zbp1-a*$^{-/-}$ mouse line was not fully congenic to the C57BL/6 genetic background[45], a finding confirmed by our own single nucleotide polymorphism (SNP) analysis **(Supplemental Figure 3A,B).** We therefore generated a second cross of *Adar*$^{P195A/p150null}$ mice to a separately derived, fully congenic *Zbp1*$^{-/-}$ strain[51] referred to here as "ZBP1-g" **(Supplemental Figure 3C).** *Adar*$^{P195A/p150null}$*::Zbp1-g*$^{-/-}$ mice also appeared phenotypically normal (**Fig S3D**). Notably, we also observed an extension of survival in *Adar*$^{P195A/p150null}$*::Zbp1-g*$^{+/-}$ animals, an effect not observed in *Adar*$^{P195A/p150null}$*:: Zbp1-a*$^{+/-}$ mice **(Supplemental Figure 2A)**. Together, these data confirm that loss of ZBP1 reverses the immunopathology observed in *Adar*$^{P195A/p150null}$ mice.

Complete ablation of the p150 isoform of ADAR1 causes uniform lethality during embryonic development, but crossing these mice to animals lacking the dsRNA sensor MDA5 (encoded by *Ifih1*) allows *Adar*$^{p150null/p150null}$ mice to survive to birth[76]. Since MDA5 is a potent inducer of type-I interferon (IFN), and since ZBP1 expression is stimulated by IFN **(Supplemental Figure 4A)**, we hypothesized that loss of MDA5 might rescue ADAR1-p150 knockout mice by preventing ZBP1 upregulation. However, in MEF cells, we observed that while loss of MDA5 completely abrogated IFN production induced by ADAR1 depletion, ZBP1 upregulation was only modestly attenuated **(Supplemental Figure 4B)**. This suggested that loss of ADAR1 could lead to ZBP1 upregulation and activation even in the absence of MDA5. Consistent with this finding, we observed that the survival of *Adar*$^{p150null/p150null}$*::Ifih1*$^{-/-}$ mice was modestly but significantly extended by concurrent deletion of ZBP1 **(Supplemental Figure 4C)**. However, deletion of ZBP1 alone did not allow *Adar*$^{p150null/p150null}$ mice to survive to birth **(Supplemental Figure 4D)**. Together, these data indicate that the developmental lethality induced by ADAR-p150 deletion is mediated by simultaneous activation of ZBP1, MDA5, and additional pathways.

An inflammatory signature remains in rescued mice

Adar$^{P195A/p150null}$ mice display aberrant activation of MDA5, which drives IFN-dependent inflammation. We hypothesized that this IFN-dependent signature would still be present in *Adar*$^{P195A/p150null}$*:: Zbp1-g*$^{-/-}$ mice, despite their normal phenotype. Consistent with this possibility, RNAseq analysis of spleens from 23-day old pups revealed that many aspects of the aberrant inflammatory and interferon stimulated gene (ISG) signature present in *Adar*$^{P195A/p150null}$ mice was also present in *Adar*$^{P195A/p150null}$*:: Zbp1*$^{-/-}$ animals, despite no alterations in splenic cellularity **(Fig 2A-C, Supplemental Figure 5A,B, Supplemental Figure 6).** Gene ontology analysis confirmed that the antiviral gene signature induced by ADAR1 mutation was conserved in *Adar*$^{P195A/p150null}$*:: Zbp1-g*$^{-/-}$ animals **(Supplemental Figure 5C).** This analysis also identified gene signatures present in *Adar*$^{P195A/p150null}$ mice but absent in *Adar*$^{P195A/p150null}$*:: Zbp1-g*$^{-/-}$ animals **(Supplemental Figure 5D).** These genes may indicate targets of ZBP1 signaling or may represent pathways upregulated as a result of the immunopathology

present in *Adar*$^{P195A/p150null}$ animals. In carrying out these analyses, we noted that while cells from *Adar*$^{P195A/p150null}$*:: Zbp1*$^{-/-}$ maintain many aspects of the ISG signature observed in *Adar*$^{P195A/p150null}$ animals, its magnitude is reduced **(Fig 2C, Supplemental Figure 5A)**. This was confirmed by direct comparison of MEF cells isolated from *Adar*$^{P195A/p150null}$ or *Adar*$^{P195A/p150null}$*:: Zbp1*$^{-/-}$ mice **(Fig 2D)**, and suggested that ZBP1 may play a role in augmenting ISG upregulation, a function previously ascribed to ZBP1 in other context[49].

We next sought to understand the pathways downstream of ZBP1 that are activated by ADAR1 mutation. We observed that culturing MEF cells from *Adar*$^{P195A/p150null}$ mice led to the ZBP1-dependent loss of RIPK3 expression **(Supplemental Figure 7A)**, suggesting that the ZBP1-RIPK3 pathway is constitutively active in these cells. Consistent with this, we observed that despite their reduced RIPK3 expression, treatment of these cells with the caspase inhibitor zVAD caused ZBP1-dependent RIPK3 phosphorylation and cell death **(Fig 2E,F, Supplemental Figure 7A,B).** Together, these results indicated that *Adar*$^{P195A/p150null}$ cells are sensitized to ZBP1-dependent necroptosis.

Cell death signaling in ADAR1 mutant mice

Given this finding, we next sought to address the role of the necroptotic pathway in the pathology of *Adar*$^{P195A/p150null}$ mice. To do this, we crossed *Adar*$^{P195A/p150null}$ mice to animals lacking different components of the necroptotic pathway. Ablation of the necroptotic effector MLKL did not alter the phenotype of *Adar*$^{P195A/p150null}$ mice **(Fig 3A, Supplemental Figure 8A)**, nor did crossing them to mice in which the kinase activity of RIPK1 is absent **(Fig 3B, Supplemental Figure 8B),** indicating that prevention of canonical necroptosis alone was not sufficient to explain the effect of ZBP1 knockout in these animals.

In contrast, ablation of RIPK3 led to a significant extension of survival in *Adar*$^{P195A/p150null}$ mice **(Fig 3C)**. However, this extension of survival was partial, with approximately 1/3rd of *Adar*$^{P195A/p150null}$*::Ripk3*$^{-/-}$ animals succumbing to death within 40 days of birth, followed by slower attrition of mice over the following 200 days. *Adar*$^{P195A/p150null}$*::Ripk3*$^{-/-}$ were severely runted, in contrast to

the overtly normal phenotype observed in *Adar*$^{P195A/p150null}$*:: Zbp1*$^{-/-}$ mice **(Fig 3D)**. These findings indicate that ZBP1 can drive pathology in *Adar*$^{P195A/p150null}$ via signaling that is independent of RIPK3. Following influenza infection, ZBP1 was reported to induce RIPK3 dependent induction of both caspase-8-dependent apoptosis and MLKL-dependent necroptosis[41,42]. Nonetheless, our finding that in *Adar*$^{P195A/p150null}$ mice ablation of RIPK3 failed to fully recapitulate the reversal of pathology observed upon ablation of ZBP1 implies RIPK3-independent functions of ZBP1 when activated downstream of ADAR1 deficiency.

ZBP1 contains three confirmed RIP homotypic interaction motifs (RHIM), which bind to similar domains present in RIPK1 and RIPK3[107]. We hypothesized that in the absence of RIPK3, ZBP1 may interact with RIPK1 to scaffold and activate caspase-8 dependent apoptosis. To study this, we turned to a reductive system in which ZBP1 could be directly activated. By replacing the ZBD of ZBP1 with tandem inducible dimerization domains derived from the protein FK506, we created a form of ZBP1 that could be activated using the cell permeable small molecule B/B **(Supplemental Figure 9A)**. In wild-type LET1, SVEC or MEF cells this construct, termed "2xFV-ZBP1", triggered cell death that was blocked only with combined inhibition of RIPK3 and the caspases, consistent with induction of both apoptosis and necroptosis downstream of ZBP1 activation **(Supplemental Figure 9B-D)**. Furthermore, B/B activation of ZBP1 resulted in phosphorylation of RIPK3 and MLKL, and when ZBP1 was directly activated in *Mlkl*$^{-/-}$ MEF cells it induced robust cell death that was dependent on caspase-8 and involved cleavage of caspase-3, consistent with apoptosis **(Fig. 3E, Supplemental Figure 10A, B).** ZBP1 activation in *Ripk3*$^{-/-}$ MEF cells also induced caspase-8-dependent cell death and caspase-3 cleavage, albeit with slower kinetics than those observed in *Mlkl*$^{-/-}$ cells **(Fig. 3E,F)**. Notably, ZBP1 activation did not trigger detectable cell death in MEF cells lacking both MLKL and caspase-8, or both RIPK3 and caspase-8 **(Fig. 3E,F)**. This finding indicates that while RIPK3 can contribute to ZBP1-dependent apoptosis, ZBP1 can still drive caspase-8-dependent cell death responses in the absence of RIPK3.

Caspase-8 suppresses lethal inflammation

We reasoned that cell death dependent on ZBP1, RIPK1 and caspase-8 could underlie the pathology observed in *Adar*$^{P195A/p150null}$*::Mlkl*$^{-/-}$ and *Adar*$^{P195A/p150null}$*::Ripk3*$^{-/-}$ mice. Deletion of caspase-8 causes embryonic lethality due to unrestrained necroptosis[29], but this phenotype is reversed by co-ablation of RIPK3 or MLKL[19,29,108]. We therefore generated *Adar*$^{P195A/p150null}$*::Mlkl*$^{-/-}$*::Casp8*$^{-/-}$ and *Adar*$^{P195A/p150null}$*::Ripk3*$^{-/-}$*::Casp8*$^{-/-}$ mice to test whether ablation of caspase-8 in addition to necroptotic signaling would recapitulate the phenotypic rescue observed upon ablation of ZBP1. Unexpectedly, *Adar*$^{P195A/p150null}$*::Ripk3*$^{-/-}$*::Casp8*$^{-/-}$ mice displayed reduced weight and survival compared to *Adar*$^{P195A/p150null}$*::Ripk3*$^{-/-}$*::Casp8*$^{+/-}$ littermates **(Fig. 4A,B, Supplemental Figure 10C)**, while *Adar*$^{P195A/p150null}$*::Mlkl*$^{-/-}$*::Casp8*$^{-/-}$ mice were born at expected frequencies but uniformly failed to survive to weaning **(Fig 4C)**. Histological analysis of these animals at birth revealed broadly normal development of the liver and kidney **(Supplemental Figure 11A-C)**, but a significant increase in Iba1-positive activated microglia in the brains of *Adar*$^{P195A/p150null}$*::Mlkl*$^{-/-}$*::Casp8*$^{-/-}$ neonates, consistent with unrestrained inflammatory signaling at this site **(Supplemental Figure 11D,E)**. These findings imply that caspase-8 suppresses ZBP1 activation in *Adar*$^{P195A/p150null}$ mice, and that caspase-8 ablation may allow unrestrained ZBP1 transcriptional signaling that is independent of canonical apoptosis or necroptosis. Consistent with this possibility, co-immunoprecipitation experiments revealed recruitment of RIPK1, or of both RIPK1 and RIPK3, upon 2xFV-ZBP1 activation in *Ripk3*$^{-/-}$*::Casp8*$^{-/-}$ or *Mlkl*$^{-/-}$*::Casp8*$^{-/-}$ MEF cells, respectively, despite the lack of cell death responses observed in these conditions **(Fig 3E,F Supplemental Figure 12A,B,).** We also observed that in *Adar*$^{P195A/p150null}$*::Mlkl*$^{-/-}$ MEF cells, zVAD treatment stabilized the interaction between ZBP1 and RIPK3, again in the absence of cell death responses **(Supplemental Figure 12C)**. These findings indicate that when necroptotic effectors are absent, loss or inhibition of caspase-8 promotes interactions between ZBP1 and the RIP kinases.

We next assessed whether loss of caspase-8 potentiated transcriptional signaling induced by ADAR1 insufficiency. We observed that while siRNA-mediated depletion of ADAR1 in *Mlkl*$^{-/-}$ cells induced the expected upregulation of ISGs, ADAR1 depletion in *Mlkl*$^{-/-}$*::Casp8*$^{-/-}$ MEFs induced a distinct

transcriptional response dominated by NF-κB targets **(Fig. 4D, Supplemental Figure 13A,B)**. Since RIPK1 is a key signaling adapter upstream of NF-κB activation[109], this finding implied that ZBP1-RIPK1 signaling may underlie these transcriptional effects. Consistent with this, we observed that 2xFV-ZBP1 activation in *Mlkl*$^{-/-}$ MEF cells induced RIPK1-dependent upregulation of the NF-κB targets CCL2 and CCL7, but not of the canonical ISG IFIT1 **(Supplemental Figure 13C).** Together, these data indicate that upon ADAR1 mutation or depletion, caspase-8 acts to suppress a ZBP1- and RIPK1-dependent program of inflammatory transcription. The modest extension of survival observed in *Adar*$^{P195A/p150null}$*::Ripk3*$^{-/-}$*::Casp8*$^{-/-}$ mice relative to *Adar*$^{P195A/p150null}$*::Mlkl*$^{-/-}$*::Casp8*$^{-/-}$ animals suggests that RIPK3 can potentiate, but is not required for ZBP1- and RIPK1-dependent inflammatory signaling.

This study does not address the identity of the ligand(s) responsible for activating ZBP1 in *Adar1*$^{P195A/p150null}$ mice. Since the P195A mutation in ADAR1 lies in its ZBD, we can speculate that ADAR1^{P195A} may be attenuated in its ability bind ZBD ligands. Interestingly, aligning the ZBD sequences of ADAR1 and ZBP1, along with those present in the fish PKR homologue PKZ[63] and the vaccinia virus effector E3L[5] reveals that ZBP1 naturally contains an alanine at position 64, the site homologous to ADAR1 P195 **(Supplemental Figure 14A).** Since substitution of proline with alanine at this site in ADAR1 limits its function, we speculate that the presence of an alanine at the homologous site within ZBP1 may reflect a naturally lower affinity for ligand by ZBP1 relative to other ZBDs. This may represent a means to limit aberrant ZBP1 activation at steady state. We sought to test this idea by creating a mouse line with a "revertant" ZBP1, in which A64 is mutated to proline. However, ZBP1^{A64P} mice did not reveal evidence of increased ZBP1 activation, either when crossed to the *Adar1*$^{P195A/p150null}$ model or in response to influenza infection, but rather appeared attenuated in their signaling in both settings **(Supplemental Figure 14 B,C).** While ZBP1^{A64P} protein was properly expressed **(Supplemental Figure 14D)**, this attenuation likely reflects a disruption of protein structure induced by this mutation, and

implies that additional mutations or larger domain swaps would be needed to effectively test this hypothesis. Future studies will clarify the identity of ZBP1 ligands that emerge upon ADAR1 mutation.

Aicardi-Goutières Syndrome refers to a family of IFN-driven congenital pathologies driven by mutations in proteins involved in nucleotide sensing and regulation[81]. Since ZBP1 is strongly induced by IFN, and has been described to bind DNA as well as RNA[49], we wondered if ZBP1 and RIPK3 signaling might play a role in AGS-like pathology driven by endogenous DNA ligands. To test this, we assessed mice lacking TREX1, a DNA exonuclease whose ablation causes aberrant activation of the cGAS-STING pathway[110,111]. However, we did not observe significant amelioration of pathology or extension of survival in *Trex1*$^{-/-}$ mice when RIPK3 was ablated, unlike the partial rescue observed in *Adar1*$^{P195A/p150null}$ animals upon RIPK3 knockout **(Fig 4E, 3C)**. This suggests that engagement the ZBP1-RIP kinase pathway is a feature of dysregulated endogenous RNA, but not DNA, sensing.

The unexpected susceptibility of *Ripk3*$^{-/-}$*::Casp8*$^{-/-}$ and *Mlkl*$^{-/-}$*::Casp8*$^{-/-}$ animals to ADAR1 mutation indicates that while these animals develop normally, they are poised for hyperactive inflammatory signaling in response to ZBP1 activation. Indeed, previous studies have found that *Fadd*$^{-/-}$*::Mlkl*$^{-/-}$ mice (comparable to *Mlkl*$^{-/-}$*::Casp8*$^{-/-}$) are highly susceptible to influenza infection[41], a setting in which ZBP1 is strongly activated. While this was interpreted as indicating a requirement for functional cell death pathways for antiviral defense, our data raise the possibility that these mice succumb to overexuberant inflammatory signaling triggered by ZBP1. Notably, we did not observe engagement of pyroptotic cell death upon ZBP1 activation in cells lacking caspase-8 in combination with RIPK3 or MLKL, though our data do not rule out contribution of pyroptotic signaling to the immunopathology we observe.

Our findings identify ZBP1 as a key effector of autoinflammatory pathology induced by mutation of the Z-DNA binding domain of ADAR1. Our data also highlight the pleiotropic nature of ZBP1 signaling; while ZBP1 ablation fully rescued the pathology of the *Adar1*$^{P195A/p150null}$ model, individual deletion of the necroptotic signaling molecules MLKL or RIPK3 did not, and ablation of caspase-8 unleashed a lethal inflammatory program, apparently in the absence of ZBP1-dependent programmed cell

death. These findings are consistent with the dual functions of caspase-8 as both an inducer of cell death and a suppressor of ZBP1-dependent necroptosis and inflammation. Indeed, both the presence and the absence of caspase-8 may drive pathology in ADAR1-mutant mice. Our *in vitro* data indicate that ZBP1 activation in the absence of RIPK3 can induce caspase-8-dependent cell death, and this pathway may contribute to the pathology of $Adar1^{P195A/p150null}::Ripk3^{-/-}$ mice; conversely, additional ablation of caspase-8 in these animals exacerbates the observed pathology by instead unleashing unrestrained inflammatory signaling. Ultimately, apoptosis, necroptosis and inflammatory transcription may all contribute to the pathology of $Adar1^{P195A/p150null}$ mice, and which of these pathways is engaged upon ADAR1 mutation likely varies between tissues and cell types depending on the abundance of the pathway components as well as of regulatory proteins such as cFLIP and the IAPs. This pleiotropy also suggests that even the combined targeting of apoptosis and necroptosis using small molecule inhibitors is unlikely to reverse AGS pathology driven by ADAR1 mutation.

2.4 Materials and Methods

Mice

Mouse strains with modifications to *Zbp1-a*[106], *Zbp1-g*[51], *Adar*$^{P195A/p150null}$[96], *Mlkl*[108], *Ripk1*^{kd}[112], *Ripk1*^{mutRHIM}[66], *Ripk3*[22] and *Casp8*[29,113], *Trex1*[111] and *Ifih1*(MDA5)[76] have been previously described. *Zbp1*^{A64P} mice were generated as previously described[114], using the sgRNA target sequence CCGCCTATGCTCCATGTTGCAGG and the repair template sequence AAAACCCTCAATCAAGTCCTTTACCGCCTGAAGAAGGAGGACAGAGTGTCCTCCCCA GAGCCTCCAACATGGAGCATAGGCGGGGCTGCTTCTGGAGATGGGGCTCCTGCAATCCCTGA GAACTCCAGT. Briefly, C57BL6/J oocytes were microinjected with Cas9 complexed with sgRNA and ssDNA donor template as described, then implanted into pseudopregnant female mice. Founder pups were screened using Surveyor assay, and resulting mice were bred to homozygosity and genotyped using a Taqman probe system to detect the Zbp1A64P g>c nucleotide change using the primer sequences CCTCAATCAAGTCCTTTACC (Sense) and GACAGATTACCAAGGCTAGG (Antisense), CAGAGCCTGCAACATGGAG
(wild type probe), CAGAGCCTCCAACATGGAG (mutant probe). All mice were housed in pathogen-free facilities at the University of Washington under 12-h light– dark cycles with access to food and water ad libitum. Temperatures were set to 74 ± 2 °F with humidity of 30–70%. All animals used were cared for and used in experiments approved by the University of Washington Institutional Animal Care and Use Committee (under protocols 4298-01 and 4190-01) in an Association for Assessment and Accreditation of Laboratory Animal Care (AAALAC)-accredited facility in accordance with the Guide for the Care and Use of Laboratory Animals and applicable laws and regulations. In breeding experiments, no specific criteria were used to determine final sample size. These experiments were not randomized or blinded.

SNP typing analysis of *Zbp1*-a and *Zbp1*-g mouse strains was performed by Taconic Biosciences using the Mouse Genome Scan Panel.

Cell lines

Mouse embryonic fibroblasts were generated from E15 pups and immortalized by retroviral transduction of the SV40 Large T antigen. HEK293T, LET1 (Lung Epithelial Type-1) and MEF (Murine Embryonic Fibroblast) cells were maintained in standard conditions: D-MEM supplemented with 10% fetal bovine serum, glutamine, penicillin and streptomycin. Following isolation and immortalization, MEF lines were tested for cell death competence by stimulation with TNF/ZVAD (RIPK3/RIPK1 dependent cell death) or IAV infection (ZBP1/RIPK3 dependent).

Plasmids and lentiviral vectors and siRNA

2xFV-ZBP1 was generated by replacing the first 146 amino acids of murine ZBP1 (corresponding to the ZBD) with tandem copies of $FKBP^{F36V}$, available from Clontech. The resulting fusion gene was cloned into the Tet-based inducible expression pSLIK vector[115], and this construct was used to create lentiviral particles for transduction of target lines using standard protocols. Expression and activation of this construct was achieved by inducing 2xFV-ZBP1 expression with 1 μg/mL doxycycline for 12 hours, then treating with 100 mM "B/B homodimerizer" (Clontech). The full ADAR1-p150 isoform was cloned from mouse cDNA directly into a 'pRRL' lentiviral backbone and subsequently sequenced to confirm identity. Wild-type and mZαβ ZBP1 were subcloned from constructs previously obtained from the lab of Jason Upton into the pRRL backbone, at which point a 3xFLAG tag was added to the C-terminus.

CRISPR-Cas9-mediated deletion was achieved using a lenti-CRISPR construct created by Dr. Daniel Stetson[96], into which guide sequences listed below were inserted. These were used to create VSV-G-pseudotyped lentivirus particle, which were used to transduce target cells. Following 10-14 days of antibiotic selection, deletion of target proteins was confirmed by Western blot. The sequences of the guide RNA (gRNA) target sites are as follows, with the protospacer adjacent motif (PAM) sequence underlined: non-targeting control gRNA: Scramble gRNA: GACGGAGGCTAAGCGTCGCAA, *Zbp1* gRNA: GAGCCTGCAACATGGAGCAT, Ifih1 (MDA5) gRNA: GTGTGGGTTTGACATAGCGCG.

SiRNA experiments were carried out by transfecting cells with SMARTpool siRNA cocktails (Dharmacon Horizon Discovery) targeting ADAR1 (siGenome mouse *Adar*, Entrez Gene 56417), RIPK1 (siGenome mouse *Ripk1*, Entrez Gene 19766), or a non-targeting 'scramble' control (siGenome Non-targeting siRNA Pool #1). Transfection of siRNA was performed using the dharmaFECT 1 transfection reagent (Cat. No. T-2001-03, Horizon Discovery) according to the manufacturer's protocols.

Antibodies and inhibitors

Where indicated, the following drugs were used at the listed concentrations: 50 μM zVAD (SM Biochemicals), 100nM GSK'843 (GlaxoSmithKline).

The following antibodies were used for Western Blots and immunoprecipitations: ADAR1 (15.8.6) SantaCruz, ZBP1 (Zippy-1) AdipoGen, actin (13E5) Cell Signaling Technology, MDA5 (D74E4) Cell Signaling Technologies, p-RIPK3 (GEN135-35-9), Genentech, RIPK3 (1G6.1.4) Genentech, or RIPK3 (2283) ProSci, p-MLKL (D6E3G) Cell Signaling Technologies, MLKL (MABC604) Millipore, Caspase-3 (9662) Cell Signaling Technologies, Cleaved Capsase-3 (9661) Cell Signaling Technologies, RIPK1 (38/RIP) BD Biosciences, anti-FLAG (M2) Sigma, anti-FKBP12, Thermo Fisher (PA1-026A). Iba1 (Cat no. 019-19741) Wako-Chem, Cleaved Caspase 3 (Clone D3E9) Cell Signaling Technologies were used in immunohistochemical analysis.

The following antibodies were used for flow cytometry analysis of splenocytes: FITC anti-CD19 (clone 1D3; BD Biosciences) PerCP-Cy5.5 anti-CD3e (clone 145-2C11; BD Biosciences), PE-Cy7 anti-Ly6C (clone HK1.4; Biolegend), APC anti-F4/80 (clone BM8; eBioscience), AF700 anti-Ly6G (clone 1A8; Biolegend), APC-Cy7 anti-NK1.1 (clone PK136; BD Biosciences), BV510 anti-CD8a (clone 53-6.7; BD Biosciences); BV605 anti-CD4 (clone RM4-5; BD Biosciences), BV650 anti-CD11b (clone M1/70; Biolegend), and BUV395 anti-CD45.2 (clone 104; BD Biosciences).

Western Blots, Immunoprecipitations and IR-CLIP

WT 293T cells or 293T cells expressing FLAG-ZBP1 or FLAG-ZBP1 mZαβ were cultured in 6-well plates and were transfected with pRRL vector expressing ADAR1 p150 or empty pRRL vector using X2 transfection reagent (Mirus). At ~24 hrs post-transfection, cells were washed in PBS and crosslinked with 254 nm UV-C light (0.3 J/cm2) or left un-crosslinked, and lysed in 200 uL IP lysis buffer (25 mM Tris pH 7.5, 150 mM NaCl, 1% Triton X-100, 0.5 mM EDTA, 5 mM $MgCl_2$ + 1X protease inhibitor). Lysates were clarified by centrifugation at 5000 xg for 10 mins at 4C, and quantified by Bradford assay. A fraction of each sample was stored for input controls. 200 ug of each lysate was incubated with Protein G Dynabeads (Thermo-Fisher) pre-conjugated with 4 ug anti-FLAG M2 antibody (Sigma) in a final volume of 500 uL IP lysis buffer for 2 hrs at 4C with rotation. Beads were then washed four times with 1 mL IP lysis buffer. Beads were then boiled in 2X Laemmli buffer (Bio-Rad) + 5% beta-mercaptoethanol to eluted protein complexes. Eluates and input controls were resolved on a 4-15% TGX gel (Bio-Rad) for SDS-PAGE, transferred to PVDF membranes. Immunoblotting were performed using HRP-conjugated anti-FLAG and anti-β-Actin antibodies, and with anti-ADAR1 primary antibody and HRP-conjugated anti-mouse secondary antibody (Jackson Immunolabs).

For RIPK3 and RIPK1 immunoprecipitations, Cells were lysed in ice-cold lysis buffer (25 mM Tris-HCl pH 7.4, 150 mM NaCl, 1% v/v Triton X-100, 10% v/v glycerol, and 0.01% w/v SDS) supplemented with 1X complete Protease Inhibitor (Roche) for 30 minutes, followed by centrifugation at 1000xg for 10 minutes. Antibodies recognizing ZBP1 or FKBP12 (Invitrogen, PA1-026A) were immobilized to Dynabeads ™ Protein G (Invitrogen) as per the manufacturer's instruction, and then incubated with total cell lysates overnight at 4ºC. Immunoprecipitates were eluted in Laemmli sample buffer (63 mM Tris-HCl, pH 8.0, 10% v/v glycerol, 2% w/v SDS, 0.01% w/v bromophenol blue, 2.5% v/v 2-mercaptoethanol) at 95ºC for 10 minutes.

We performed irCLIP as described by Zarnegar et al.[116] with slight modifications. Wild-type 293T cells or 293T cells stably expressing FLAG-ZBP1 or FLAG-ZBP1 mZαβ were cultured in 6-well plates. Cells were washed with PBS, crosslinked with 254 nm UV-C light (0.3 J/cm2), and lysed in 200 uL irCLIP lysis buffer (50 mM Tris pH 7.5, 150 mM NaCl, 1 mM EDTA, 1% Triton X-100, 0.1% SDS,

1X protease inhibitor). After sonication in ice slurry, lysates were clarified by centrifugation at 5000 x g for 10 mins at 4C, and quantified by Bradford assay (Bio-Rad). A fraction of each sample was stored for input controls. 200 ug of each lysate was incubated with Protein G Dynabeads (Thermo-Fisher) pre-conjugated with 4 ug anti-FLAG M2 antibody (Sigma) in a final volume of 500 uL irCLIP lysis buffer for 2 hrs at 4C with rotation. The beads were then sequentially washed with the following ice-cold buffers: once with 1 mL irCLIP lysis buffer, once with 1 mL high stringency buffer (20 mM Tris pH 7.5, 120 mM NaCl, 25 mM KCl, 5 mM EDTA, 1% Triton X-100, 1% NaDOC, 0.1% SDS), once with 1 mL high salt buffer (20 mM Tris pH 7.5, 500 mM NaCl, 5 mM EDTA, 1% Triton X-100, 1% NaDOC), once with with 1 mL low salt buffer (20 mM Tris pH 7.5, 5 mM NaCl, 5 mM EDTA, 1% Triton X-100), and twice with 0.5 mL NT2 buffer (50 mM Tris pH 7.5, 150 mM NaCl, 1 mM $MgCl^2$, 0.05% NP-40). Beads were then resuspended in 30 uL NT2 buffer containing 25 ng/mL RNase A (Thermo-Fisher) and 15% PEG400 (Sigma) for on-bead RNase digestion at 30C for 15 mins with shaking (1200 rpm) in a Thermomixer. RNase digestion was quenched by the addition of 0.5 mL high stringency buffer. Beads were washed twice with 0.3 mL PNK wash buffer (50 mM Tris pH 7.0, 10 mM MgCl2), and then resuspended in 30 uL PNK dephosphorylation mix (1X PNK buffer (Promega), 0.5 uL RNaseIN (Promega), 1 uL T4 PNK (Promega), 4 uL PEG400) . Dephosphorylation reactions were conducted at 37C for 60 mins with shaking (1200 rpm) in a Thermomixer. Dephosphorylation mix was removed and beads were washed with 0.25 mL PNK wash buffer. For ligation of IR-Dye conjugated oligo to RNA crosslinked to protein, beads were resuspended in 30 uL RNA ligation mix (1X RNA ligase I buffer (NEB), 1 uL RNA ligase I (NEB), 1 uL IR-Dye-labeled oligo (cite: PMID: 27111506), 5 uL PEG400, and 0.5 uL RNaseIN) and incubated for 16 hrs at 16C with shaking in Thermomixer (1200 rpm). Ligation mix was then removed and beads were washed twice with 0.25 mL PNK wash buffer, prior to elution of RNA-protein complexes in 20 uL 1X LDS Buffer (Thermo-Fisher) + 10% beta-mercaptoethanol at 80C for 10 mins. 5 uL of eluates, as well as input controls, were then resolved by SDS-PAGE on 4-12% Bis-Tris NuPAGE gels (Thermo-Fisher), and transferred to nitrocellulose membranes. Fluorescent RNA-protein complexes in the eluates were visualized on a LiCOR Odyssey FC imager.

Flow Cytometry

Splenocytes were blocked with Fc block (BD Biosciences) in PBS + 2% heat inactivated FBS for 10 minutes at 4 degrees prior to cell surface staining by subsequent addition of a pre-mixed antibody cocktail. Cells were incubated with fluorescently labeled antibodies, each at a dilution of 1:200 for 30 minutes at 4 degrees, washed, and fixed with 2% paraformaldehyde in PBS for 10 minutes. Data were acquired on a BD FACSymphony A3 Cell Analyzer and using the BD Diva acquisition software (version 9.0) analyzed using FlowJo (Tree Star, version 10.8.1).

Cell death analysis

Cell death was measured using an IncuCyte imaging system, as described previously[117]. Briefly, cells were imaged in the presence of the cell impermeable DNA intercalator Sytox Green (Thermo Fisher, R37168), and Sytox positive cells quantified at each timepoint using custom processing definitions, available upon request. In parallel, separate cells plated in identical numbers were treated with the cell permeable dye Syto Green (Thermo Fisher, S34854) and quantified using the same approach, and percent cell death was calculated as $Sytox^{+}/Syto^{+}$ at each timepoint. For siRNA knockdown cell death assays, to avoid excessive non-specific toxicity, cells were transfected with siRNA for 8 hours, at which point cells (adherent) were washed and dye/inhibitors were added at final concentrations just prior to IncuCyte imaging.

Pathology

Pathology analysis for the *Adar*$^{P195A/p150null}$*:: Zbp1* experiments (Supplemental Figure 2) was performed by the same personnel and using a similar scoring system recently described for analysis of *Adar*$^{P195A/p150null}$ mice[96]. Briefly, littermate mice 21 days of age were euthanized via CO_2 asphyxiation and livers and kidneys were harvested and washed in PBS and fixed in 10% neutral buffered formalin. Tissues were embedded in paraffin and cut into ~4mm sections for hematoxylin and eosin (HE) staining.

Additionally, liver and kidney sections were periodic acid-Schiff (PAS) stained. Slides were evaluated by a board-certified veterinary pathologist, who was blinded to genotype and experimental setup. For kidney, expansion of the glomerular mesangial matrix was scored from 0-4, with 0=normal, 1=minimal, 2=mild, 3=moderate, and 4=severe. For the liver, microvesicular and lesser macrovesicular cytoplasmic vacuolation were scored from 0-5, with 0 = normal; 1 = minimal changes affecting only a small region (< 5%) of the liver; 2 = mild changes throughout the liver but without enlargement of hepatocytes, coalescing lesions, or necrosis; 3 = mild to moderate cytoplasmic vacuolation throughout liver with enlargement of hepatocytes but no necrosis or loss of parenchyma; 4 = moderate, coalescing throughout liver with multifocal mild regions of loss of parenchyma or necrosis; and 5 = severe with moderate multifocal regions of cavitation and necrosis.

Tissues for the *Adar*$^{P195A/p150null}$*::Mlkl*$^{-/-}$*::Casp8*$^{-/-}$ experiments (Supplemental Figure 11) were collected from pups euthanized by decapitation on the day of birth, and spleen, kidney, liver, heart, head with brain, and gastrointestinal tract were routinely paraffin embedded and HE stained. PAS stains were also obtained for liver and kidney. These slides were reviewed blindly, with the exception of gastrointestinal tissues, for which the pathologist was not blinded to genotype.

Representative images were captured from scanned slides or from glass slides taken using NIS-Elements BR 3.2 64-bit and plated in Adobe Photoshop. Image white balance, lighting, and contrast were adjusted using auto corrections applied to the entire image. Original magnification is stated.

Iba1 and Cleaved Caspase-3 analysis for Mlkl::Casp8::Adar$^{p150/P195A}$ pups was performed through the University of Washington Histology and Imaging Core (UW-HIC) utilizing the Leica Bond Rx Automated Immunostainer (Leica Microsystems, Buffalo Grove, IL), Slides were deparaffinized with Leica Dewax solution at 72°C for 30 seconds. Antigen retrieval was performed on all slides with EDTA, pH 9, at 100°C for 20 minutes. All subsequent steps were performed at room temperature. Initial blocking consisted of 10% normal goat serum (Jackson ImmunoResearch, cat no. 005-000-121) in tris-buffered saline for 20 minutes and Additional blocking with Leica Bond Peroxide Block for 5 minutes. Slides were incubated with Iba1 (1:1000) or CC3 (1:250) primary antibodies in Leica Primary Antibody Diluent.

Slides were scanned in brightfield with a 20X objective using a NanoZoomer Digital Pathology System (Hamamatsu City, Japan). CC3 and Iba1 quantification was performed using the Visiopharm Image Analysis module.

Quantitative PCR analysis

RNA was isolated from primary MEFs or LET1s using Trizol extraction and first strand cDNA synthesis was performed with SuperScript III Reverse Transcriptase (Invitrogen, Cat. No. 18080044). QPCR was performed using a ViiA 7 Real Time PCR System (Thermo Fischer Scientific) using SYBR reagents (Thermo Fisher) The following primers were used for QPCR: *Zbp1*, S: AAGAGTCCCCTGCGATTATTTG, AS: TCTGGATGGCGTTTGAATTGG , *Ripk1*, S: GAAGACAGACCTAGACAGCGG, AS: CCAGTAGCTTCACCACTCGAC, *Ccl2*, S: TGGCTCAGCCAGATGCAGT, AS: TTGGGATCATCTTGCTGGTG, *Ccl7*, S: CCACATGCTGCTATGTCAAGA, AS: ACACCGACTACTGGTGATCCT, *Ifit1*, S: GCCATTCAACTGTCTCCTG, AS: GCTCTGTCTGTGTCATATACC, *Ifnb*, S: CTGGAGCAGCTGAATGGAAAG, AS: CTTCTCCGTCATCTCCATAGGG, *Gapdh*, S: GGCAAATTCAACGGCACAGT, AS: AGATGGTGATGGGCTTCCC.

RNA-seq and Nanostring analysis

For RNAseq and Nanostring experiments, RNA was isolated from day 23 spleens (RNAseq) or treated cells using Trizol. An on-column DNAse treatment was included for RNAseq experiments. Total RNA was added directly to lysis buffer from the SMART-Seq v4 Ultra Low Input RNA Kit for Sequencing (Takara), and reverse transcription was performed followed by PCR amplification to generate full-length amplified cDNA. Sequencing libraries were constructed using the NexteraXT DNA sample preparation kit (Illumina) to generate Illumina-compatible barcoded libraries. Libraries were pooled and quantified using a Qubit Fluorometer (Life Technologies). Dual-index, single-read sequencing of pooled

libraries was carried out on a HiSeq2500 sequencer (Illumina) with 58-base reads, using HiSeq v4 Cluster and SBS kits (Illumina) with a target depth of 10 million reads per sample.

For Nanostring, two hundred fifty-four transcripts were quantified from total RNA using the mouse nCounter Inflammation V2 panel (Nanostring). The nSolver Analysis Software 4.0 with the nCounter Advanced Analyses package (Version 2.0.134) was used to normalize the data and perform differential gene expression analysis to generate log2-fold-change values and p-values. Data visualizations were carried out in R (version 4.1.1). Differentially expressed genes were visualized as heatmaps and volcano plots using the packages "pheatmap" (version 1.0.12), and "ggplot2" (version 3.3.5).

For RNA seq analysis of day 23 spleens, reads were aligned using kallisto[118] to the mouse reference genome (GRCm39) using default parameters. Quality control was performed on raw reads using fastqc and then combined with aligned reads using multiqc[119], with no samples removed from the final dataset due to QC checks. Analysis of aligned read was performed with R using DESeq2[120] using standard parameters to generate differential gene expressions for each of the conditions against wild type, and significant differential expression was defined by adjust P-value < 0.01 and absolute log2 fold change > 1. The differential expression data was annotated using the bioMaRt package[121,122]. Fold changes against wild-type between ADAR1 deficient (*Adar*$^{P195A/p150null}$), with and without Zbp1-a knockout were compared, defining high recovery genes as those with a >50% regression to a fold change of 0 after Zbp1-a knockout and as low recovery otherwise. Gene ontology analysis was performed using the clusterProfiler package[123] using standard parameters comparing both high and low recovery genes against background separately.

Statistical analysis

Comparison of survival cures was done using a Log-rank (Mantel-Cox) test. P values less than 0.0001 were a result of the statistical analysis package and are represented as ">0.0001". Data shown in

graphs are mean or mean ± SD. If the data fulfilled the criteria for Gaussian distribution tested by column statistics, an unpaired parametric *t*-test with Welch's correction was performed for statistical analysis. All statistical tests listed in the figure legends were two-sided and were performed using Graphpad Prism, or Microsoft Excel (Chi-Square Power values for mendelian distributions). *P* values are presented in the figure or figure legends. All *in vitro* experiments, unless otherwise stated were independently replicated a minimum of two times, and details on replication of displayed data is stated in the figure legends.

Data and code availability

The R analysis was performed using publicly available code, described above; Custom R scripts are available on https://github.com/OberstLab/Hubbard-et-al-2022-Nature. RNAseq and Nanostring data are available via the NIH Gene Expression Omnibus, accession numbers GSE200854 (RNAseq) and GSE200985 and GSE200986 (NanoString).

Acknowledgements:

This work is supported by grants R01 AI153246 (to AO and DBS), R01 CA228098 (to AO), R01 AI084914 (to DBS), R01 AI143227 and R01 AI147177 (to RS), by the Titus Fellowship (to NWH), T32 T32AR7108-41 (to JMA), and by the Helen Hay Whitney Foundation award (to NSG). Supplemental figure 10A was created using Biorender.com. The authors thank Dr. Pooja Jain, Isabel Silva and Ricky Lee for technical assistance.

Author Contributions:

Conceptualization: NWH, MM, DBS, AO; Methodology: NWH, MM, RS, LHC, NSG, DBS, AO; Analysis: NWH (all), JMA (Nanostring data), KS (RNAseq data analysis), JMS (histopathological analysis and scoring), AO; Investigation: NWH (all), JMA (Nanostring, tissue culture and cell death assays), NSG (Fig. S1 co-IPs), LHC (tissue culture, Western blot and co-IP), KL (flow cytometry), MW

(RIPK3/TREX1 cross); Resources: RS, DBS, AO; Writing-Original draft: NWH, AO; Writing-review and editing: All authors.

2.5 Acknowledgements

This work is supported by grants R01 AI153246 (to AO and DBS), R01 CA228098 (to AO), R01 AI084914 (to DBS), R01 AI143227 and R01 AI147177 (to RS), by the Titus Fellowship (to NWH), T32 T32AR7108-41 (to JMA), and by the Helen Hay Whitney Foundation award (to NSG). Supplemental figure 10A was created using Biorender.com. The authors thank Dr. Pooja Jain, Isabel Silva and Ricky Lee for technical assistance.

Author contributions:

Conceptualization: NWH, MM, DBS, AO; Methodology: NWH, MM, RS, LHC, NSG, DBS, AO; Analysis: NWH (all), JMA (Nanostring data), KS (RNAseq data analysis), JMS (histopathological analysis and scoring), AO; Investigation: NWH (all), JMA (Nanostring, tissue culture and cell death assays), NSG (Fig. S1 co-IPs), LHC (tissue culture, Western blot and co-IP), KL (flow cytometry), MW (RIPK3/TREX1 cross); Resources: RS, DBS, AO; Writing-Original draft: NWH, AO; Writing-review and editing: All authors.

2.6 Figures

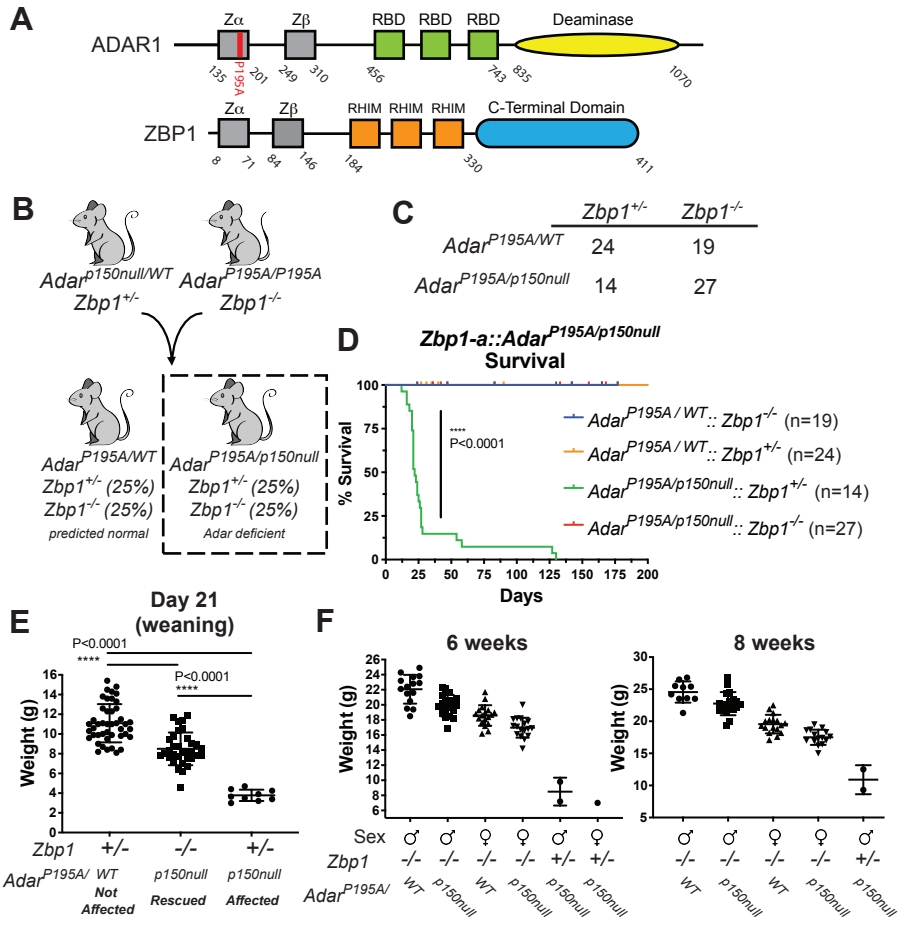

<u>Figure 1</u>: Immunopathology in ADAR1-mutant mice is driven by ZBP1. **A**: Schematic of ADAR1 and ZBP1. Zα and Zβ, Z-DNA Binding Domains; RBD, RNA binding domain; RHIM, RIP homotypic interaction motif **B-D**: Parental and expected offspring genotypes **(B),** observed genotypes **(C)** and percent survival for each genotype produced **(D)** by the cross of *Adar*$^{p150null/WT}$*::Zbp1-a*$^{+/-}$ mice to *Adar*$^{P195A/P195A}$*::Zbp1-a*$^{-/-}$ mice. **E-F**: Observed weights for mice of indicated genotypes at 3 **(E),** 6 or 8 **(F)** weeks of age. Survival curves in **D** represent littermates across 18 litters, *Adar*$^{P195A\,/\,WT}$*:: Zbp1*$^{-/-}$ (n=19), *Adar*$^{P195A\,/\,WT}$*:: Zbp1*$^{+/-}$ (n=24), *Adar*$^{P195A/p150null}$*:: Zbp1*$^{+/-}$ (n=14), *Adar*$^{P195A/p150null}$*:: Zbp1*$^{-/-}$ (n=27). **** = $p \leq 0.0001$ (Log-Rank Mantel Cox). Litter weights: *Adar*$^{P195A/WT}$*:: Zbp1*$^{+/+}$ (n=17), *Adar*$^{P195A/p150null}$*:: Zbp1*$^{+/+}$

(n=18), $Adar^{P195A/p150null}$:: $Zbp1^{+/+}$ (n=5). **** = $p \leq 0.0001$, unpaired t test, two-tailed. 6 week weights, from left to right n = 15, 19, 18, 17, 2, 1. 8 week weights, from left to right n = 10, 18, 17, 15, 2. Whisker bars (1E,F) are presented as mean +/- SD.

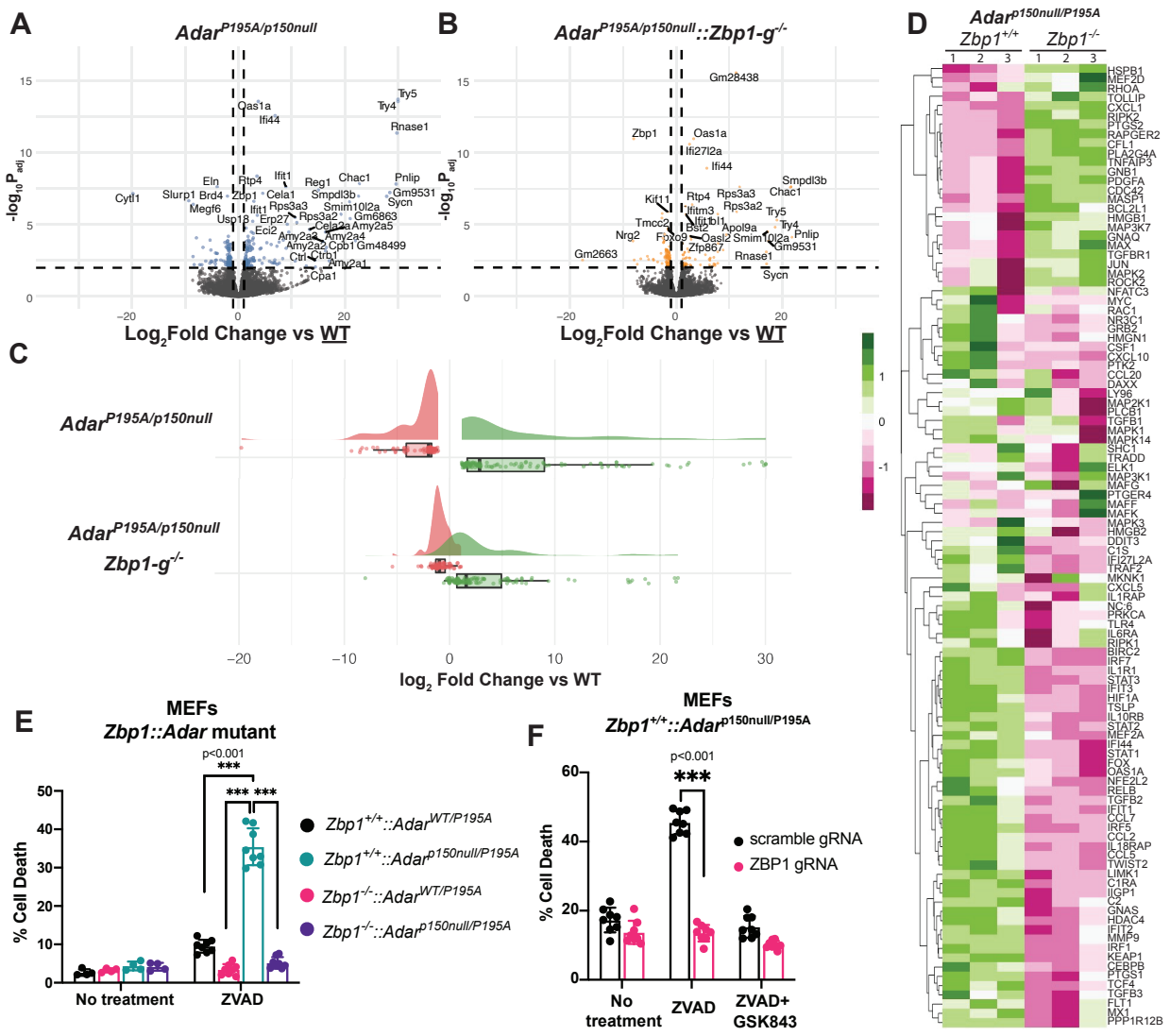

Figure 2: **The inflammatory program initiated by ADAR1 mutation remains intact upon ZBP1 knockout.** **A-B**: Volcano plots depicting differential expression of genes detected by RNA sequencing of whole spleen tissue derived from 23 day old mice of the genotypes **(A)** *Adar*$^{P195A/p150null}$ (affected) n=4 or **(B)** *Adar*$^{P195A/p150null}$*::Zbp1-g*$^{-/-}$ (rescued) n=5, in each case compared to spleens derived from wild-type pups (n=4). **C:** Raincloud plots of affected (n=4) and ZBP1 (n=5) rescued animals depicting the statistically significant up- and down-regulated ADAR signature identified in **A.** in. ADAR1 signature was identified from the differential analysis of ADAR vs WT from genes with a $\log_2$ fold change > 1 and adjusted p-value < 0.01. **D.**

Heatmap analysis of differential gene expression from Nanostring analysis of wild-type vs. *Zbp1*$^{-/-}$ ADAR mutant MEFs. **E-F.** Cell death, as measured by loss of plasma membrane integrity using an IncuCyte imager, of *Adar* mutant MEFs after 8 hour ZVAD treatment on **(E)** *Adar*::*Zbp1* mutant MEFs (genetic knockout/mutants) or **(F)** *Adar* mutant MEFs with CRISPR-Cas9 knockout of ZBP1. Each experimental group (bar) contains n=8 biologic replicates (8 wells). Statistical significance determined by unpaired student t-tests, two-tailed. Incucyte analyses (E and F) are single representatives of independently duplicated experiments. Whisker bars (2E,F) are presented as mean +/- SD.

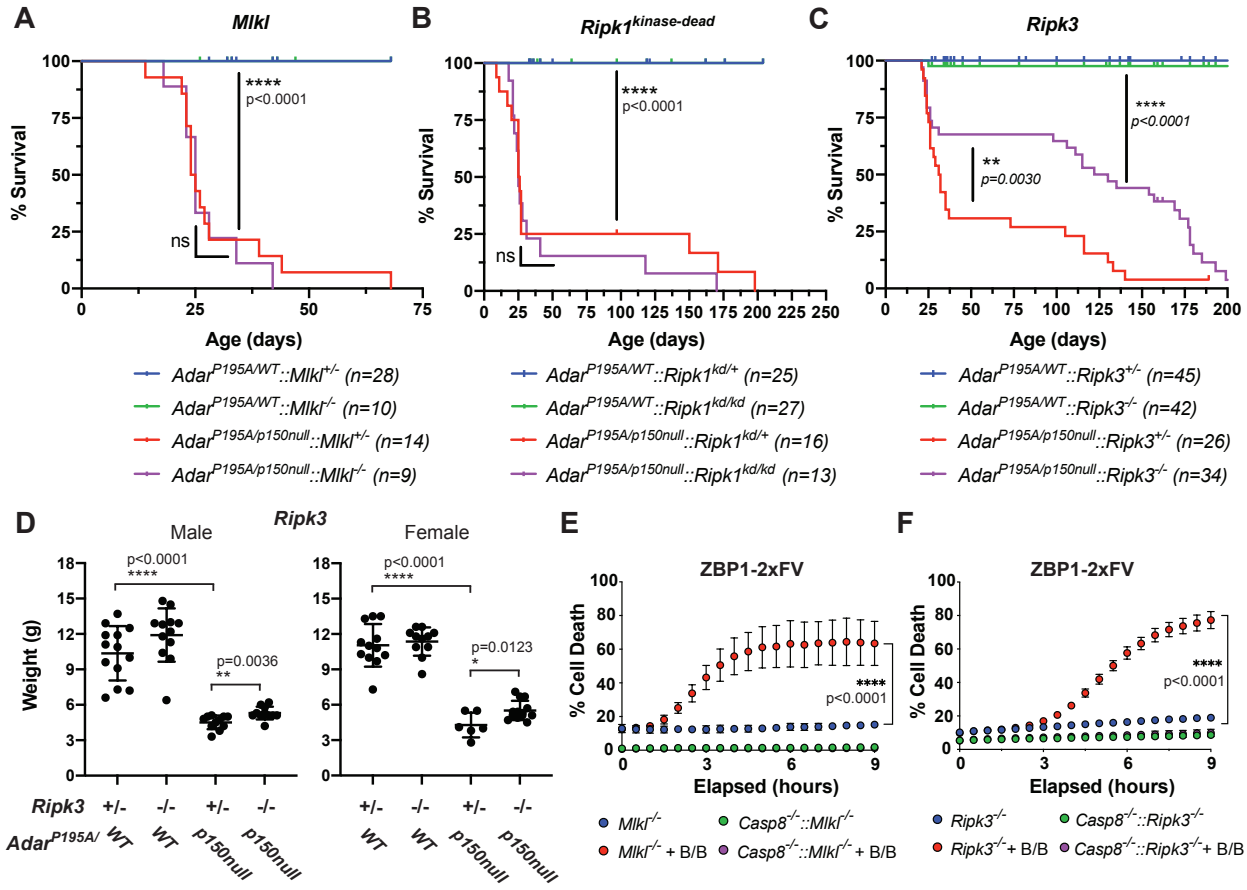

<u>Figure 3</u>: ZBP1-induced necroptosis does not underlie immunopathology induced by ADAR1 mutation. A-C: Survival proportions for *Adar*$^{P195A/p150null}$ mice crossed to animals lacking MLKL **(A)**, carrying a point mutation abrogating the kinase activity of RIPK1 (*Ripk1*^{kd}) **(B)** or lacking RIPK3 **(C).** In each case, the result of a breeding scheme analogous to that depicted in Fig. 1B is shown. Survival proportions (**A-C**) represent littermates from 9 (A, *Mlkl*), 10 (B, *Ripk1*^{kd}) or 18 (C, *Ripk3)* litters; *Adar*$^{P195A\,/\,WT}$*:: Mlkl*$^{+/-}$ (n=28), *Adar*$^{P195A\,/\,WT}$*:: Mlkl*$^{-/-}$ (n=10), *Adar*$^{P195A/p150null}$*:: Mlkl*$^{+/-}$ (n=14), *Adar*$^{P195A/p150null}$*:: Mlkl*$^{-/-}$ (n=9). *Adar*$^{P195A\,/\,WT}$*:: Ripk1*$^{kd/+}$ (n=25), *Adar*$^{P195A\,/\,WT}$*:: Ripk1*$^{kd/kd}$ (n=27), *Adar*$^{P195A/p150null}$*:: Ripk1*$^{kd/+}$ (n=16), *Adar*$^{P195A/p150null}$*:: Ripk1*$^{kd/kd}$ (n=13). *Adar*$^{P195A\,/\,WT}$*:: Ripk3*$^{+/-}$ (n=45), *Adar*$^{P195A\,/\,WT}$*:: Ripk3*$^{-/-}$

(n=42), *Adar*$^{P195A/p150null}$*:: Ripk3*$^{+/-}$ (n=26), *Adar*$^{P195A/p150null}$*:: Ripk3*$^{-/-}$ (n=34). Survival statistics determined by Log-Rank (Mantel-Cox) test, exact p values indicated on curves. **D:** Weights of male or female Ripk3$^{-/-}$ mice, observed at 21 days after birth. Litter weights: *Adar*$^{P195A/WT}$*:: Ripk3*$^{+/-}$ (m/f n=13/12), *Adar*$^{P195A/WT}$*:: Ripk3*$^{-/-}$ (m/f n=12/11), *Adar*$^{P195A/p150null}$*:: Ripk3*$^{-/-}$ (m/f n=11/6), *Adar*$^{P195A/p150null}$*:: Ripk3*$^{+/-}$ (m/f n=11/13). Statistical differences determined by individual unpaired t tests (two-tailed), exact p values indicated on plots. **E-F:** Cell death, as measured by loss of plasma membrane integrity, observed in MEFs from **(E)** *Mlkl*$^{-/-}$ and *Mlkl*$^{-/-}$*::Casp8*$^{-/-}$ (n=3 for each group) and **(F)** *Ripk3*$^{-/-}$ and *Ripk3*$^{-/-}$*::Casp8*$^{-/-}$ (n=4 for each group) genotypes stably expressing 2xFV-ZBP1, following treatment with the activating drug B/B. E and F are representative of three independently replicated experiments. Whisker bars (3D-F) are presented as mean +/- SD.

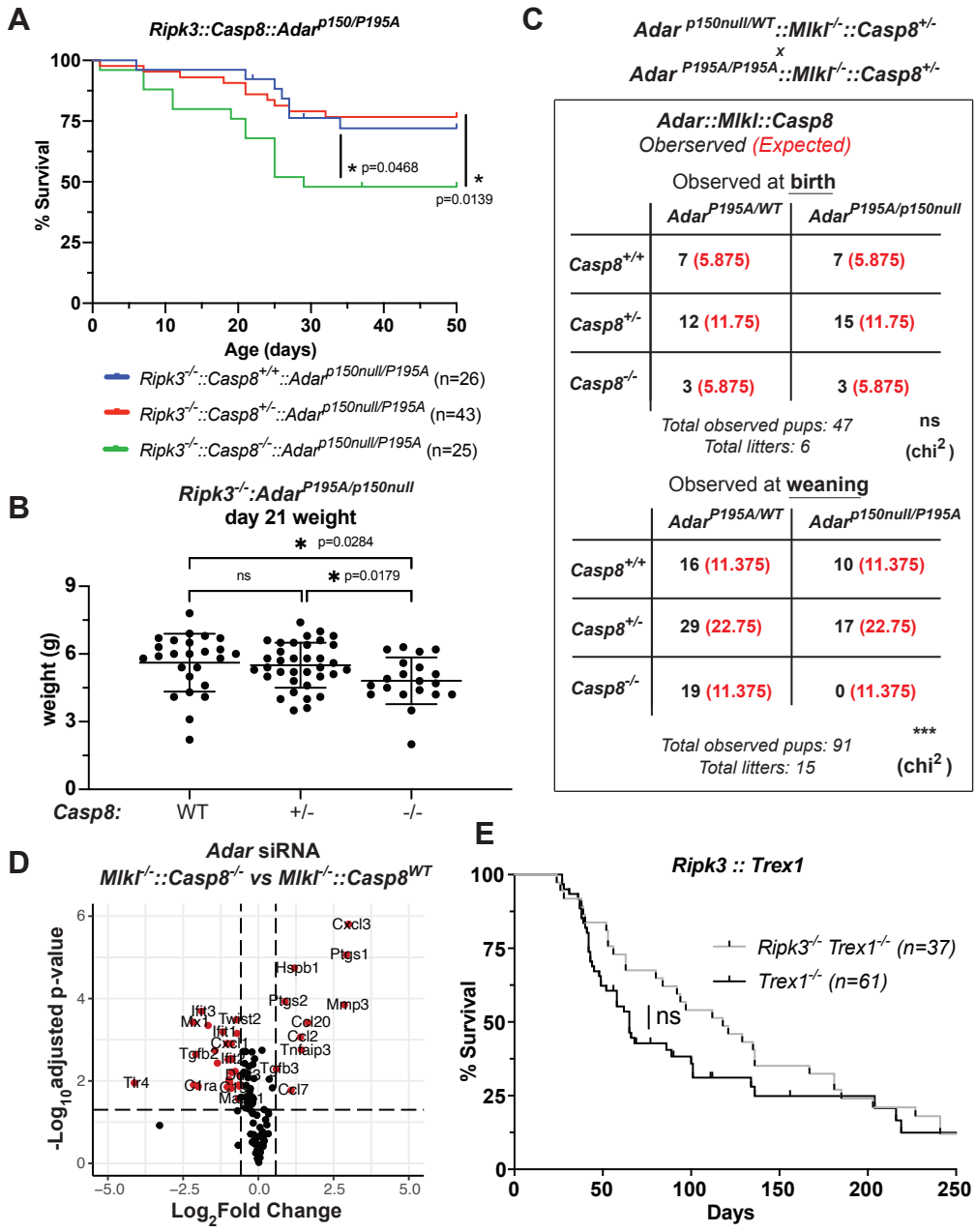

Figure 4: Caspase-8 suppresses lethal inflammatory signaling in ADAR1-mutant mice. A-B: *Ripk3*$^{-/-}$*::Casp8*$^{-/-}$*::Adar*$^{P195A/p150null}$ cross **(A)** survival and **(B)** weight at weaning (d.21). **A:** Log-rank (Mantel-Cox) statistical test performed on survival curves for survival to day 50 between Ripk3$^{-/-}$::Adar^{p150nullP195A} littermates (Adar$^{P195A/WT}$ mice excluded from comparison) which were Casp8$^{+/+}$ (n=26), Casp8$^{+/-}$ (n=43) and Casp8$^{-/-}$ (n=25) showed a significant decrease

in survival proportion of $Casp8^{-/-}$ mice compared to $Casp8^{+/+}$ (p=0.0468) and $Casp8^{+/-}$ (p=0.0139) mice. **B:** Difference between $Casp8^{+/+}$ and $Casp8^{+/-}$ was not significant. Individual student t-tests performed on affected mouse weights (*Adar*$^{p150null/P195A}$) show a statistically significant decrease in $Casp8^{-/-}$ (n=20) compared to $Casp8^{+/+}$ (n=25), p=0.0284 and $Casp8^{+/-}$ (n=35), p=0.0179 mice. **C:** Observed (black) and expected (red) mice from *Mlkl*$^{-/-}$*::Casp8*$^{-/-}$*::Adar*$^{P195A/p150null}$ cross at birth (day 0) and at weaning (day 21)**.** Chi square power analysis was performed on observed:expected frequencies at birth (not significant) and weaning (p=0.000596**). **D**: Volcano plots showing differential gene expression from Nanostring analysis of MEF cells derived from *Mlkl*$^{-/-}$ or *Mlkl*$^{-/-}$*::Casp8*$^{-/-}$ embryos, following siRNA-mediated depletion of ADAR1.

E. Survival proportions for *Trex1*$^{-/-}$ *(n=61)* or *Trex1*$^{-/-}$*::Ripk3*$^{-/-}$ *(n=37)* mice. Not significant (Mantel-Cox Log-Rank). Whisker bars (4B) are presented as mean +/- SD.

2.7 Supplemental Figures

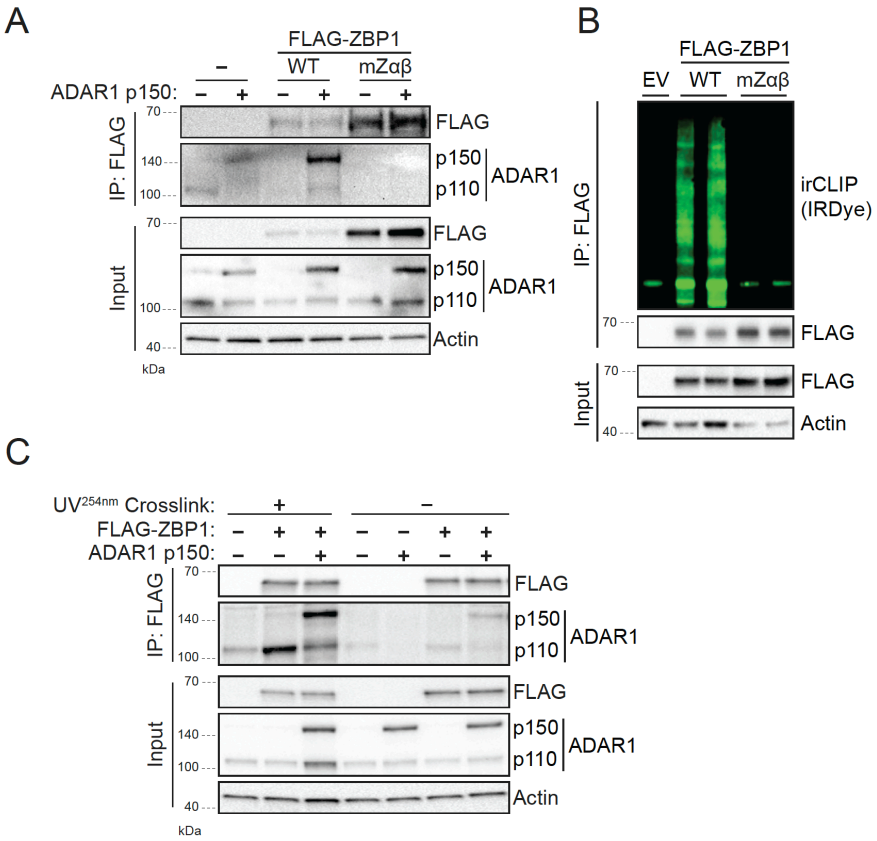

<u>Supplemental Figure 1</u>: Interaction of ZBP1 with RNA and ADAR1. A. Co-precipitation ADAR1 with WT or mutant Zαβ (mZαβ) Flag-tagged ZBP1 (FLAG-ZBP1) after FLAG immunoprecipitation. **B.** Immunoprecipitation and IR-CLIP analysis for RNA binding by of WT or mZαβ FLAG-ZBP1. **C.** Co-precipitation of ADAR1 and FLAG-tagged ZBP1 after UV-crosslinking. These experiments were performed in HEK293T cells.

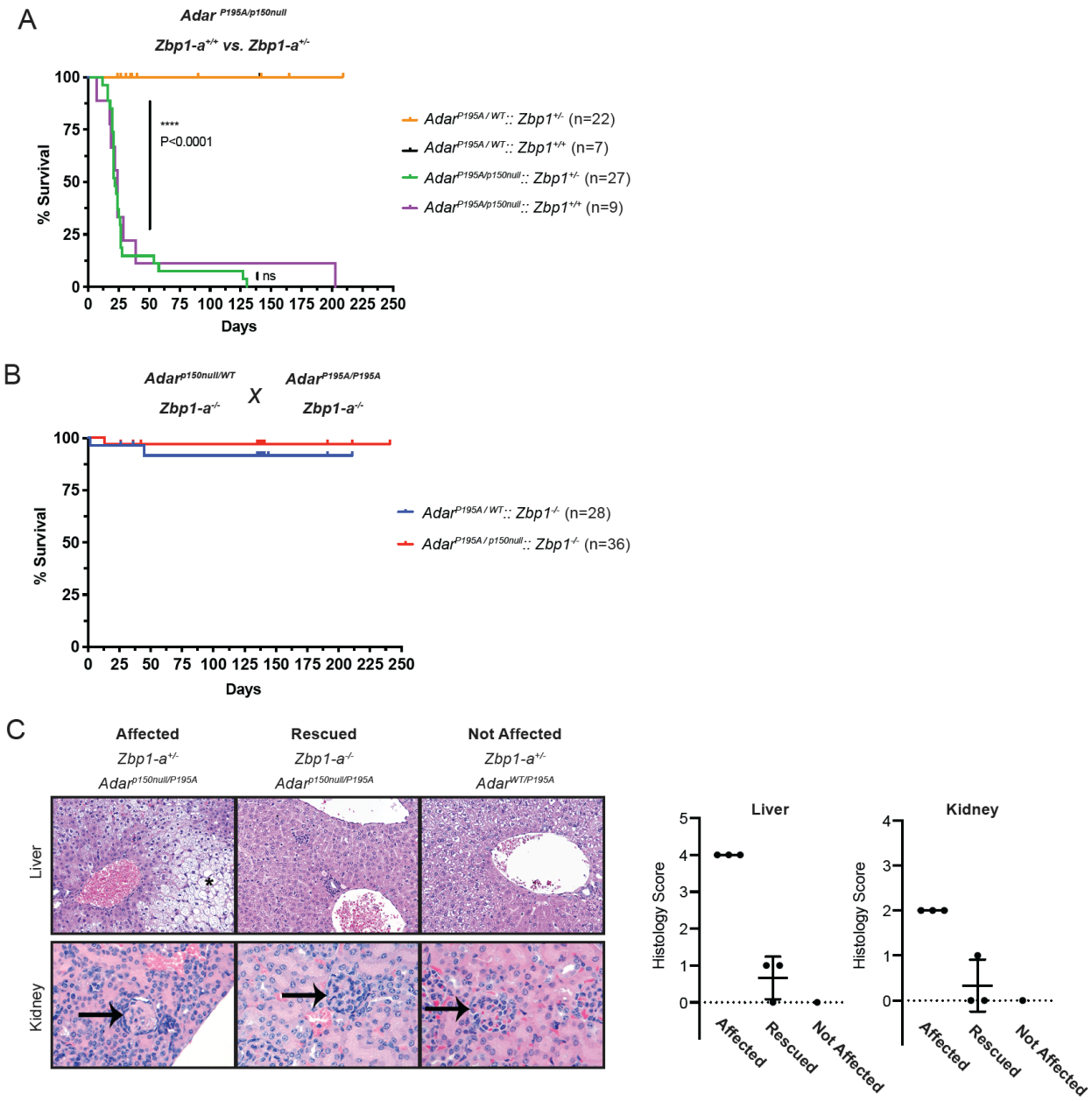

<u>Supplemental Figure 2</u>: Immunopathology in ADAR-mutant mice is ZBP1 dependent.

Survival proportions observed upon cross of *Adar*$^{p150null/WT}$*::Zbp1-a*$^{+/-}$ mice to *Adar*$^{P195A/P195A}$*::Zbp1-*$^{+/-}$, **** p<0.0001 (Mantel-Cox Log-Rank test) **(A)** or *Adar*$^{p150null/WT}$*::Zbp1-a*$^{-/-}$ mice to *Adar*$^{P195A/P195A}$*::Zbp1-a*$^{-/-}$, not significant (Mantel-Cox Log-Rank test) **(B). (C)** Histopathological analysis of liver and kidney from affected, rescued and unaffected mice (genotypes indicated.) For liver samples, regions of cytoplasmic vacuolation

indicated with asterisk. Original magnification 20x, HE staining. For kidney, glomeruli are indicated with arrows, from original magnification 40x HE staining.

A

Genotype	% C57BL/6J
ZBP1-a$^{-/-}$::ADAR$^{p150null/+}$	92.56 %
ZBP1-a$^{-/-}$::ADAR$^{p150null/+}$	85.35 %
ZBP1-a$^{-/-}$::ADAR$^{P195A/P195A}$	92.03 %
ZBP1-a$^{-/-}$::ADAR$^{P195A/P195A}$	90.36 %
ZBP1-a$^{-/-}$::ADAR$^{p150null/P195A}$	91.59 %
ZBP1-a$^{-/-}$::ADAR$^{p150null/P195A}$	92.15 %
ZBP1-a$^{-/-}$::ADAR$^{p150null/P195A}$	91.27 %
ZBP1-a$^{-/-}$::ADAR$^{p150null/P195A}$	89.31 %
Control C57BL/6J	100.0 %
ZBP1-a$^{-/-}$	84.29 %
ZBP1-a$^{-/-}$	85.32 %

B

Genotype	% C57BL/6J
ZBP1-g$^{-/-}$::ADAR$^{p150null/P195A}$	98.38 %
ZBP1-g$^{-/-}$::ADAR$^{p150null/P195A}$	98.16 %
ZBP1-g$^{-/-}$::ADAR$^{P195A/P195A}$	98.13 %
ZBP1-g$^{-/-}$::ADAR$^{P195A/P195A}$	98.21 %

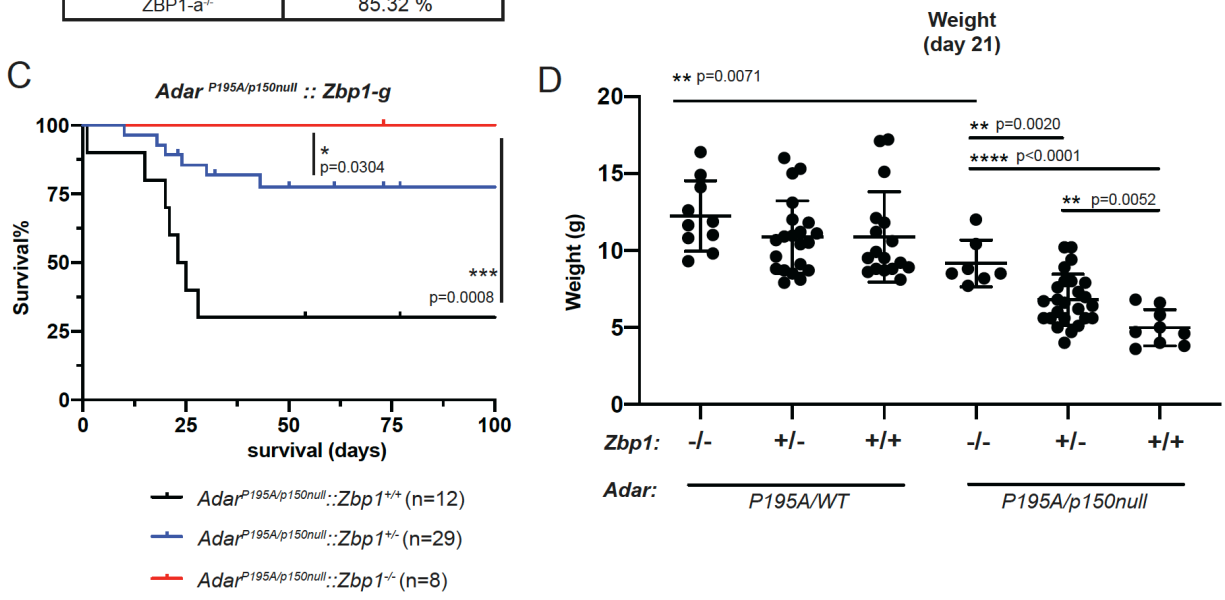

<u>Supplemental Figure 3</u>: Cross of *Adar*$^{P195A/p150null}$ mice to a separately derived, fully congenic *Zbp1*$^{-/-}$*-g* strain. A-B. SNP typing analysis of ZBP1-g **(A)** and ZBP1-a **(B)** mice. **C-D.** *Zbp1*$^{-/-}$*-g::Adar*$^{P195A/p150null}$ survival proportions**(C)** and observed weight **(D)** at 21 days (weaning). Combined male & female, Zbp1$^{+/+}$::Adar$^{P195A/WT}$ (n=17), Zbp1$^{+/-}$::Adar$^{P195A/WT}$ (n=21), Zbp1$^{-/-}$::Adar$^{P195A/WT}$ (n=10), Zbp1$^{+/+}$::Adar$^{P195A/p150null}$ (n=9), Zbp1$^{+/-}$::Adar$^{P195A/WT}$ (n=25), Zbp1$^{-/-}$::Adar$^{P195A/WT}$ (n=7).

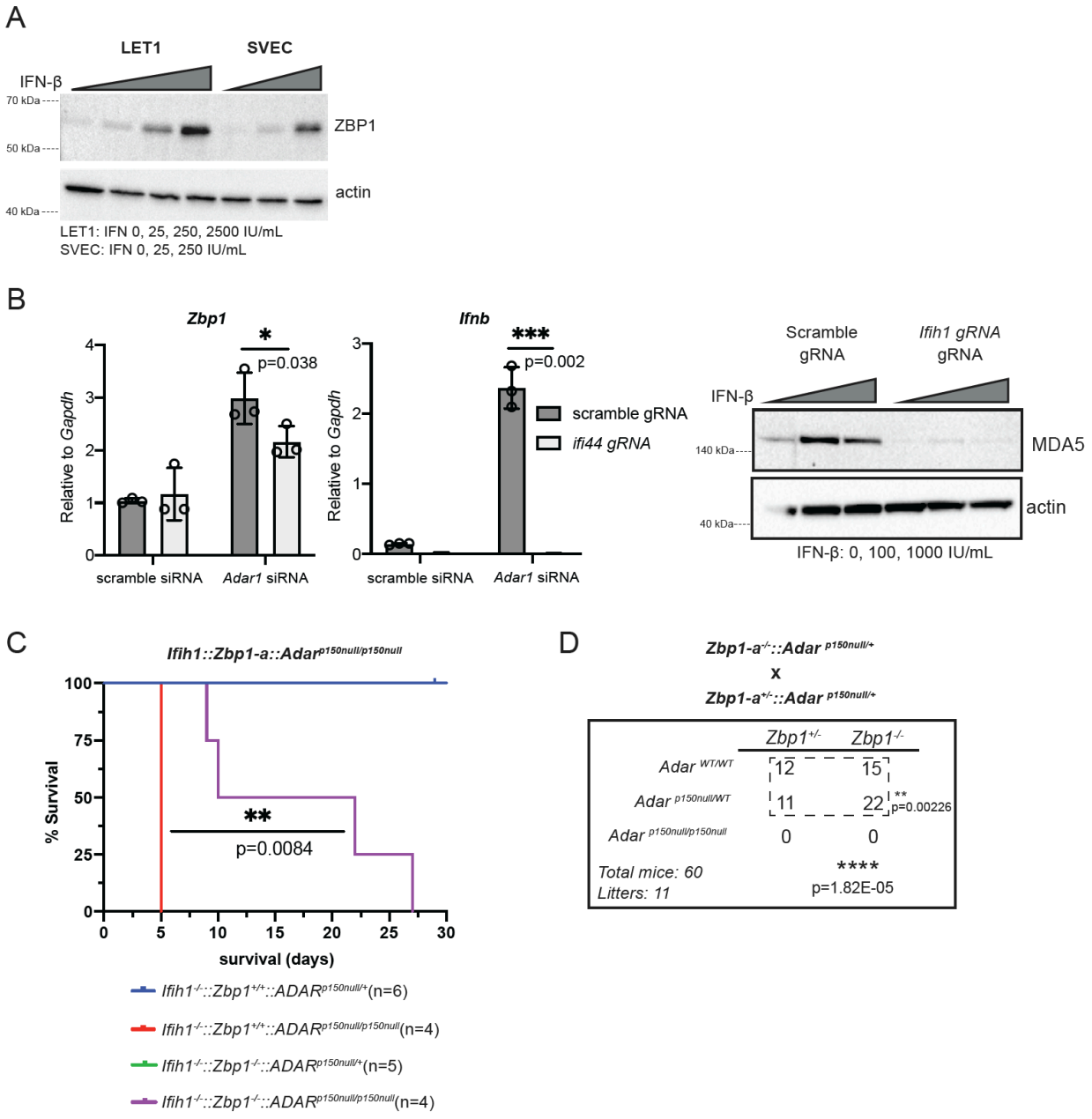

<u>Supplemental Figure 4:</u> ZBP1 is IFN dependent and partially dependent on MDA5. A. Twelve-hour stimulation of LET1 and SVEC cells with varying concentrations of IFN-β followed by Western Blot analysis for ZBP1 protein. **B.** Quantitative PCR analysis for *Zbp1* and *Ifnb* after ADAR1 depletion in wild-type (scramble gRNA) or MDA5 knockout LET1. Gene was normalized against *Gapdh.* Significance determined by individual student t-tests. Each group (*Zbp and Ifnb*)

contains 3 biologic replicates, each comprising the average of 4 technical replicates). This experiment is representative of two independent repeats. Whisker bars are presented as mean +/- SD. **C.** Survival of $Zbp1^{-/-}$::$MDA5^{-/-}$::$ADAR^{p150null/p150null}$ mice. Zbp1-$a^{+/+}$::$Ifih1^{-/-}$::$Adar^{p150null/+}$ n=6, Zbp1-$a^{+/+}$::$Ifih1^{-/-}$::$Adar^{p150null/p150null}$ n=4, Zbp1-$a^{-/-}$::$Ifih1^{-/-}$::$Adar^{p150null/+}$ n=5, Zbp1-$a^{-/-}$::$Ifih1^{-/-}$::$Adar^{p150null/p150null}$ n=3. Statistical significance determined by Mantel-Cox (Log-Rank) test. **D.** Survival proportions of *$Zbp1^{-/-}$-a::$Adar^{p150/WT}$ intercross.* Chi square power analysis performed, indicating significance at $p=1.82x10^{-5}$.

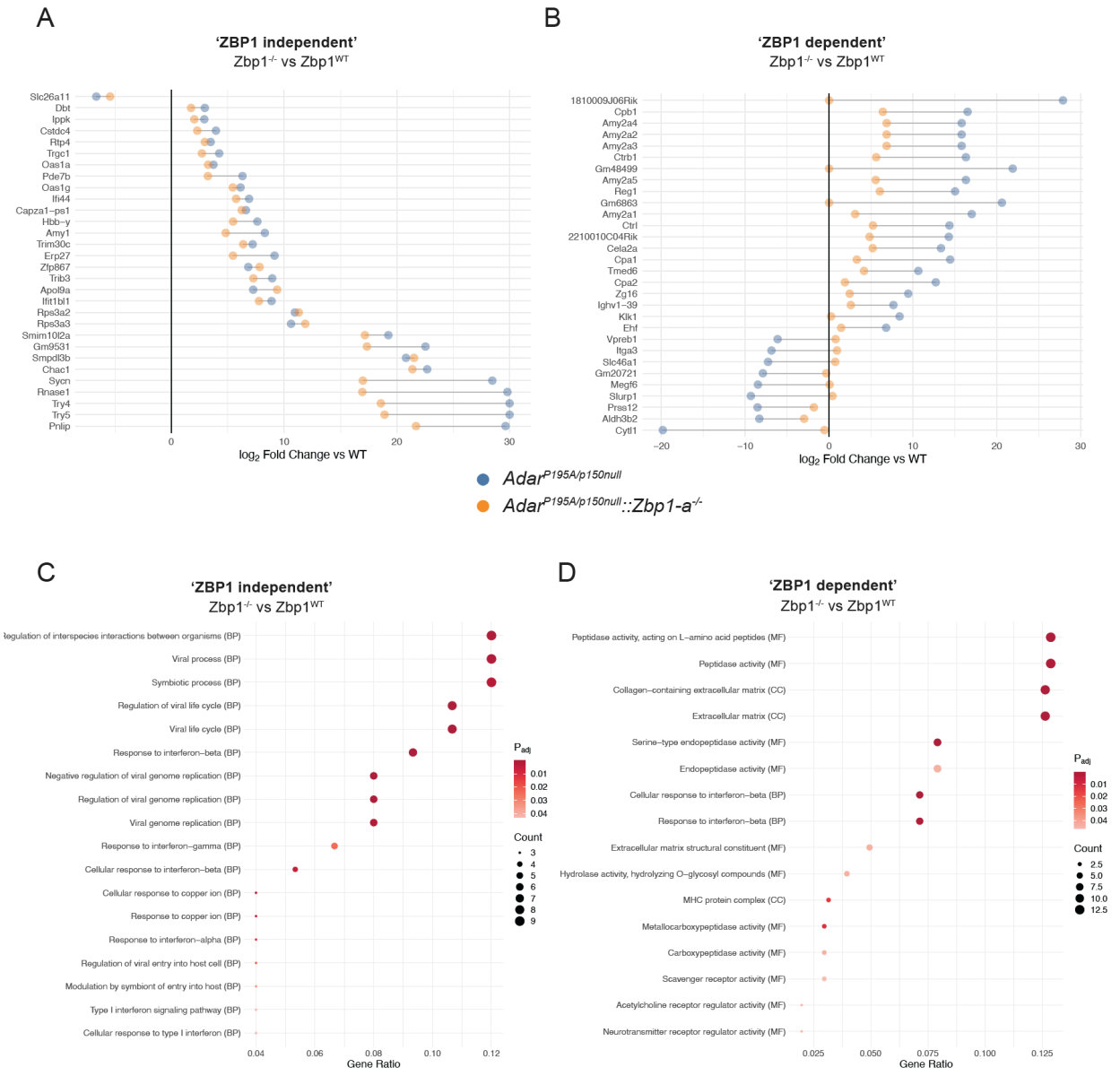

<u>Supplemental Figure 5:</u> Identification of ZBP1 dependent and independent aspects of the ADAR1 inflammatory signature. A-B: Cleveland plots indicating changes in the ADAR1 dependent gene signature observed in the spleens of 23 day old mice, indicating most- **(A)** and least- **(B)** changed genes upon ZBP1 ablation in *Adar*$^{P195A/p150null}$ mice. Gene selection is the top 30 largest contributors to the ZBP1 dependent **(A)** and independent **(B)** signature from ADAR$^{P195A/p150null}$ mice, in comparison to WT mice. Gene Ontology analysis was performed on

the signatures from **A** and **B**. **C-D:** GO-terms analysis for ZBP1-independent signature **(C)**, and the ZBP1 dependent signature analysis **(D).**

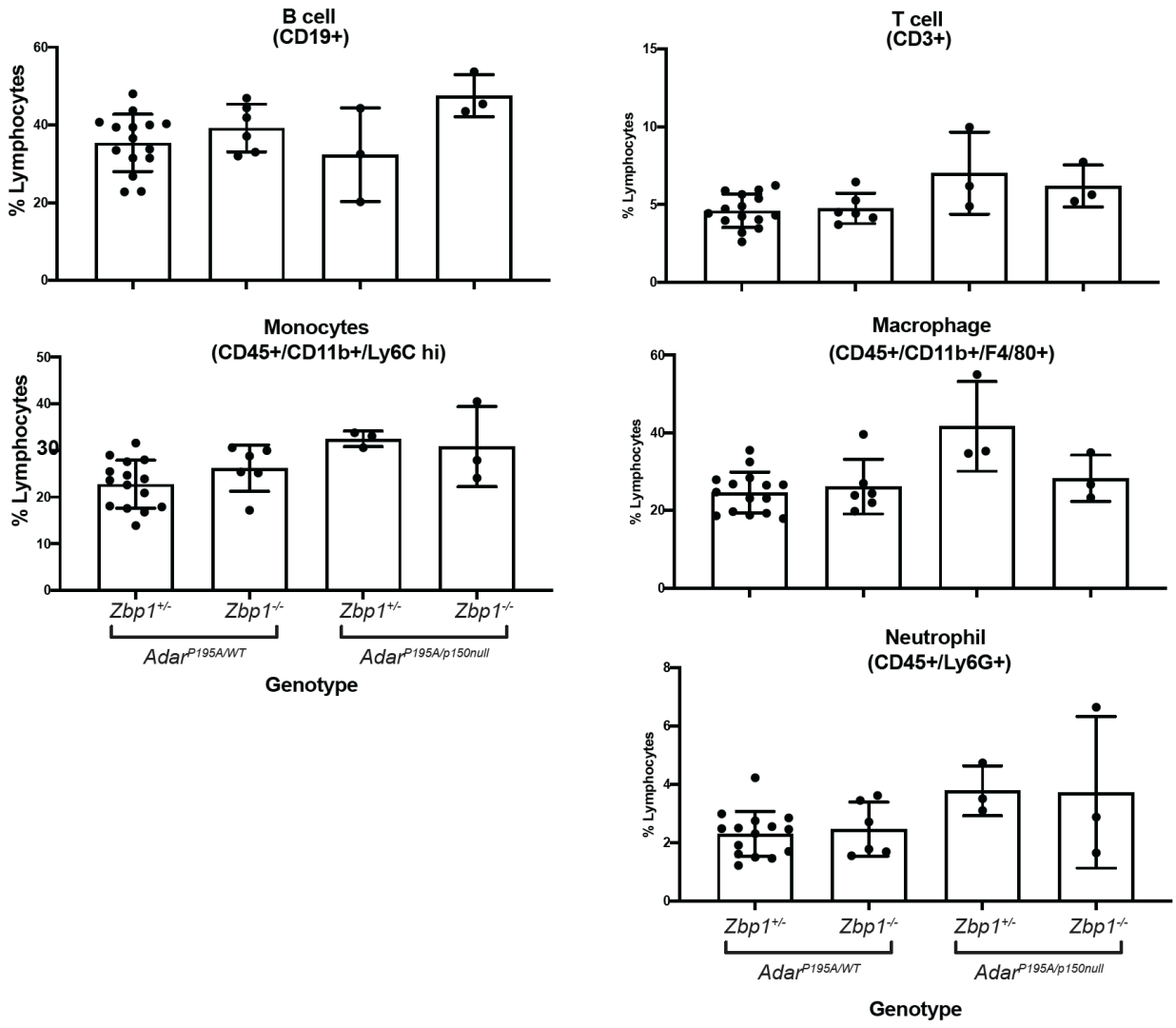

<u>Supplemental Figure 6:</u> Flow cytometry analysis of splenic cellular subsets. B cell, T cell, monocyte, macrophage percentages from day 23 spleens of *Zbp1::Adar*$^{p150/P195A}$ mice.

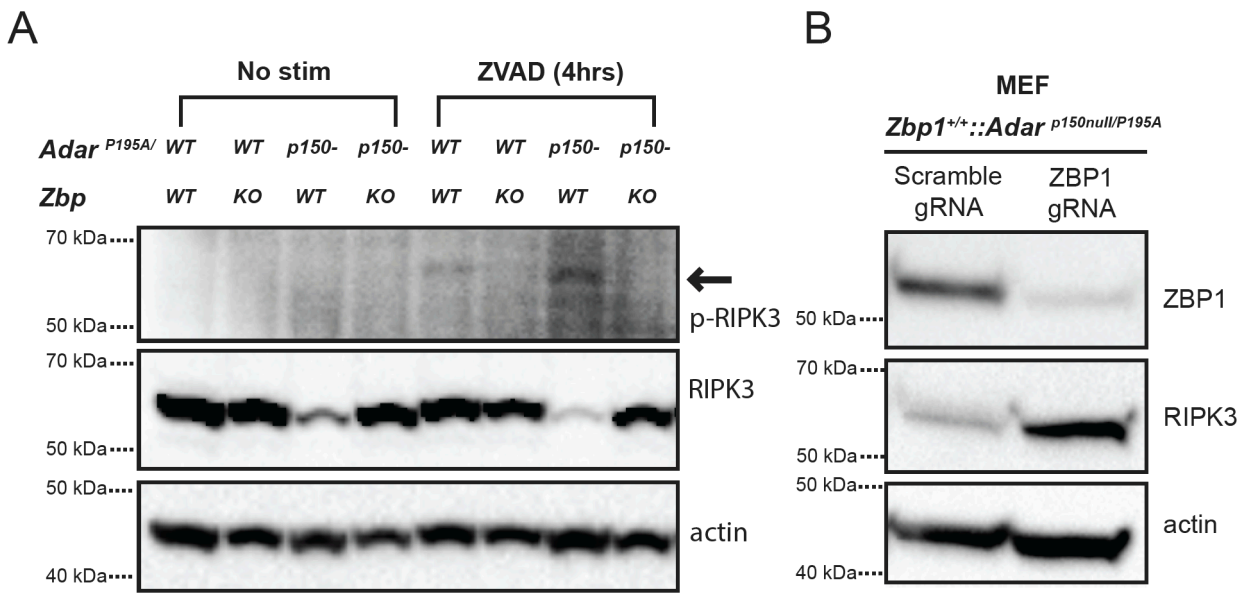

Supplemental Figure 7: ZVAD treatment induces phosphorylation of RIPK3 in ADAR mutant MEFs in a ZBP1 dependent fashion. A. Analysis of phospho-RIPK3 in ADAR1 mutant MEFs after 4 hour ZVAD treatment. **B.** Confirmation of ZBP1 gRNA knockout in ADAR1 mutant MEFs.

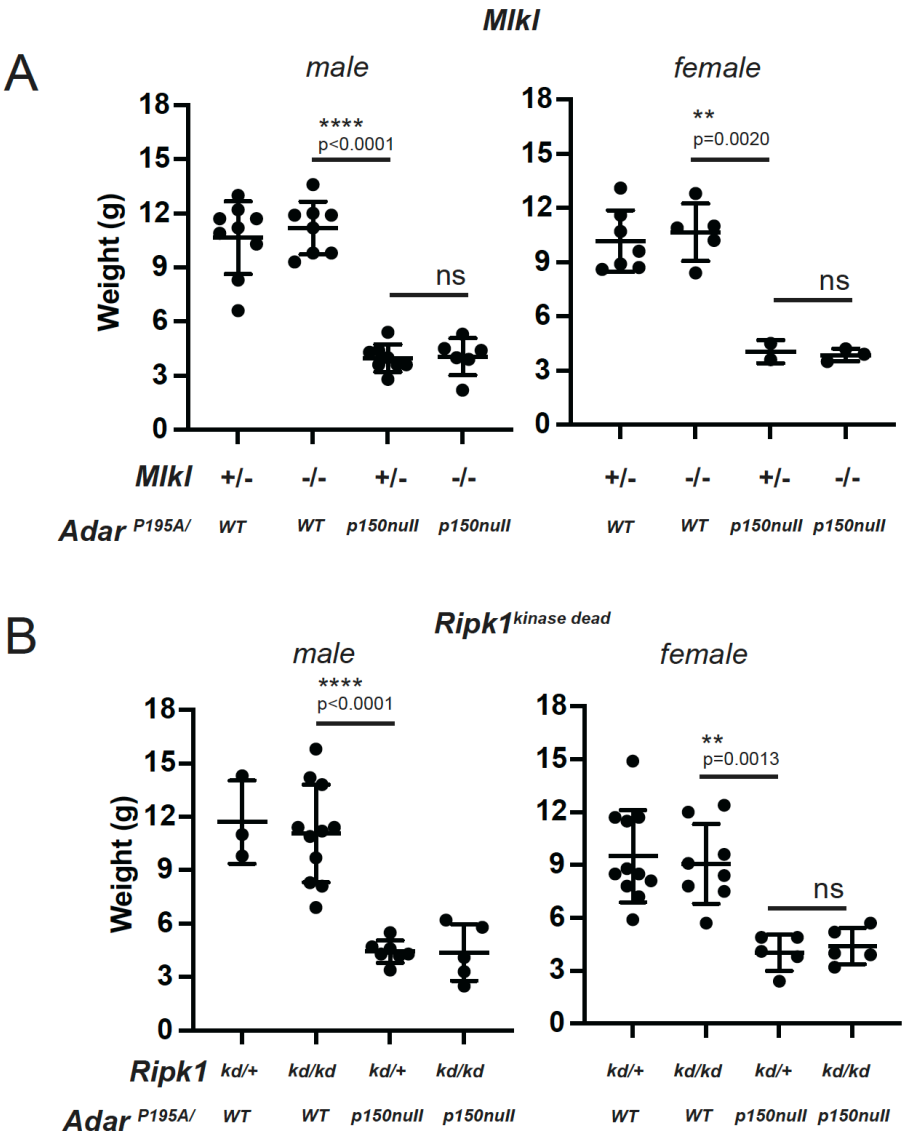

<u>Supplemental Figure 8:</u> MLKL or RIPK1$^{\text{kinase dead}}$ mutations do not rescue ADAR$^{\text{P195A/p150null}}$ mutation. Three-week-old weights (weaning) of male or female *Adar*$^{P195A/p150null}$ mice crossed to animals lacking, **A:** MLKL. Mlkl$^{+/-}$::Adar$^{\text{P195A/WT}}$ (m/f n=9/7), Mlkl$^{+/-}$::Adar$^{\text{P195A/p150null}}$ (m/f n=8/2), Mlkl$^{-/-}$::Adar$^{\text{P195A/WT}}$ (m/f n=8/5), Mlkl$^{-/-}$::Adar$^{\text{P195A/p150null}}$ (m/f n=6/3). or **B:** carrying a point mutation abrogating the kinase activity of RIPK1 (*Ripk1*^{kd}). Ripk1$^{\text{kd/+}}$::Adar$^{\text{P195A/WT}}$ (m/f n=3/11), Ripk1$^{\text{kd/+}}$::Adar$^{\text{P195A/p150null}}$ (m/f n=7/5), Ripk1$^{\text{kd/kd}}$::Adar$^{\text{P195A/WT}}$ (m/f n=11/8),

Ripk1$^{kd/kd}$::Adar$^{P195A/p150null}$ (m/f n=5/5). Statistical differences determined by individual student t-tests (two tailed). All genotypes are littermates from mixed litters.

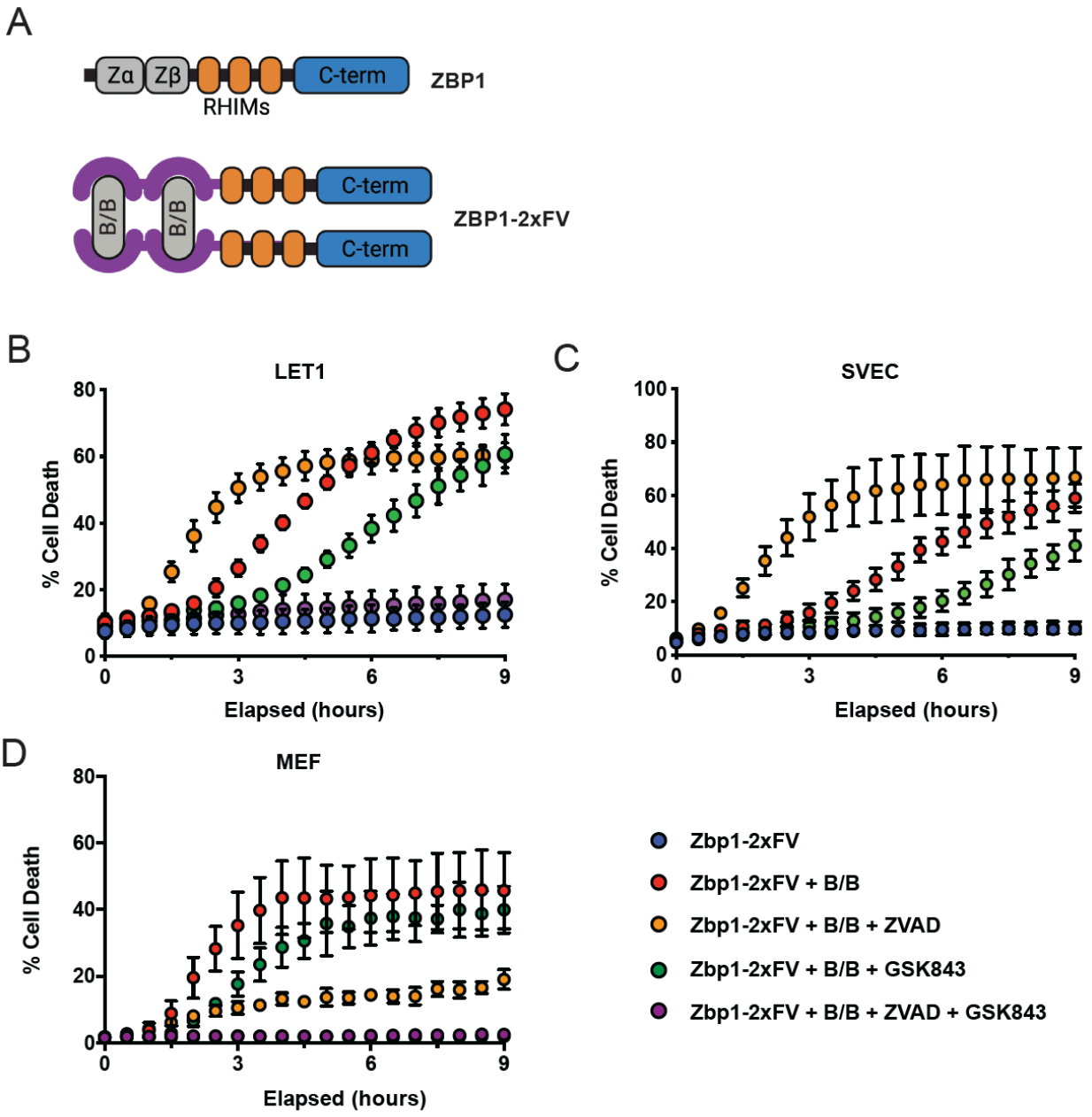

<u>Supplemental Figure 9:</u> Oligomerization of ZBP1 triggers necroptotic cell death. A. Schematic indicating the replacement of ZBP1's Z-DNA binding domain with a tandem FKBP domain. **B-D:** Cell death following addition of B/B homodimerizer with indicated combinations of ZVAD and GSK843 in LET1s (each group, n=4 biologic replicates) **(B)**, SVECs (each group n=4 biologic replicates) **(C)** or MEFs (each group n=3 biologic replicates) **(D)**. Statistical

significance was determined by unpaired t tests (two-tailed). Experiments B and C are representative of two independent experiments, and D is representative of 3 independent experiments. All whisker bars are presented as mean +/- SD.

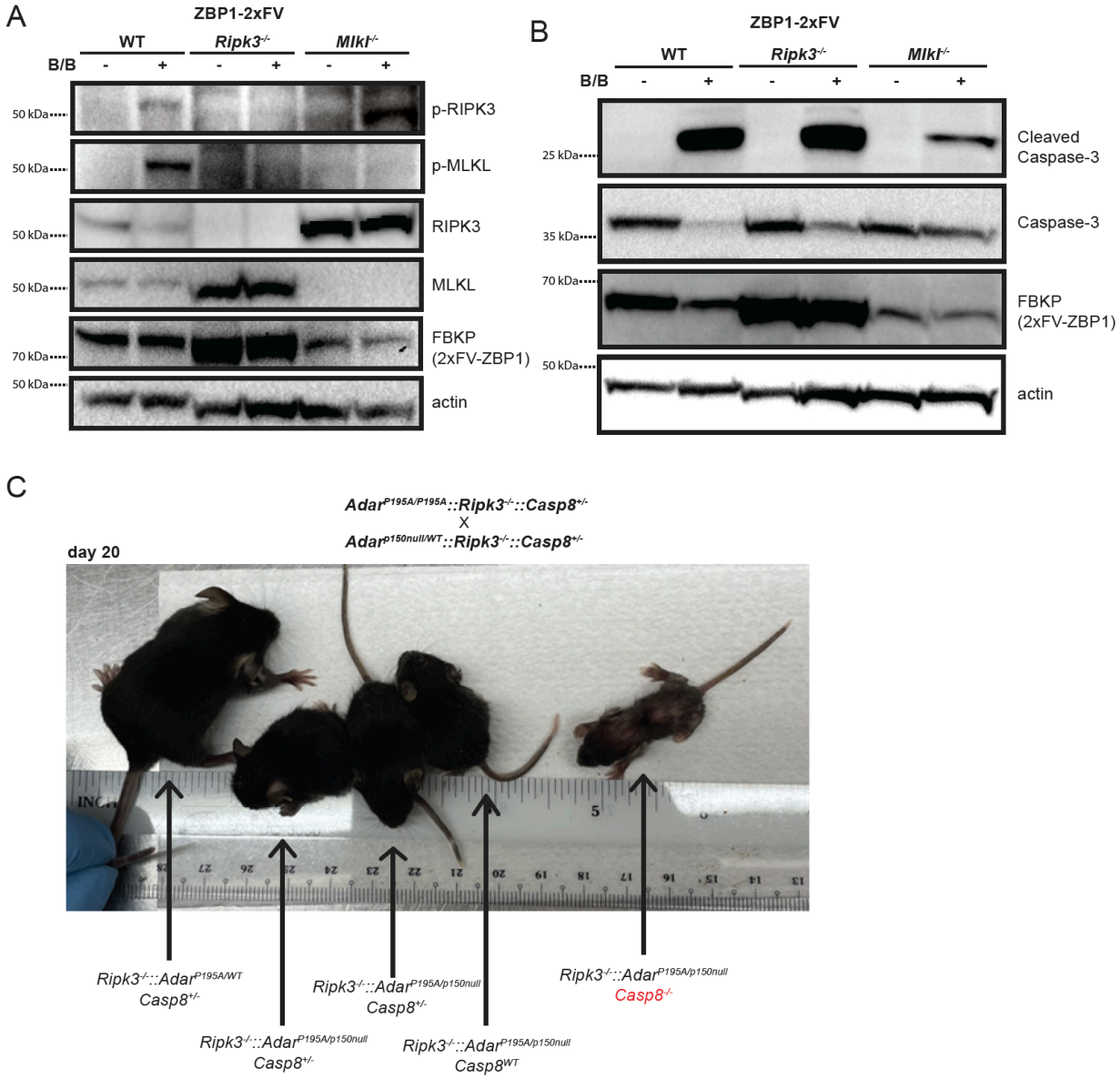

<u>Supplemental Figure 10:</u> Molecular analysis of cell death induced by ZBP1-2xFV homodimerization. A. Phospho-MLKL analysis of ZBP1-2xFV MEFs (wild-type, Ripk3$^{-/-}$, MLKL$^{-/-}$) after 1 hour stimulation with B/B homodimerizer. **B.** Cleaved-caspase 3 analysis of ZBP1-2xFV MEFs (wild-type, Ripk3$^{-/-}$, MLKL$^{-/-}$) after 3 hour stimulation with B/B homodimerizer. **C.** Representative image depicting Caspase-8 deficiency exacerbation of disease

phenotype in ADAR$^{P195A/p150null}$::RIPK3$^{-/-}$ mice. Image of 20-day old littermates from the cross depicted in Fig. 4B.

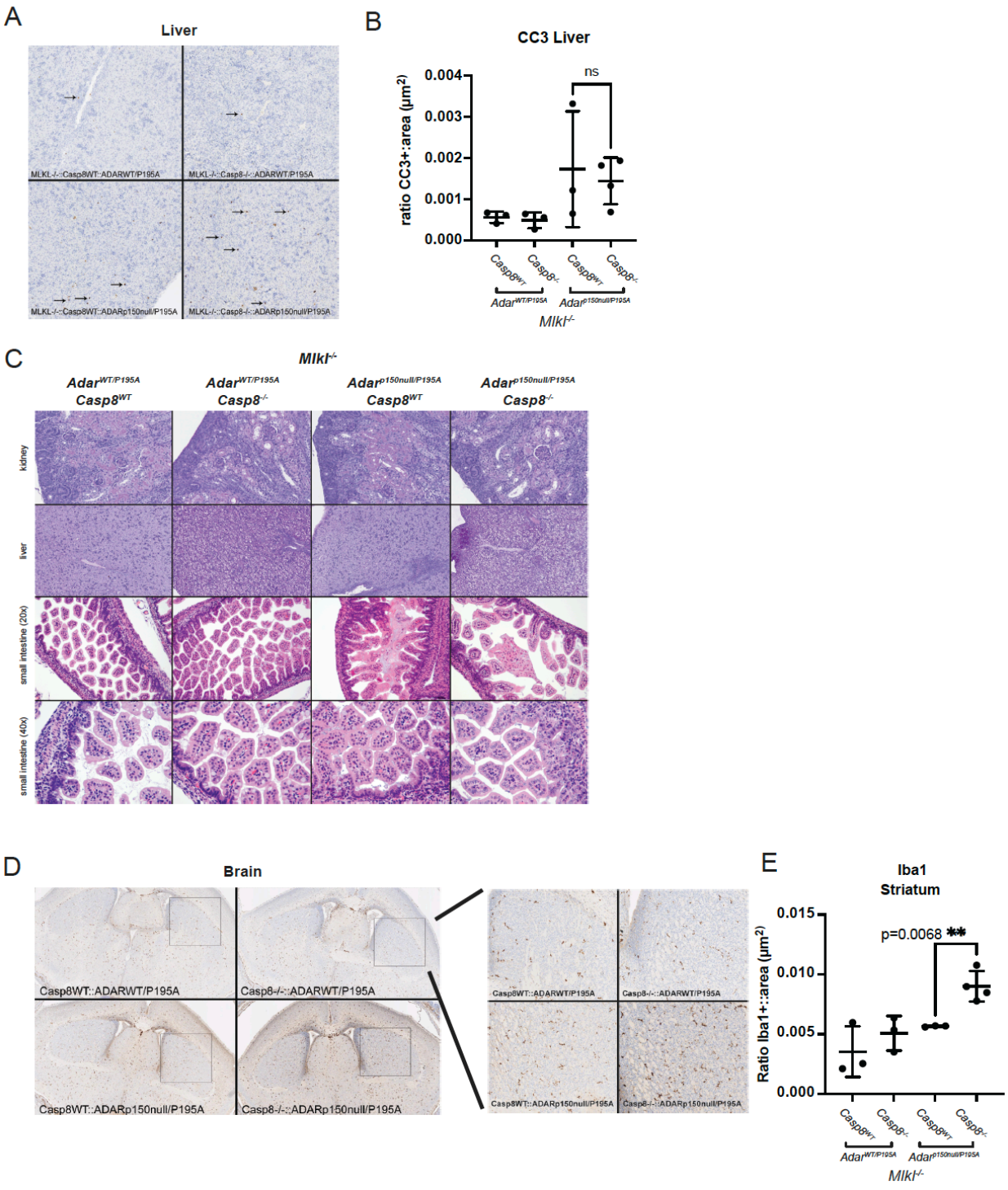

<u>Supplemental Figure 11:</u> Pathologic analysis of Mlkl-/-::Casp8$^{-/-}$::$^{Adarp150null/P195A}$ mice. A-B. Immunohistochemical staining **(A)** and quantification (**B)** in liver for cleaved-caspase 3. (n=3 d.0 pups, each group) Original magnification 10x. **C.** Additional histological images of other tissue

sites (kidney, liver and small intestine). Kidney (20x) and liver (10x) PAS staining, small intestine HE staining (original magnification as stated). **D-E.** Immunohistochemical staining, with 2.5x and 10x images **(D)** and quantification (**E)** in brain for Iba1 (n=3 d.0 pups, each group). **B & E** use tissues from matched animals.

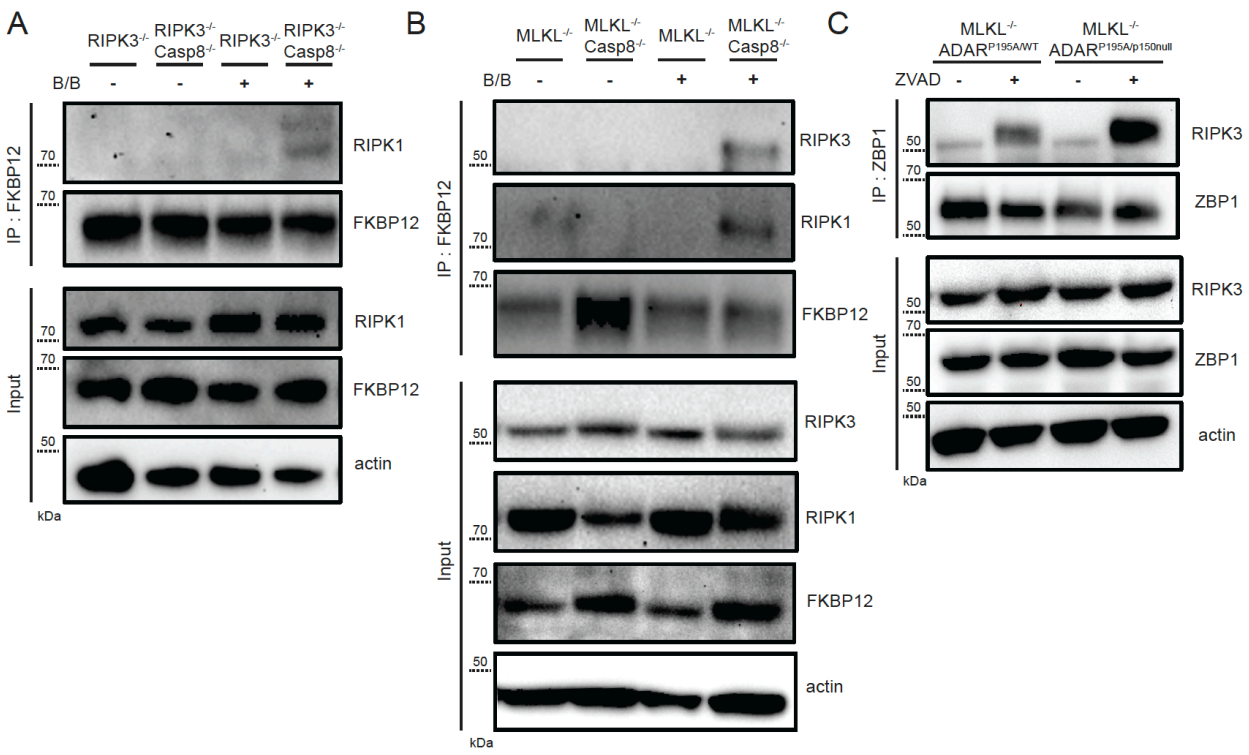

<u>Supplemental Figure 12</u>: Immunoprecipitation of RIPK3 and RIPK1 by ZBP1 is enhanced by Casp8 deficiency. A. Pulldown of ZBP1-2xFV (FKBP) and co-precipitation of RIPK1 in *Ripk3$^{-/-}$::Casp8$^{-/-}$ MEFs.* **B.** Pulldown of ZBP1-2xFV (FKBP) and co-precipitation of RIPK1 and RIPK3 in *Mkl$^{-/-}$::Casp8$^{-/-}$ MEFs.* **C.** Pulldown of ZBP1 and co-precipitation of RIPK3 and in *Mlkl$^{-/-}$::Adar$^{p150null/P195A}$ MEFs.*

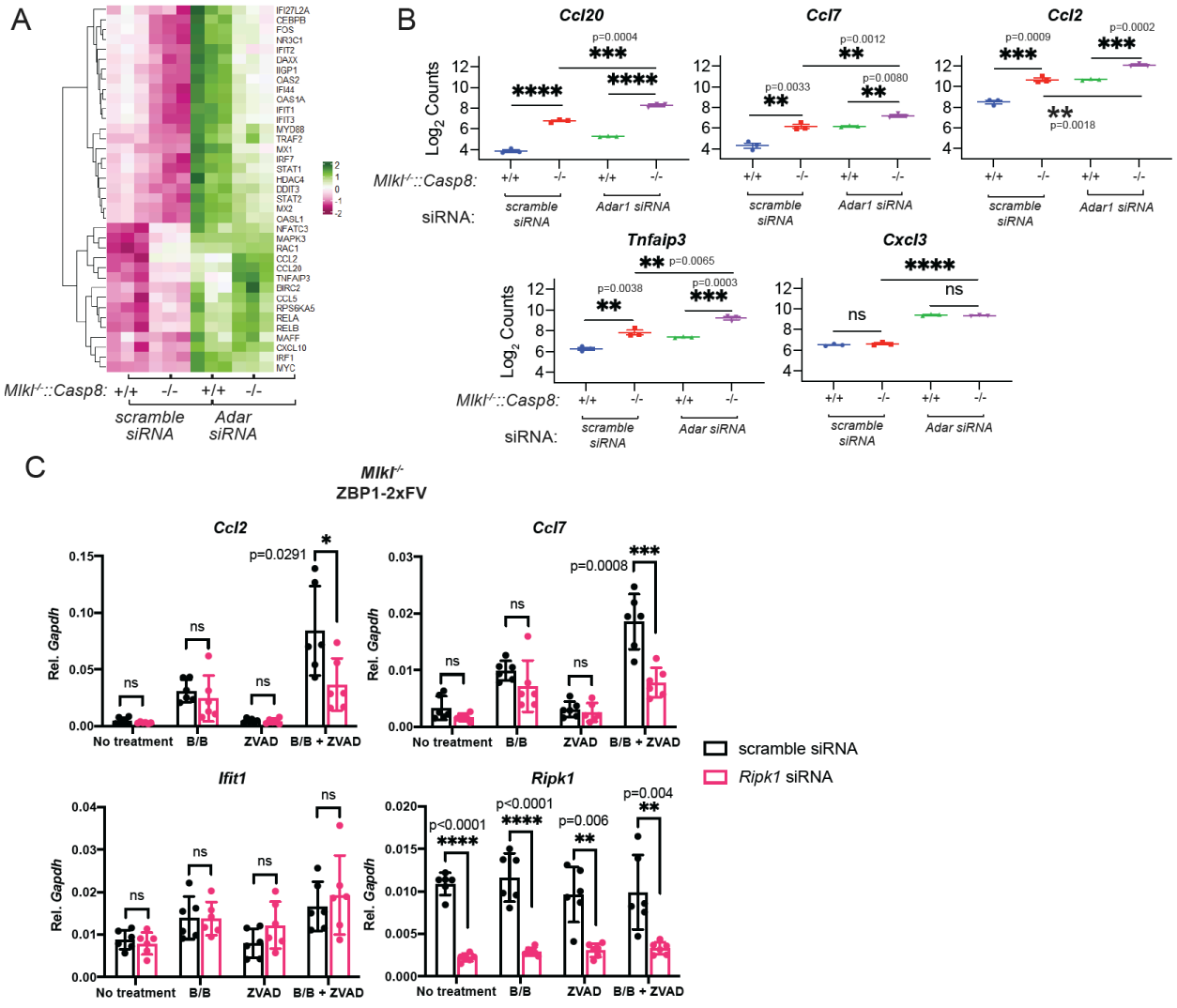

<u>Supplemental Figure 14</u>: ZBP1 activation results in RIPK1 dependent, RIPK3 independent gene transcription which is enhanced by knockout of *Casp8*. A-B Differential transcript analysis of *Mlkl*$^{-/-}$*::*Casp8$^{+/+}$ and Mlkl$^{-/-}$::Casp8$^{-/-}$ MEFs (n=3) following ADAR depletion, by **(A)** Heatmap analysis and **(B)** individual quantification of the top 5 differentially expressed genes. Statistical significance determined by individual unpaired t tests (two-tailed). Where not indicated: **** p<0.0001. **C.** QPCR analysis of top 5 differentially expressed genes identified (B) in MEFs expressing ZBP1-2xFV after B/B activation after depletion of RIPK1. n=6 biologic replicates for each treatment group, each representing the average of three technical replicates.

Data is compiled from two independent experiments. Statistical significance determined by individual unpaired t tests (two-tailed). Where indicated: **** $p<0.0001$. Whisker bars represent the mean +/- SD.

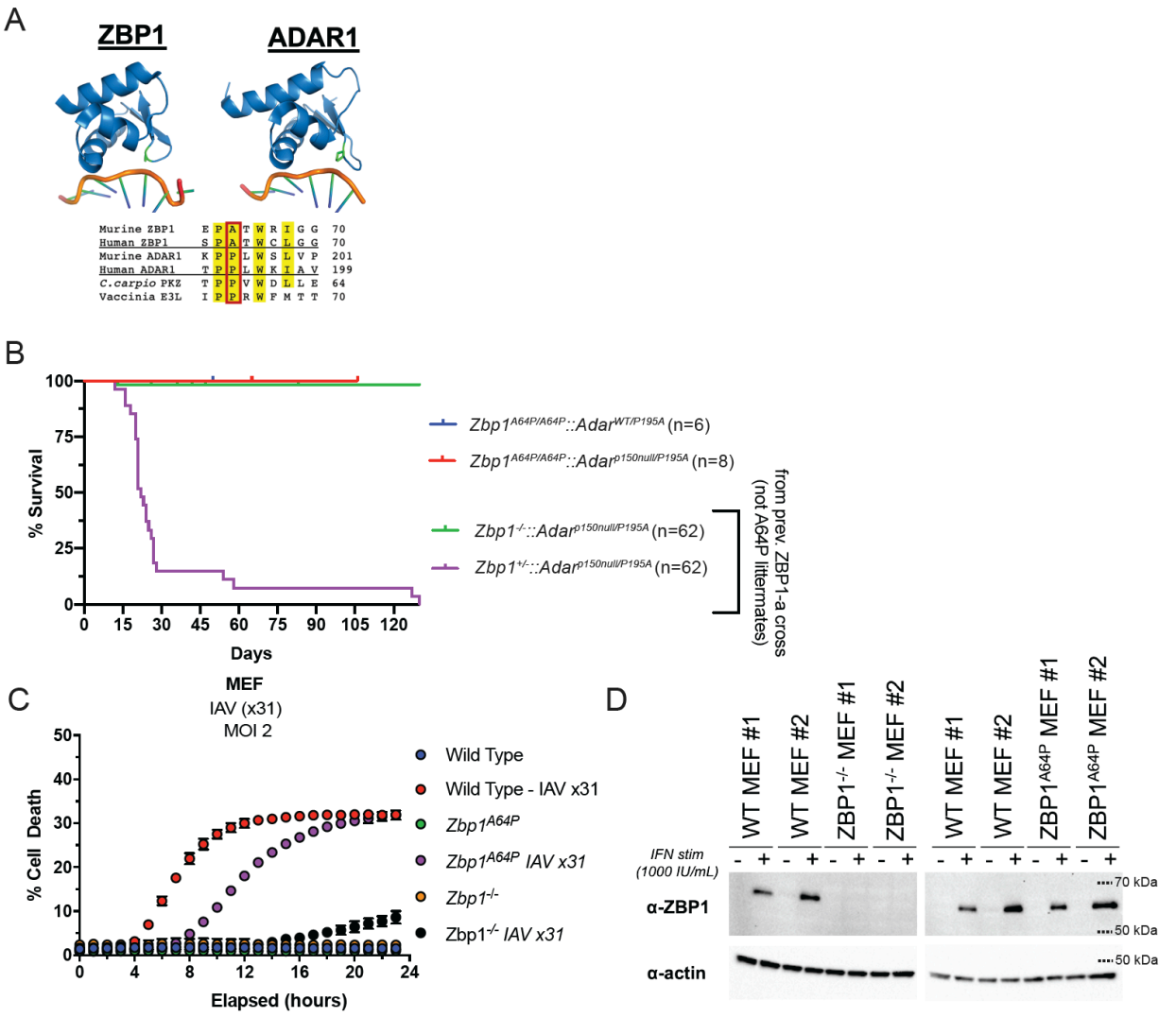

Supplemental Figure 14: ZBP1^{A64P} mutation attenuates ZBP1 activity in ADAR deficiency model and during influenza infection. **A.** Previously-reported structures of the ZBDs of ZBP1 (left) and ADAR1 (right), with A64 and P195A (respectively) highlighted in green. PDB accession #s: 1J75 and 3F21. **B.** Survival proportions of *Adar1*$^{P195A/p150null}$*::ZBP1*^{A64P} mice (n=9 animals) compared with previous survival statistics of *Adar*$^{P195A/p150null}$*::ZBP1-a*$^{+/-}$ animals. **C.** Cell death analysis following influenza (X31, MOI 2) infection of primary MEFs derived from Wild Type (B6/J), *Zbp1*$^{-/-}$ or ZBP1$^{A64P/A64P}$ mice. Each group, n=2 biologic replicates. Whisker bars represent the mean +/- SD. Experiment was independently replicated using MEFs derived

from a different embryo. **D.** Expression of ZBP1 in wild-type, *Zbp1*$^{-/-}$, and *Zbp1*$^{A64P/A64P}$ MEFs following 24 stimulation with 1000 IU/mL murine IFN-β.

Chapter 3

Summary and Future Directions

3.1 Summary

The research presented in Chapter 2 of this dissertation demonstrate that ZBP1 is a key distal effector mediating the pathology in a model of human autoinflammatory disease. Despite a robust steady-state IFN signature in *Adar*$^{P195A/p150null}$ animals, deletion of ZBP1 renders these mice phenotypically normal. Although ZBP1 is clearly responsible for pathology, the individual contributions of the pathways downstream of ZBP1 on this pathology remains somewhat unclear; our knockout analysis suggests that apoptosis, necroptosis and inflammatory (NFκB) transcription may all contribute, neither ruling out or specifically identifying one key mechanism.

This work further shows that Casp8 represents a critical mechanism for controlling ZBP1 dependent inflammation; based on previous studies, we anticipate that this control is due to Casp8/cFLIP proteolytic regulation of the necrosome. Alternatively, it is interesting to consider a potential anti-inflammatory effect mediated by cell death, that is, deletion of a cell engaged in inflammatory transcription/translation may counterintuitively represent an anti-inflammatory mechanism, in particular, by non-lytic immunologically silent apoptotic cell death[124]. Therefore, in addition to Casp8/cFLIP heterodimers regulating ZBP1 dependent inflammation, it is also conceivable that apoptosis following Casp8 homodimerization may represent an important mechanism for controlling pathology.

RIPK1 engagement and signaling by ZBP1 independently of RIPK3 was an unexpected finding of this study. Although RIPK1 was previously appreciated to regulate ZBP1 signaling at homeostasis[51], studies investigating viral activation of ZBP1 suggested that its effects were entirely mediated via RIPK3[41]. The partial attenuation of pathology both in the RIPK3 knockout and RIPK3::Casp8 vs MLKL::Casp8 double knockouts may suggest that RIPK3 participates in

potentiating the recruitment and activation of RIPK1, but RIPK1 also appears capable of signaling independently of RIPK3 downstream of ZBP1. Previous studies investigating RIPK3/RIPK1 interactions have identified dynamics of RHIM oligomer assembly as important for necroptotic signaling[125–127]; given that ZBP1 contains three central RHIM domain, it is interesting consider how its inclusion in the necrosome may modify these signaling dynamics. Furthermore, based on our observation of these ZBP1-RIPK1 interactions, crosstalk between TNF and ZBP1 dependent activation the necroptotic pathway also seems possible.

Implied, but not directly stated in Chapter 2, is the implication that RIPK1 is mediating the pathology in mice associated with the RIPK3 or MLKL::Casp8 double knockouts; we therefore predict that *Adar*$^{P195A/p150null}$*::Ripk3*$^{-/-}$*::Ripk1*$^{mutRHIM/mutRHIM}$ mice would phenocopy the ZBP1 rescue effect. To our surprise, combined RIPK3/RIPK1^{mutRHIM} mutation also failed to rescue the disease phenotype (**Fig. 1**). Although preliminary at the time of this dissertation's writing, there does appear to be some minor improvement in the survival conferred by the additional mutation of RIPK1. In light of this surprising observation, it should be noted that the innate adapter molecule TRIF (TIR-domain-containing adapter-inducing interferon-β) also contains a RHIM domain, and indeed, several studies have recently investigated the effects of ZBP1-TRIF signaling[109,128,129]. Current efforts are being made to generate *Adar*$^{P195A/p150null}$*::Ripk3-/-::Ripk1*$^{mutRHIM/mutRHIM}$*::Trif*$^{-/-}$ mice. Although it is unclear if this genotype will phenocopy the effects of ZBP1 knockout, this mouse will provide important insight into ZBP1 signaling. In the instance that further TRIF knockout <u>does</u> fully rescue, this would represent a novel finding as, engagement of the TRIF:ZBP1 signaling axis has only been identified in the context of TLR4 signaling[109,128,129], and it remains unclear what, if any role it plays in other settings. In the instance that TRIF knockout <u>does not</u> rescue, this would suggest

entirely unidentified RHIM-independent ZBP1 functions and provide a useful platform for their further characterization. While this increasing complexity surrounding the necroptotic pathway is undeniably overwhelming, that ZBP1 appears to be the unifying hub of so many unique signaling processes may serve as an important touchstone for future studies and further highlights it as an important innate immune signaling molecule.

The location and timing of ZBP1 dependent pathology observed in these studies, while not a focus of the previous chapter, is nonetheless intriguing. The pathology associated with the $ADAR^{P195A/p150null}$ seems almost entirely confined to the liver and kidneys. The time course of disease is also surprising: affected pups are born at mendelian frequencies, with most pups dying around day 15-21. Interestingly, few pups die prior to day 15, and of those pups that survive past day 21, these mice commonly survive beyond 100 days. Together, these observations suggest that ZBP1 dependent pathology may be restricted both by tissue and age-related regulatory mechanisms; alternatively, the same may be true of ADAR1 activity. Intriguingly, a previous report described RIPK3 downregulation in adult mouse hepatocytes[130]. Therefore, future studies investigating the tissue restriction of ZBP1 expression and signaling may provide important insights into the mechanisms of ZBP1 signaling and regulation.

The $ADAR1^{P195A/p150null}$ model highlights an important shortfall of many models where embryonic lethality results from a gene deletion: the effects of these critical knockouts are often so pleiotropic that it becomes nearly impossible to understand the individual consequences of the many pathways involved. A full deletion of ADAR1 illustrates this, as ZBP1 knockout has little or no discernable effect in this setting. The $ADAR^{P195A/p150null}$ model seems to represent a unique convergence of a ZBD-dependent dysregulated ligand effect (P195A mutation) and a decreased ability to control MDA5 dependent production of type-I interferon ($ADAR^{p150null}$

haploinsufficiency), resulting in the specific activation of ZBP1. How the molecular mechanisms of the ADAR$^{P195A/p150null}$ model overlap with ZBP1 activation during viral infections is somewhat unclear, but suggest that subtle shifts in ligand availability in the context of type-I interferon production appear to be key factors balancing the activity of ZBP1.

Finally, this work suggests that ZBP1 may represent a critical factor in the pathogenesis in patients with AGS due to mutations in ADAR1. Although this model of ADAR1 deficiency fails to recapitulate several key factors of human disease, most notably the neuropathology associated with AGS, the rescue of this model by ZBP1 is striking. Despite this, it seems unlikely that other causative mutations of AGS (Trex1, MDA5, SAMHD1, etc.) would be mediated by ZBP1 - indeed our own studies indicate that necroptosis does not play a role in the disease associated with Trex1 knockout in mice. This is likely due the very specific circumstances arising in this model of disease, which have allowed us to specifically activate ZBP1. Further work is therefore needed to investigate roles for ZBP1 in other inflammatory disease settings.

3.2 Outstanding Questions and Future Directions

The work described in chapter 2 identified a novel relationship whereby ADAR1 deficiency results in the sterile, *in vivo* activation of ZBP1 and the associated necroptotic pathway. In the wake of these findings and establishment of this model, we may now be well-positioned to address the following two longstanding questions surrounding necroptotic cell death: 1) What is the ZBP1 ligand? And 2) How is Casp8 control of the necrosome modulated to allow necroptotic cell death? In this section, I will briefly discuss a few key preliminary findings

attempting to address these questions and hypothesize (speculate) about some potential mechanisms which may begin to answer these important questions.

In response to the first question, 'What is the ZBP1 ligand?', from the perspective of our model we might begin by asking, 'Do ZBP1 and ADAR1 share a ligand?'. In chapter two, we observed that when co-expressed, ADAR1 and ZBP1 co-immunoprecipitated, and that this interaction is stabilized by UV-crosslinking. We followed up on this experiment by performing IR-CLIP, and observed that ZBP1 appeared to bind RNA (see Supplemental Fig.1 in Chapter 2). Next, we sought to understand how expression of ADAR1 might modulate ZBP1 binding of RNA; our prediction was, that overexpression of the long p150 isoform of ADAR1 would disrupt the RNA binding of ZBP1. Surprisingly, we found that overexpression of ADAR1 instead resulted in significantly enhanced binding of ZBP1 to RNA species **(Fig. 2)**. These unexpected results led us to wonder about the nature of ADAR1 effects on RNA, and specifically the effect of deamination on the thermodynamics of Z-Nucleic Acid. A rough observation of ZBD:Z-DNA crystal structures[54–57,131] might suggest that the conformational change from a right-handed to a left-handed structure would be highly unlikely from a thermodynamic perspective; with this in mind, we hypothesize that the double-stranded nucleic acid 'bubble' associated with deamination may underlie the creation of 'Z-prone' regions associated with ADAR1 editing. Under this hypothesis, upon deamination of a dsRNA structure and creation of a Z-prone region, the ADAR1 ZBD may serve to protect these structures from recognition by ZBP1. Furthermore, a previously mentioned recent study suggested that ZBDs may actually provide a stabilizing influence on Z-NA[65], therefore it follows that as Z-NA is stabilized by the presence of ZBDs, the relative abundance of these structures (as regulated by type-I interferon) might determine the outcome of the response, specifically, ZBP1 binding and oligomerization.

Future experiments will explore these possibilities more thoroughly by investigating the effects of mutations disrupting either ADAR1 deaminase function, or ADAR1 Z-NA binding function. Under this model, we hypothesize that co-expression of a deaminase dead ADAR1 would result in creation of fewer Z-prone structures, thereby decreasing ZBP1 binding to RNA; similarly, mutation of the ADAR1 ZBD would be expected to enhance ZBP1 RNA binding, as ADAR1 would be less capable of protecting these Z-prone regions from ZBP1 binding. In addition to providing support for the molecular basis of ZBP1 activation in the *Adar*$^{P195A/p150null}$ model, it is interesting to consider how this careful balance between the interferon inducible ZBP1 and the p150 isoform of ADAR1 may be at play during viral infections; while it is tempting to think that ZBP1 is responding to a virus specific ligand, perhaps ZBP1 is instead responding to an altered perception of self-ligand.

The question, 'How is Casp8 modulated such that necroptosis may take place?', has existed since the first description of necroptotic cell death, when inhibition of Casp8 (using the drug zVAD) in combination with TNF was described to trigger this phenomenon[17]. In other words, how do we take the brakes off necroptosis? Although a there is not a clear physiologic paralog of direct Casp8 inhibition, a similar sensitization to TNF induced necroptosis is observed when translation is blocked using the drug cycloheximide.[108,132] This sensitization is mediated by the rapid decrease in cFLIP protein levels upon translational inhibition.[133–135] Intriguingly, translation inhibition also occurs upon ADAR1 loss due to activation of the dsRNA sensor PKR (Protein Kinase R) which triggers the Integrated Stress Response (ISR) and the associated block in cap dependent translation[75,96,98,101] Furthermore, knockout of PKR also completely rescues the *Adar*$^{P195A/p150null}$ disease phenotype[96], suggesting that PKR may be playing a role in ZBP1 activation of necroptosis. To test this, we depleted ADAR1 in LET1 cells where either PKR was

deleted, or the ISR was inhibited with the drug ISRIB. Interestingly, we found that the cell death associated with ADAR1 depletion was completely rescued in PKR knockout or ISRIB treated cells **(Fig. 3A)**. We also observed a marked decrease in cFLIP protein levels of ADAR1 depleted cells which was reversed by PKR knockout or ISRIB treatment **(Fig 3B)**. Finally, to test the effect of cFLIP expression on cell death during ADAR1 depletion, we simultaneously depleted cFLIP in LET1 cells and observed that cFLIP depletion restored sensitivity to cell death in the presence of ISRIB (**Fig 3A**). These preliminary results indicate that the translation inhibition associated with PKR during ADAR1 deficiency may be playing a role in sensitization to necroptotic cell death by the translational control of cFLIP and potentially other pro-survival proteins. Although future studies are needed to further understand these preliminary results and hypotheses, we believe that PKR and the Integrated Stress Response may represent an important component to answering this longstanding question regarding how Casp8 inhibition of necroptosis is modulated. This observation may also suggest an interesting two-signal model where type-I interferon production (ZBP1 upregulation) in the presence of cellular stress may activate this pathway. This model is intriguing as it does not actually require any direct recognition of a viral component, but instead would respond to the circumstances associated with infection (**Fig. 4**); this may provide an explanation for how ZBP1 is able to respond to such a wide variety of unrelated DNA and RNA viruses.

Alternatively, it is interesting to consider the role of ADAR1 during a viral infection; although an antiviral role of ADAR1 in animals is unclear and often contradictory,[141–145] it feasible to consider that the ancestral ADARs may have originated as antiviral effector molecules. Indeed, ADAR1 arose in early metazoans, where its original functions are somewhat unclear[146], but the fact that ADAR1 is now strongly associated with type-I interferon, a pathway

that did not evolve until much later, is intriguing. This raises the possibility that type-I interferon production following viral restriction of ADAR1 could have originated as a sort of surveillance mechanism safeguarding the integrity of its antiviral function. Moreover, no instances of ADAR1 restriction by viruses have been reported, either indicating that ADAR1 has no antiviral function, or that disruption of ADAR1 is strongly disadvantageous for the virus due to this IFN-surveillance mechanism. A recent report describing a similar Self-Guard Theory mechanism involving the protein MORC3 and the SUMOylation pathway upstream of type-I IFN production may lend some credence to this idea[147,148]. Finally, it is interesting to consider the relationship between ADAR1 and ZBP1 as an added layer on this self-guard theory perspective: due to ZBD domain similarity between ADAR1 and ZBP1, any restriction in these sites would likely also disrupt ADAR1, thereby triggering a further type-I interferon response. As ZBP1 and ADAR1 are the only ZBD containing proteins in the mammalian genome, and ZBP1 (a clearly antiviral protein) appears to have evolved after ADAR1, this seems to further indicate that the original function of ADAR1's ZBD domain may have been antiviral in origin.

3.3. Final Remarks

Despite an awareness that interferon mediates immune pathology in a wide variety of pathogen and non-pathogen settings, the interferon response is comprised of hundreds of downstream effector components, and the contributions of these individual pathways to broader immune pathology is unclear and often generalized. Using a model of Aicardi-Goutiéres Syndrome we identify ZBP1 as a critical distal effector of interferon mediated pathology. Although AGS represents a severe example of an extremely rare interferon mediated disease, the

mechanisms responsible for its pathology may be at play in a variety of less aggressive settings. While our observations lend credence to the idea that a small handful of effector mechanisms may be contributing disproportionately to immune pathology, we are also distinctly aware that the highly specific set of circumstances leading to ZBP1 activation in this model may not be present in other instances of inflammatory disease. With that in mind, a more detailed understanding is required for how the multitude of host immune effector mechanisms downstream of pleiotropic signals such as type-I interferon or TNF may mediate pathology in different inflammatory disease contexts. The challenge of this endeavor is potentially highlighted when comparing the effects of a full ADAR1 knockout to the $ADAR1^{P195A/p150null}$ model used here; the traditional approach of understanding a pathway by complete genetic knockout, while certainly useful for implicating broad classes of associated mechanisms (for instance, an MDA5 driven type-I interferon response), individual yet important components of those mechanisms may be obscured (like ZBP1) in these extreme settings. To this end, new systems based on the genetics of human disease (not embryonic lethality), like the ADAR1 model used here, represent invaluable tools for our increasingly granular and complex understanding of the immune system.

The severe ZBP1 dependent disease described in Chapter 2 highlights the highly dangerous pathogenic potential of this host effector mechanism, and begs the question, would we be better off without this pathway? More generally though, is there ever an evolutionary pressure to lose an effector mechanism which has developed too much pathogenic potential? There is some evidence for this across the animal kingdom, with a variety of potent antiviral pathways – for example, OAS1 is lost in a large range of primate species[136]; AIM2 and the ALRs are lost in cats, dogs cows and dolphins[137]; the inflammasome is largely defunct in cats and dogs due to a variety of different components being lost across individual sub-speies[138]; MLKL is lost across

carnivores[139]; and finally neither RIPK3 or ZBP1 is found in birds[140]. Although it is hard to ascribe a direct cause to these losses, the inflammatory potential of these individual pathways is undeniable; it is conceivable that in certain circumstances, their loss may confer a fitness advantage. It is also interesting to consider how long-term co-evolution of host effectors with viruses may ultimately result in extremely potent mechanisms, that are essentially dormant due to inevitable viral escape. Take for example many of the herpesviruses: we appreciate that co-evolution with these viruses has largely shaped our immune responses, and a result of this is that many of us are infected by herpesviruses yet suffer no immune pathology or adverse effects. Extending the common metaphor of the evolutionary arms race, we might consider our immune system to be akin to a minefield from a bygone arms race which has been carefully mapped by these co-evolved viruses so they can be navigated safely. What then might be the effect of an infection by a similar zoonotic virus that manages to infect us? Without the careful co-evolution with our own immune effector mechanisms, it is concerning to think that these novel pathogens would not be able to effectively navigate this extremely dangerous evolutionary landscape, and stumbling into this 'minefield', may trigger enormously damaging consequences. Referring to the last section identifying the need to identify these distal effector mechanisms of immune pathology, perhaps this evolutionary perspective may offer a useful framework. Either by identifying conserved interferon stimulated pathways which been intermittently lost in other species during their recent evolutionary history, or differential analysis of how infection by closely related zoonotic virus families trigger different sets of effectors, perhaps we can identify new critical pathways that further our understanding of inflammation and immune pathology. Overall, the work described in this dissertation provides an example of the surprisingly damaging

potential of a single effector pathway, and highlights the importance for expanding our understanding on the distal mechanisms mediating inflammatory pathology.

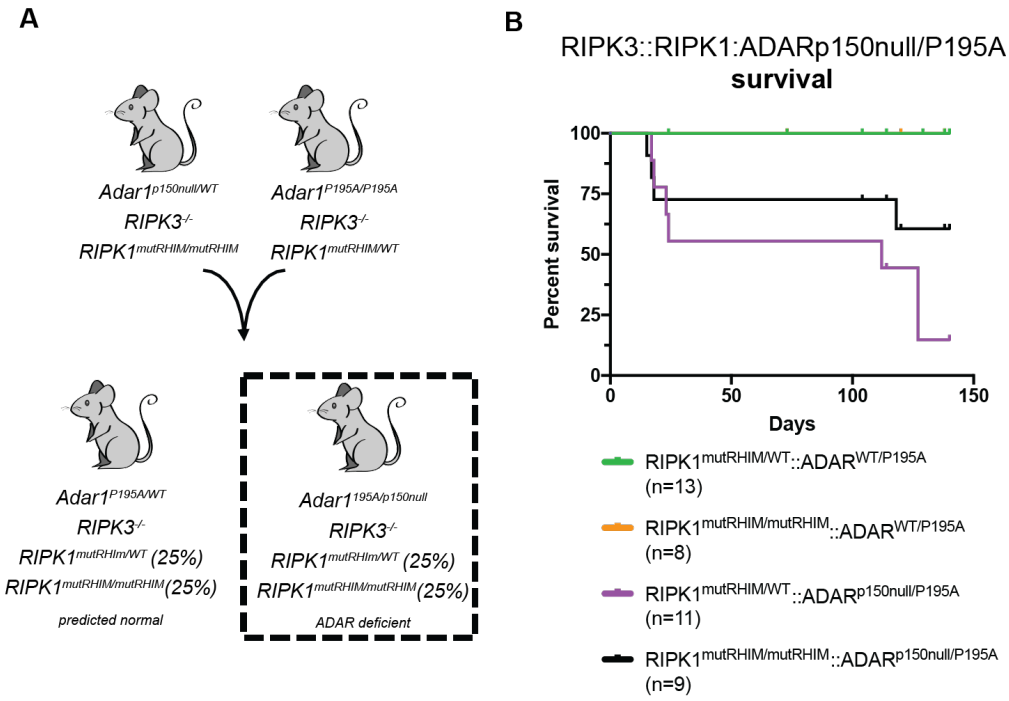

Figure 1. RIPK3$^{-/-}$::ADAR1$^{p150null/P195A}$ is not rescued by additional RIPK1$^{RHIM/RHIM}$ knockout. (A) Schematic showing the cross strategy and observed genotype outcomes. **(B)** Percent survival for each genotype produced by the cross of *Adar*$^{p150null/WT}$*::Ripk3*$^{-/-}$*::Ripk1*$^{mutRHIM/mutRHIM}$ mice to *Adar*$^{P195A/P195A}$*::Ripk3*$^{-/-}$*::Ripk1*$^{mutRHIM/WT}$ mice.

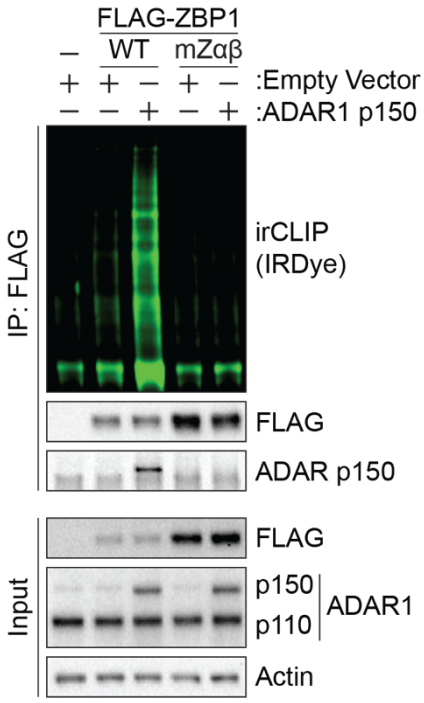

Figure 2. Co-expression of ADAR1 enhances ZBP1 binding so RNA. Immunoprecipitation and IR-CLIP analysis for RNA binding by of WT or mZαβ FLAG-ZBP1 in the presence or absence of the co-transfected ADAR1 p150 isoform.

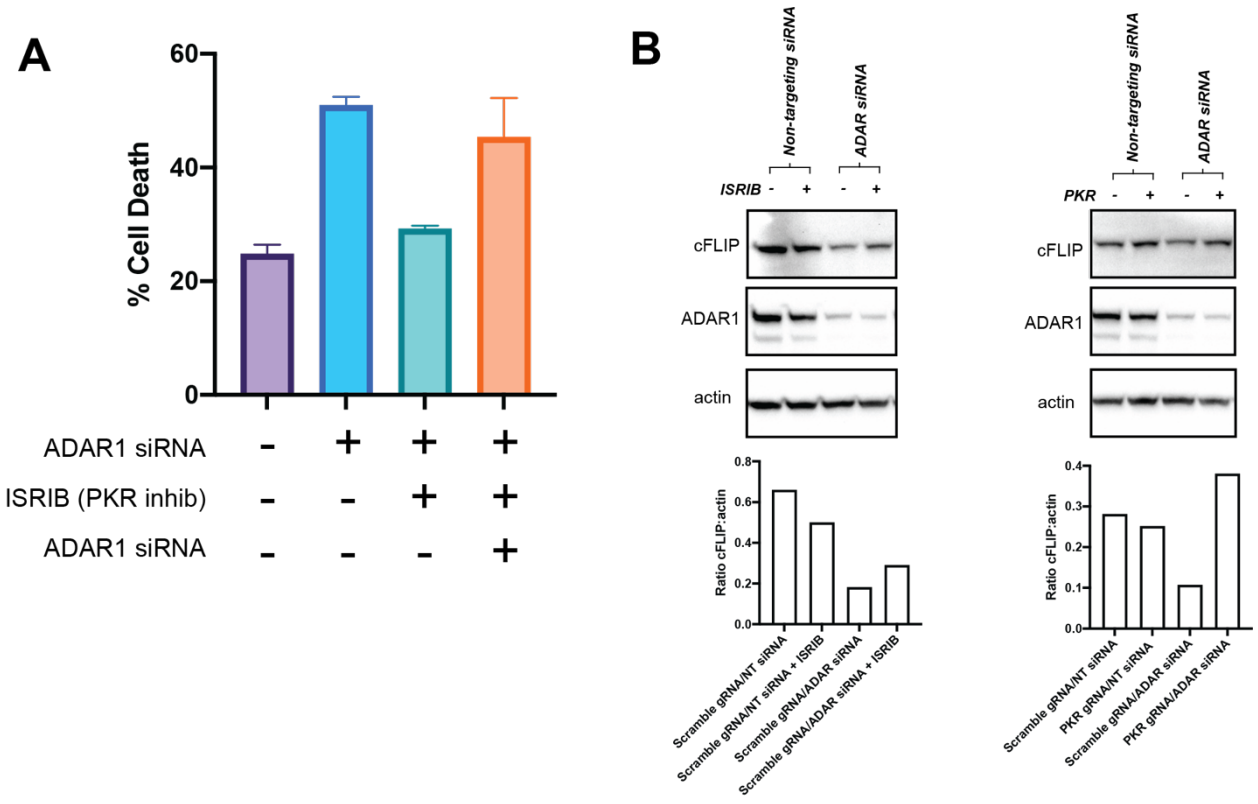

Figure 3. Regulation of cFLIP expression by the Integrated Stress Response during ADAR1 depletion regulates sensitivity to cell death. (A) Cell death analysis in LET1 cells treated with a combination of ADAR1 and cFLIP siRNAs in combination with the drug ISRIB. Cell death observed at the 36 hour timepoint, post siRNA transfection. **(B)** cFLIP expression in LET1s 24 houors following ADAR1 depletion and treatment with ISRIB.

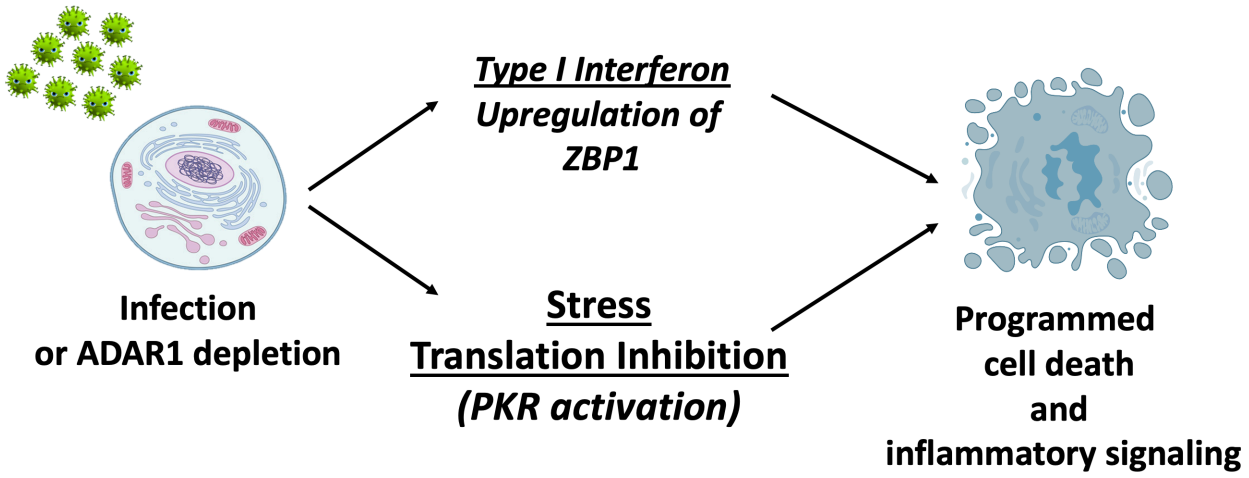

Figure 4. Schematic of proposed model for viral and non-viral activation of ZBP1. ZBP1 activation may by triggered by a coincidental detection of interferon and cellular stress. Under this model, although ZBP1 may not directly respond to a viral ligand, it would only be activated by a cell in the environmental context of infection (interferon) and currently undergoing a stress response, possibly indicative of infection. This proposed model may help explain the observation that ZBP1 activation during ADAR1 deficiency does not require any viral infection.

References

1. Oberst A. Death in the fast lane: what's next for necroptosis? *Febs J*. 2015;283(14):2616-2625. doi:10.1111/febs.13520

2. Orozco S, Oberst A. RIPK3 in cell death and inflammation: the good, the bad, and the ugly. *Immunol Rev*. 2017;277(1):102-112. doi:10.1111/imr.12536

3. Green DR. The Coming Decade of Cell Death Research: Five Riddles. *Cell*. 2019;177(5):1094-1107. doi:10.1016/j.cell.2019.04.024

4. Ali M, Roback L, Mocarski ES. Herpes simplex virus 1 ICP6 impedes TNF receptor 1–induced necrosome assembly during compartmentalization to detergent-resistant membrane vesicles. *J Biol Chem*. 2019;294(3):991-1004. doi:10.1074/jbc.ra118.004651

5. Koehler H, Cotsmire S, Zhang T, et al. Vaccinia virus E3 prevents sensing of Z-RNA to block ZBP1-dependent necroptosis. *Cell Host Microbe*. 2021;29(8):1266-1276.e5. doi:10.1016/j.chom.2021.05.009

6. Upton JW, Kaiser WJ, Mocarski ES. Virus Inhibition of RIP3-Dependent Necrosis. *Cell Host Microbe*. 2010;7(4):302-313. doi:10.1016/j.chom.2010.03.006

7. Green DR. The cell's dilemma, or the story of cell death: an entertainment in three acts. *Febs J*. 2016;283(14):2568-2576. doi:10.1111/febs.13658

8. Galluzzi L, Vitale I, Aaronson SA, et al. Molecular mechanisms of cell death: recommendations of the Nomenclature Committee on Cell Death 2018. *Cell Death Differ*. 2018;25(3):486-541. doi:10.1038/s41418-017-0012-4

9. Bergsbaken T, Fink SL, Cookson BT. Pyroptosis: host cell death and inflammation. *Nat Rev Microbiol*. 2009;7(2):99-109. doi:10.1038/nrmicro2070

10. Alvarez-Diaz S, Dillon CP, Lalaoui N, et al. The Pseudokinase MLKL and the Kinase RIPK3 Have Distinct Roles in Autoimmune Disease Caused by Loss of Death-Receptor-Induced Apoptosis. *Immunity*. 2016;45(3):513-526. doi:10.1016/j.immuni.2016.07.016

11. Green DR. Pseudokiller, qu'est-ce que c'est? *Immunity*. 2013;39(3):421-422. doi:10.1016/j.immuni.2013.08.020

12. Yatim N, Jusforgues-Saklani H, Orozco S, et al. RIPK1 and NF-κB signaling in dying cells determines cross-priming of $CD8^+$ T cells. *Sci New York N Y*. 2015;350(6258):328-334. doi:10.1126/science.aad0395

13. Snyder AG, Hubbard NW, Messmer MN, et al. Intratumoral activation of the necroptotic pathway components RIPK1 and RIPK3 potentiates antitumor immunity. *Sci Immunol*. 2019;4(36). doi:10.1126/sciimmunol.aaw2004

14. Deets KA, Doyle RN, Rauch I, Vance RE. Inflammasome activation leads to cDC1-independent cross-priming of CD8 T cells by epithelial cell-derived antigen. *Elife*. 2021;10:e72082. doi:10.7554/elife.72082

15. Deets KA, Vance RE. Inflammasomes and adaptive immune responses. *Nat Immunol*. 2021;22(4):412-422. doi:10.1038/s41590-021-00869-6

16. Burke TP, Engström P, Chavez RA, Fonbuena JA, Vance RE, Welch MD. Inflammasome-mediated antagonism of type I interferon enhances Rickettsia pathogenesis. *Nat Microbiol*. 2020;5(5):688-696. doi:10.1038/s41564-020-0673-5

17. Vercammen D, Beyaert R, Denecker G, et al. Inhibition of Caspases Increases the Sensitivity of L929 Cells to Necrosis Mediated by Tumor Necrosis Factor. *J Exp Medicine*. 1998;187(9):1477-1485. doi:10.1084/jem.187.9.1477

18. Huang Z, Wu SQ, Liang Y, et al. RIP1/RIP3 Binding to HSV-1 ICP6 Initiates Necroptosis to Restrict Virus Propagation in Mice. *Cell Host Microbe*. 2015;17(2):229-242. doi:10.1016/j.chom.2015.01.002

19. Kaiser WJ, Upton JW, Long AB, et al. RIP3 mediates the embryonic lethality of caspase-8-deficient mice. *Nature*. 2011;471(7338):368-372. doi:10.1038/nature09857

20. Zhang DW, Shao J, Lin J, et al. RIP3, an Energy Metabolism Regulator That Switches TNF-Induced Cell Death from Apoptosis to Necrosis. *Science*. 2009;325(5938):332-336. doi:10.1126/science.1172308

21. He S, Wang L, Miao L, et al. Receptor Interacting Protein Kinase-3 Determines Cellular Necrotic Response to TNF-α. *Cell*. 2009;137(6):1100-1111. doi:10.1016/j.cell.2009.05.021

22. Newton K, Sun X, Dixit VM. Kinase RIP3 is dispensable for normal NF-kappa Bs, signaling by the B-cell and T-cell receptors, tumor necrosis factor receptor 1, and Toll-like receptors 2 and 4. *Mol Cell Biol*. 2004;24(4):1464-1469.

23. Vandenabeele P, Galluzzi L, Berghe TV, Kroemer G. Molecular mechanisms of necroptosis: an ordered cellular explosion. *Nat Rev Mol Cell Bio*. 2010;11(10):700-714. doi:10.1038/nrm2970

24. Aggarwal BB. Signalling pathways of the TNF superfamily: a double-edged sword. *Nat Rev Immunol*. 2003;3(9):745-756. doi:10.1038/nri1184

25. Kondylis V, Kumari S, Vlantis K, Pasparakis M. The interplay of IKK, NF-κB and RIPK1 signaling in the regulation of cell death, tissue homeostasis and inflammation. *Immunol Rev*. 2017;277(1):113-127. doi:10.1111/imr.12550

26. Gough P, Myles IA. Tumor Necrosis Factor Receptors: Pleiotropic Signaling Complexes and Their Differential Effects. *Front Immunol*. 2020;11:585880. doi:10.3389/fimmu.2020.585880

27. Wajant H. TRAIL- and TNF-induced signaling complexes—so similar yet so different. *Embo J*. 2017;36(9):1117-1119. doi:10.15252/embj.201796997

28. Li X, Zhang M, Huang X, et al. Ubiquitination of RIPK1 regulates its activation mediated by TNFR1 and TLRs signaling in distinct manners. *Nat Commun*. 2020;11(1):6364. doi:10.1038/s41467-020-19935-y

29. Oberst A, Dillon CP, Weinlich R, et al. Catalytic activity of the caspase-8-FLIP(L) complex inhibits RIPK3-dependent necrosis. *Nature*. 2011;471(7338):363-367. doi:10.1038/nature09852

30. Chan FKM, Shisler J, Bixby JG, et al. A Role for Tumor Necrosis Factor Receptor-2 and Receptor-interacting Protein in Programmed Necrosis and Antiviral Responses*. *J Biol Chem*. 2003;278(51):51613-51621. doi:10.1074/jbc.m305633200

31. Safa AR. c-FLIP, a master anti-apoptotic regulator. *Exp Oncol*. 2012;34(3):176-184.

32. Newton K, Wickliffe KE, Dugger DL, et al. Cleavage of RIPK1 by caspase-8 is crucial for limiting apoptosis and necroptosis. *Nature*. 2019;574(7778):428-431. doi:10.1038/s41586-019-1548-x

33. Shamas-Din A, Bindner S, Zhu W, et al. tBid Undergoes Multiple Conformational Changes at the Membrane Required for Bax Activation*. *J Biol Chem*. 2013;288(30):22111-22127. doi:10.1074/jbc.m113.482109

34. Garrido C, Galluzzi L, Brunet M, Puig PE, Didelot C, Kroemer G. Mechanisms of cytochrome c release from mitochondria. *Cell Death Differ*. 2006;13(9):1423-1433. doi:10.1038/sj.cdd.4401950

35. Riedl SJ, Salvesen GS. The apoptosome: signalling platform of cell death. *Nat Rev Mol Cell Bio*. 2007;8(5):405-413. doi:10.1038/nrm2153

36. Kalkavan H, Green DR. MOMP, cell suicide as a BCL-2 family business. *Cell Death Differ*. 2018;25(1):46-55. doi:10.1038/cdd.2017.179

37. Brentnall M, Rodriguez-Menocal L, Guevara RLD, Cepero E, Boise LH. Caspase-9, caspase-3 and caspase-7 have distinct roles during intrinsic apoptosis. *Bmc Cell Biol*. 2013;14(1):32-32. doi:10.1186/1471-2121-14-32

38. Moriwaki K, Chan FKM. Necroptosis-independent signaling by the RIP kinases in inflammation. *Cell Mol Life Sci Cmls*. 2016;73(11-12):2325-2334. doi:10.1007/s00018-016-2203-4

39. Weinlich R, Oberst A, Beere HM, Green DR. Necroptosis in development, inflammation and disease. *Nat Rev Mol Cell Bio*. 2016;18(2):127-136. doi:10.1038/nrm.2016.149

40. Belizário J, Vieira-Cordeiro L, Enns S. Necroptotic Cell Death Signaling and Execution Pathway: Lessons from Knockout Mice. *Mediat Inflamm*. 2015;2015:128076. doi:10.1155/2015/128076

41. Thapa RJ, Ingram JP, Ragan KB, et al. DAI Senses Influenza A Virus Genomic RNA and Activates RIPK3-Dependent Cell Death. *Cell Host Microbe*. 2016;20(5):674-681. doi:10.1016/j.chom.2016.09.014

42. Nogusa S, Thapa RJ, Dillon CP, et al. RIPK3 Activates Parallel Pathways of MLKL-Driven Necroptosis and FADD-Mediated Apoptosis to Protect against Influenza A Virus. *Cell Host Microbe*. 2016;20(1):13-24. doi:10.1016/j.chom.2016.05.011

43. Upton JW, Kaiser WJ, Mocarski ES. DAI/ZBP1/DLM-1 Complexes with RIP3 to Mediate Virus-Induced Programmed Necrosis that Is Targeted by Murine Cytomegalovirus vIRA. *Cell Host Microbe*. 2012;11(3):290-297. doi:10.1016/j.chom.2012.01.016

44. Koehler H, Cotsmire S, Langland J, et al. Inhibition of DAI-dependent necroptosis by the Z-DNA binding domain of the vaccinia virus innate immune evasion protein, E3. *Proc National Acad Sci*. 2017;114(43):11506-11511. doi:10.1073/pnas.1700999114

45. Koehler HS, Feng Y, Mandal P, Mocarski ES. Recognizing limits of Z-nucleic acid binding protein (ZBP1/DAI/DLM1) function. *Febs J*. 2020;287(20):4362-4369. doi:10.1111/febs.15242

46. Rebsamen M, Heinz LX, Meylan E, et al. DAI/ZBP1 recruits RIP1 and RIP3 through RIP homotypic interaction motifs to activate NF-κB. *Embo Rep*. 2009;10(8):916-922. doi:10.1038/embor.2009.109

47. Daniels BP, Snyder AG, Olsen TM, et al. RIPK3 Restricts Viral Pathogenesis via Cell Death-Independent Neuroinflammation. *Cell*. 2017;169(2):301-313.e11. doi:10.1016/j.cell.2017.03.011

48. Daniels BP, Kofman SB, Smith JR, et al. The Nucleotide Sensor ZBP1 and Kinase RIPK3 Induce the Enzyme IRG1 to Promote an Antiviral Metabolic State in Neurons. *Immunity*. 2019;50(1):64-76.e4. doi:10.1016/j.immuni.2018.11.017

49. Takaoka A, Wang Z, Choi MK, et al. DAI (DLM-1/ZBP1) is a cytosolic DNA sensor and an activator of innate immune response. *Nature*. 2007;448(7152):501-505. doi:10.1038/nature06013

50. Kaiser WJ, Upton JW, Mocarski ES. Receptor-Interacting Protein Homotypic Interaction Motif-Dependent Control of NF-κB Activation via the DNA-Dependent Activator of IFN Regulatory Factors. *J Immunol*. 2008;181(9):6427-6434. doi:10.4049/jimmunol.181.9.6427

51. Newton K, Wickliffe KE, Maltzman A, et al. RIPK1 inhibits ZBP1-driven necroptosis during development. *Nature*. 2016;540(7631):129-133. doi:10.1038/nature20559

52. Kuriakose T, Man SM, Malireddi RKS, et al. ZBP1/DAI is an innate sensor of influenza virus triggering the NLRP3 inflammasome and programmed cell death pathways. *Sci Immunol*. 2016;1(2):aag2045. doi:10.1126/sciimmunol.aag2045

53. Herbert A, Alfken J, Kim YG, Mian IS, Nishikura K, Rich A. A Z-DNA binding domain present in the human editing enzyme, double-stranded RNA adenosine deaminase. *Proc National Acad Sci*. 1997;94(16):8421-8426. doi:10.1073/pnas.94.16.8421

54. Schwartz T, Rould MA, Lowenhaupt K, Herbert A, Rich A. Crystal Structure of the Zα Domain of the Human Editing Enzyme ADAR1 Bound to Left-Handed Z-DNA. *Science*. 1999;284(5421):1841-1845. doi:10.1126/science.284.5421.1841

55. Schwartz T, Behlke J, Lowenhaupt K, Heinemann U, Rich A. Structure of the DLM-1–Z-DNA complex reveals a conserved family of Z-DNA-binding proteins. *Nat Struct Biol*. 2001;8(9):761-765. doi:10.1038/nsb0901-761

56. Ha S, Kim D, Hwang HY, Rich A, Kim YG, Kim K. The crystal structure of the second Z-DNA binding domain of human DAI (ZBP1) in complex with Z-DNA reveals an unusual binding mode to Z-DNA. *P Natl Acad Sci Usa*. 2008;105(52):20671-20676. doi:10.1073/pnas.0810463106

57. Athanasiadis A, Placido D, Maas S, Brown BA, Lowenhaupt K, Rich A. The Crystal Structure of the Zβ Domain of the RNA-editing Enzyme ADAR1 Reveals Distinct Conserved Surfaces Among Z-domains. *J Mol Biol*. 2005;351(3):496-507. doi:10.1016/j.jmb.2005.06.028

58. Herbert A. Z-DNA and Z-RNA in human disease. *Commun Biology*. 2019;2(1):7. doi:10.1038/s42003-018-0237-x

59. Maelfait J, Liverpool L, Bridgeman A, Ragan KB, Upton JW, Rehwinkel J. Sensing of viral and endogenous RNA by ZBP 1/ DAI induces necroptosis. *Embo J*. 2017;36(17):2529-2543. doi:10.15252/embj.201796476

60. Guo H, Gilley RP, Fisher A, et al. Species-independent contribution of ZBP1/DAI/DLM-1-triggered necroptosis in host defense against HSV1. *Cell Death Dis*. 2018;9(8):816. doi:10.1038/s41419-018-0868-3

61. Hall K, Cruz P, Tinoco I, Jovin TM, Sande JH van de. 'Z-RNA'--a left-handed RNA double helix. *Nature*. 1984;311(5986):584-586. doi:10.1038/311584a0

62. Placido D, Brown BA, Lowenhaupt K, Rich A, Athanasiadis A. A Left-Handed RNA Double Helix Bound by the Zα Domain of the RNA-Editing Enzyme ADAR1. *Structure*. 2007;15(4):395-404. doi:10.1016/j.str.2007.03.001

63. Rothenburg S, Deigendesch N, Dittmar K, et al. A PKR-like eukaryotic initiation factor 2α kinase from zebrafish contains Z-DNA binding domains instead of dsRNA binding domains. *Proc National Acad Sci*. 2005;102(5):1602-1607. doi:10.1073/pnas.0408714102

64. Neidle S. Principles of Nucleic Acid Structure. 2008;(Nucleic Acids Res.161988):38-80. doi:10.1016/b978-012369507-9.50004-2

65. Nichols PJ, Bevers S, Henen M, Kieft JS, Vicens Q, Vögeli B. Recognition of non-CpG repeats in Alu and ribosomal RNAs by the Z-RNA binding domain of ADAR1 induces A-Z junctions. *Nat Commun*. 2021;12(1):793. doi:10.1038/s41467-021-21039-0

66. Lin J, Kumari S, Kim C, et al. RIPK1 counteracts ZBP1-mediated necroptosis to inhibit inflammation. *Nature*. 2016;540(7631):124-128. doi:10.1038/nature20558

67. Jiao H, Wachsmuth L, Kumari S, et al. Z-nucleic-acid sensing triggers ZBP1-dependent necroptosis and inflammation. *Nature*. 2020;580(7803):391-395. doi:10.1038/s41586-020-2129-8

68. Barraud P, Allain F. ADAR proteins: double-stranded RNA and Z-DNA binding domains. *Curr Top Microbiol*. 2012;353:35-60. doi:10.1007/82_2011_145

69. Brown BA, Lowenhaupt K, Wilbert CM, Hanlon EB, Rich A. The Zα domain of the editing enzyme dsRNA adenosine deaminase binds left-handed Z-RNA as well as Z-DNA. *Proc National Acad Sci*. 2000;97(25):13532-13536. doi:10.1073/pnas.240464097

70. Liddicoat BJ, Hartner JC, Piskol R, et al. Adenosine-to-inosine RNA editing by ADAR1 is essential for normal murine erythropoiesis. *Exp Hematol*. 2016;44(10):947-963. doi:10.1016/j.exphem.2016.06.250

71. Galipon J, Ishii R, Suzuki Y, Tomita M, Ui-Tei K. Differential Binding of Three Major Human ADAR Isoforms to Coding and Long Non-Coding Transcripts. *Genes-basel*. 2017;8(2):68. doi:10.3390/genes8020068

72. Bahn J, Ahn J, Lin X, et al. Genomic analysis of ADAR1 binding and its involvement in multiple RNA processing pathways. *Nat Commun*. 2015;6(1):6355. doi:10.1038/ncomms7355

73. George CX, Ramaswami G, Li JB, Samuel CE. Editing of Cellular Self-RNAs by Adenosine Deaminase ADAR1 Suppresses Innate Immune Stress Responses*. *J Biol Chem*. 2016;291(12):6158-6168. doi:10.1074/jbc.m115.709014

74. Bass BL. RNA Editing by Adenosine Deaminases That Act on RNA. *Annu Rev Biochem*. 2002;71(1):817-846. doi:10.1146/annurev.biochem.71.110601.135501

75. Chung H, Calis JJA, Wu X, et al. Human ADAR1 Prevents Endogenous RNA from Triggering Translational Shutdown. *Cell*. 2018;172(4):811-824.e14. doi:10.1016/j.cell.2017.12.038

76. Pestal K, Funk CC, Snyder JM, Price ND, Treuting PM, Stetson DB. Isoforms of RNA-Editing Enzyme ADAR1 Independently Control Nucleic Acid Sensor MDA5-Driven Autoimmunity and Multi-organ Development. *Immunity*. 2015;43(5):933-944. doi:10.1016/j.immuni.2015.11.001

77. Liddicoat BJ, Piskol R, Chalk AM, et al. RNA editing by ADAR1 prevents MDA5 sensing of endogenous dsRNA as nonself. *Science*. 2015;349(6252):1115-1120. doi:10.1126/science.aac7049

78. Mannion NM, Greenwood SM, Young R, et al. The RNA-Editing Enzyme ADAR1 Controls Innate Immune Responses to RNA. *Cell Reports*. 2014;9(4):1482-1494. doi:10.1016/j.celrep.2014.10.041

79. Rice GI, Kasher PR, Forte GMA, et al. Mutations in ADAR1 cause Aicardi-Goutières syndrome associated with a type I interferon signature. *Nat Genet*. 2012;44(11):1243-1248. doi:10.1038/ng.2414

80. Walkley CR, Liddicoat B, Hartner JC. Role of ADARs in mouse development. *Curr Top Microbiol*. 2012;353:197-220. doi:10.1007/82_2011_150

81. Crow YJ, Chase DS, Schmidt JL, et al. Characterization of human disease phenotypes associated with mutations in TREX1, RNASEH2A, RNASEH2B, RNASEH2C, SAMHD1, ADAR, and IFIH1. *Am J Med Genet A*. 2015;167(2):296-312. doi:10.1002/ajmg.a.36887

82. Rodero MP, Crow YJ. Type I interferon–mediated monogenic autoinflammation: The type I interferonopathies, a conceptual overview. *J Exp Medicine*. 2016;213(12):2527-2538. doi:10.1084/jem.20161596

83. Rodero MP, Tesser A, Bartok E, et al. Type I interferon-mediated autoinflammation due to DNase II deficiency. *Nat Commun*. 2017;8(1):2176. doi:10.1038/s41467-017-01932-3

84. Herbert A. Mendelian Disease caused by variants affecting recognition of Z-DNA and Z-RNA by the Zα domain of the double-stranded RNA Editing Enzyme ADAR. doi:10.31219/osf.io/4mja3

85. Kleinova R, Leuchtenberger AF, Giudice CL, et al. The ADAR1 editome reveals drivers of editing-specificity for ADAR1-isoforms. *Biorxiv*. 2021:2021.11.24.469911. doi:10.1101/2021.11.24.469911

86. Duany Y del T, Wu B, Hur S. MDA5-filament, dynamics and disease. *Curr Opin Virol*. 2015;12:20-25. doi:10.1016/j.coviro.2015.01.011

87. Ahmad S, Mu X, Yang F, et al. Breaching Self-Tolerance to Alu Duplex RNA Underlies MDA5-Mediated Inflammation. *Cell*. 2018;172(4):797-810.e13. doi:10.1016/j.cell.2017.12.016

88. Pichlmair A, Schulz O, Tan CP, et al. Activation of MDA5 requires higher-order RNA structures generated during virus infection. *J Virol*. 2009;83(20):10761-10769. doi:10.1128/jvi.00770-09

89. Loo YM, Fornek J, Crochet N, et al. Distinct RIG-I and MDA5 Signaling by RNA Viruses in Innate Immunity. *J Virol*. 2008;82(1):335-345. doi:10.1128/jvi.01080-07

90. Oda H, Nakagawa K, Abe J, et al. Aicardi-Goutières syndrome is caused by IFIH1 mutations. *Am J Hum Genet*. 2014;95(1):121-125. doi:10.1016/j.ajhg.2014.06.007

91. Yu Q, Valle AH del, Singh R, Modis Y. MDA5 disease variant M854K prevents ATP-dependent structural discrimination of viral and cellular RNA. *Nat Commun*. 2021;12(1):6668. doi:10.1038/s41467-021-27062-5

92. Häsler J, Strub K. Alu elements as regulators of gene expression. *Nucleic Acids Res*. 2006;34(19):5491-5497. doi:10.1093/nar/gkl706

93. Deininger P. Alu elements: know the SINEs. *Genome Biol*. 2011;12(12):236-236. doi:10.1186/gb-2011-12-12-236

94. Yang CC, Chen YT, Chang YF, et al. ADAR1-mediated 3′ UTR editing and expression control of antiapoptosis genes fine-tunes cellular apoptosis response. *Cell Death Dis*. 2017;8(5):e2833-e2833. doi:10.1038/cddis.2017.12

95. Rice GI, Kitabayashi N, Barth M, et al. Genetic, Phenotypic, and Interferon Biomarker Status in ADAR1-Related Neurological Disease. *Neuropediatrics*. 2017;48(03):166-184. doi:10.1055/s-0037-1601449

96. Maurano M, Snyder JM, Connelly C, Henao-Mejia J, Sidrauski C, Stetson DB. Protein kinase R and the integrated stress response drive immunopathology caused by mutations in the RNA deaminase ADAR1. *Immunity*. 2021;54(9):1948-1960.e5. doi:10.1016/j.immuni.2021.07.001

97. Fu Y, Comella N, Tognazzi K, Brown LF, Dvorak HF, Kocher O. Cloning of DLM-1, a novel gene that is up-regulated in activated macrophages, using RNA differential display. *Gene*. 1999;240(1):157-163. doi:10.1016/s0378-1119(99)00419-9

98. CLEMENS MJ, ELIA A. The Double-Stranded RNA-Dependent Protein Kinase PKR: Structure and Function. *J Interf Cytokine Res*. 1997;17(9):503-524. doi:10.1089/jir.1997.17.503

99. Morgan MJ, Kim YS. The serine threonine kinase RIP3: lost and found. *Bmb Rep*. 2015;48(6):303-312. doi:10.5483/bmbrep.2015.48.6.068

100. Ishizuka JJ, Manguso RT, Cheruiyot CK, et al. Loss of ADAR1 in tumours overcomes resistance to immune checkpoint blockade. *Nature*. 2019;565(7737):43-48. doi:10.1038/s41586-018-0768-9

101. John L, Samuel CE. Induction of stress granules by interferon and down-regulation by the cellular RNA adenosine deaminase ADAR1. *Virology*. 2014;454:299-310. doi:10.1016/j.virol.2014.02.025

102. Mok CC. Rituximab for the treatment of rheumatoid arthritis: an update. *Drug Des Dev Ther*. 2013;8:87. doi:10.2147/dddt.s41645

103. Crow YJ, Stetson DB. The type I interferonopathies: 10 years on. *Nat Rev Immunol*. 2021:1-13. doi:10.1038/s41577-021-00633-9

104. Serhan CN. Treating inflammation and infection in the 21st century: new hints from decoding resolution mediators and mechanisms. *Faseb J*. 2017;31(4):1273-1288. doi:10.1096/fj.201601222r

105. Coutinho AE, Chapman KE. The anti-inflammatory and immunosuppressive effects of glucocorticoids, recent developments and mechanistic insights. *Mol Cell Endocrinol*. 2011;335(1):2-13. doi:10.1016/j.mce.2010.04.005

106. Ishii KJ, Kawagoe T, Koyama S, et al. TANK-binding kinase-1 delineates innate and adaptive immune responses to DNA vaccines. *Nature*. 2008;451(7179):725-729. doi:10.1038/nature06537

107. Varfolomeev EE, Schuchmann M, Luria V, et al. Targeted Disruption of the Mouse Caspase 8 Gene Ablates Cell Death Induction by the TNF Receptors, Fas/Apo1, and DR3 and Is Lethal Prenatally. *Immunity*. 1998;9(2):267-276. doi:10.1016/s1074-7613(00)80609-3

108. Murphy JM, Czabotar PE, Hildebrand JM, et al. The Pseudokinase MLKL Mediates Necroptosis via a Molecular Switch Mechanism. *Immunity*. 2013;39(3):443-453. doi:10.1016/j.immuni.2013.06.018

109. Najjar M, Saleh D, Zelic M, et al. RIPK1 and RIPK3 Kinases Promote Cell-Death-Independent Inflammation by Toll-like Receptor 4. *Immunity*. 2016;45(1):46-59. doi:10.1016/j.immuni.2016.06.007

110. Gray EE, Treuting PM, Woodward JJ, Stetson DB. Cutting Edge: cGAS Is Required for Lethal Autoimmune Disease in the Trex1-Deficient Mouse Model of Aicardi–Goutières Syndrome. *J Immunol*. 2015;195(5):1939-1943. doi:10.4049/jimmunol.1500969

111. Gall A, Treuting P, Elkon KB, et al. Autoimmunity Initiates in Nonhematopoietic Cells and Progresses via Lymphocytes in an Interferon-Dependent Autoimmune Disease. *Immunity*. 2012;36(1):120-131. doi:10.1016/j.immuni.2011.11.018

112. Berger SB, Kasparcova V, Hoffman S, et al. Cutting Edge: RIP1 Kinase Activity Is Dispensable for Normal Development but Is a Key Regulator of Inflammation in SHARPIN-Deficient Mice. *J Immunol*. 2014;192(12):5476-5480. doi:10.4049/jimmunol.1400499

113. Salmena L, Lemmers B, Hakem A, et al. Essential role for caspase 8 in T-cell homeostasis and T-cell-mediated immunity. *Gene Dev*. 2003;17(7):883-895. doi:10.1101/gad.1063703

114. Henao-Mejia J, Williams A, Rongvaux A, Stein J, Hughes C, Flavell RA. Generation of Genetically Modified Mice Using the CRISPR–Cas9 Genome-Editing System. *Cold Spring Harb Protoc*. 2016;2016(2):pdb.prot090704. doi:10.1101/pdb.prot090704

115. Shin KJ, Wall EA, Zavzavadjian JR, et al. A single lentiviral vector platform for microRNA-based conditional RNA interference and coordinated transgene expression. *Proc National Acad Sci*. 2006;103(37):13759-13764. doi:10.1073/pnas.0606179103

116. Zarnegar BJ, Flynn RA, Shen Y, Do BT, Chang HY, Khavari PA. irCLIP platform for efficient characterization of protein–RNA interactions. *Nat Methods*. 2016;13(6):489-492. doi:10.1038/nmeth.3840

117. Orozco S, Yatim N, Werner MR, et al. RIPK1 both positively and negatively regulates RIPK3 oligomerization and necroptosis. *Cell Death Differ*. 2014;21(10):1511-1521. doi:10.1038/cdd.2014.76

118. Bray NL, Pimentel H, Melsted P, Pachter L. Near-optimal probabilistic RNA-seq quantification. *Nat Biotechnol*. 2016;34(5):525-527. doi:10.1038/nbt.3519

119. Ewels P, Magnusson M, Lundin S, Käller M. MultiQC: summarize analysis results for multiple tools and samples in a single report. *Bioinformatics*. 2016;32(19):3047-3048. doi:10.1093/bioinformatics/btw354

120. Love MI, Huber W, Anders S. Moderated estimation of fold change and dispersion for RNA-seq data with DESeq2. *Genome Biol*. 2014;15(12):550. doi:10.1186/s13059-014-0550-8

121. Durinck S, Moreau Y, Kasprzyk A, et al. BioMart and Bioconductor: a powerful link between biological databases and microarray data analysis. *Bioinformatics*. 2005;21(16):3439-3440. doi:10.1093/bioinformatics/bti525

122. Durinck S, Spellman PT, Birney E, Huber W. Mapping identifiers for the integration of genomic datasets with the R/Bioconductor package biomaRt. *Nat Protoc*. 2009;4(8):1184-1191. doi:10.1038/nprot.2009.97

123. Yu G, Wang LG, Han Y, He QY. clusterProfiler: an R Package for Comparing Biological Themes Among Gene Clusters. *Omics J Integr Biology*. 2012;16(5):284-287. doi:10.1089/omi.2011.0118

124. Kearney CJ, Martin SJ. An Inflammatory Perspective on Necroptosis. *Mol Cell*. 2017;65(6):965-973. doi:10.1016/j.molcel.2017.02.024

125. Chen X, Zhu R, Zhong J, et al. Mosaic composition of RIP1–RIP3 signalling hub and its role in regulating cell death. *Nat Cell Biol*. 2022;24(4):471-482. doi:10.1038/s41556-022-00854-7

126. Cho Y, Challa S, Moquin D, et al. Phosphorylation-Driven Assembly of the RIP1-RIP3 Complex Regulates Programmed Necrosis and Virus-Induced Inflammation. *Cell*. 2009;137(6):1112-1123. doi:10.1016/j.cell.2009.05.037

127. Wu XN, Yang ZH, Wang XK, et al. Distinct roles of RIP1–RIP3 hetero- and RIP3–RIP3 homo-interaction in mediating necroptosis. *Cell Death Differ*. 2014;21(11):1709-1720. doi:10.1038/cdd.2014.77

128. Muendlein HI, Connolly WM, Magri Z, et al. ZBP1 promotes LPS-induced cell death and IL-1β release via RHIM-mediated interactions with RIPK1. *Nat Commun*. 2021;12(1):86. doi:10.1038/s41467-020-20357-z

129. Muendlein HI, Connolly WM, Magri Z, et al. ZBP1 promotes inflammatory responses downstream of TLR3/TLR4 via timely delivery of RIPK1 to TRIF. *Proc National Acad Sci*. 2022;119(24):e2113872119. doi:10.1073/pnas.2113872119

130. Dara L, Liu ZX, Kaplowitz N. A murder mystery in the liver: who done it and how? *J Clin Investigation*. 2016;126(11):4068-4071. doi:10.1172/jci90830

131. Wolf U, Wolf M, Heusser P, Thurneysen A, Baumgartner S. Homeopathic Preparations of Quartz, Sulfur and Copper Sulfate Assessed by UV-Spectroscopy. *Evid-based Compl Alt*. 2011;2011:1-11. doi:10.1093/ecam/nep036

132. Kreuz S, Siegmund D, Scheurich P, Wajant H. NF-kappaB inducers upregulate cFLIP, a cycloheximide-sensitive inhibitor of death receptor signaling. *Mol Cell Biol*. 2001;21(12):3964-3973. doi:10.1128/mcb.21.12.3964-3973.2001

133. Poukkula M, Kaunisto A, Hietakangas V, et al. Rapid turnover of c-FLIPshort is determined by its unique C-terminal tail. *J Biological Chem*. 2005;280(29):27345-27355. doi:10.1074/jbc.m504019200

134. Fulda S. Targeting c-FLICE-like inhibitory protein (CFLAR) in cancer. *Expert Opin Ther Tar*. 2012;17(2):195-201. doi:10.1517/14728222.2013.736499

135. Piccirillo CA, Bjur E, Topisirovic I, Sonenberg N, Larsson O. Translational control of immune responses: from transcripts to translatomes. *Nat Immunol*. 2014;15(6):503-511. doi:10.1038/ni.2891

136. Carey CM, Govande AA, Cooper JM, Hartley MK, Kranzusch PJ, Elde NC. Recurrent Loss-of-Function Mutations Reveal Costs to OAS1 Antiviral Activity in Primates. *Cell Host Microbe*. 2019;25(2):336-343.e4. doi:10.1016/j.chom.2019.01.001

137. Brunette RL, Young JM, Whitley DG, Brodsky IE, Malik HS, Stetson DB. Extensive evolutionary and functional diversity among mammalian AIM2-like receptors. *J Exp Medicine*. 2012;209(11):1969-1983. doi:10.1084/jem.20121960

138. Digby Z, Tourlomousis P, Rooney J, et al. Evolutionary loss of inflammasomes in the Carnivora and implications for the carriage of zoonotic infections. *Cell Reports*. 2021;36(8):109614. doi:10.1016/j.celrep.2021.109614

139. Águeda-Pinto A, Alves LQ, Neves F, et al. Convergent Loss of the Necroptosis Pathway in Disparate Mammalian Lineages Shapes Viruses Countermeasures. *Front Immunol*. 2021;12:747737. doi:10.3389/fimmu.2021.747737

140. Basavaraju S, Mishra S, Jindal R, Kesavardhana S. Emerging Role of ZBP1 in Z-RNA Sensing, Influenza Virus-Induced Cell Death, and Pulmonary Inflammation. *Mbio*. 2022;13(3):e0040122. doi:10.1128/mbio.00401-22

141. Lamers MM, Hoogen BG van den, Haagmans BL. ADAR1: “Editor-in-Chief” of Cytoplasmic Innate Immunity. *Front Immunol*. 2019;10:1763. doi:10.3389/fimmu.2019.01763

142. Piontkivska H, Wales-McGrath B, Miyamoto M, Wayne ML. ADAR Editing in Viruses: An Evolutionary Force to Reckon with. *Genome Biol Evol*. 2021;13(11):evab240. doi:10.1093/gbe/evab240

143. Ringlander J, Fingal J, Kann H, et al. Impact of ADAR-induced editing of minor viral RNA populations on replication and transmission of SARS-CoV-2. *Proc National Acad Sci*. 2022;119(6):e2112663119. doi:10.1073/pnas.2112663119

144. Samuel CE. ADARs: viruses and innate immunity. *Curr Top Microbiol*. 2011;353:163-195. doi:10.1007/82_2011_148

145. Gélinas JF, Clerzius G, Shaw E, Gatignol A. Enhancement of replication of RNA viruses by ADAR1 via RNA editing and inhibition of RNA-activated protein kinase. *J Virol*. 2011;85(17):8460-8466. doi:10.1128/jvi.00240-11

146. Jin Y, Zhang W, Li Q. Origins and evolution of ADAR-mediated RNA editing. *Iubmb Life*. 2009;61(6):572-578. doi:10.1002/iub.207

147. Gaidt MM, Morrow A, Fairgrieve MR, Karr JP, Yosef N, Vance RE. Self-guarding of MORC3 enables virulence factor-triggered immunity. *Nature*. 2021;600(7887):138-142. doi:10.1038/s41586-021-04054-5

148. Crowl JT, Stetson DB. SUMO2 and SUMO3 redundantly prevent a noncanonical type I interferon response. *P Natl Acad Sci Usa*. 2018;115(26):6798-6803. doi:10.1073/pnas.1802114115